ELECTRICAL EFFECTS OF GASES ON LEAD TELLURIDE THIN FILMS

by

Surinder Pal Singh Sangha, M.Sc., D.I.C.

A thesis submitted for the degree of Doctor of Philosophy in the University of London

Department of Electrical Engineering,
Imperial College of Science & Technology,
London, S.W.7.

November 1979

Abstract

Interaction of oxygen and atomic hydrogen with thin films of lead telluride was studied by performing in situ Hall measurements. The films were grown in a vacuum of $\sim 1 \times 10^{-6}$ torr on air-cleaved muscovite mica using a single source evaporation technique. The carrier concentration at room temperature was in the range 10^{16}-10^{18} cm^{-3} and the values of the Hall mobilities at room temperature ranged from 400-900 $cm^2 v^{-1} s^{-1}$. The thickness of the films varied from 2000Å to 5000Å.

The effect of oxygen and atomic hydrogen on the electrical properties of the films was examined by continuously monitoring the Hall coefficient, R_H and the resistivity, ρ during the gas exposure. Results were interpreted in terms of two models, namely surface adsorption model and diffusion model. Theoretical expressions for R_H and ρ were developed for both models in order to compare the experimental and the theoretical R_H vs ρ curves. The accuracy of the fit between the two curves was taken as evidence for the validity of the model. The shape of R_H vs ρ curve was successfully predicted by the theoretical models under appropriate conditions.

Kinetic studies were also undertaken in an attempt to gain further insight into the mechanisms of gas uptake. In addition, mechanisms of ionisation of H were also considered. Based on the combined evidence of the theoretical models and the kinetic studies, it was proposed that the mechanism of gas uptake was not uniquely defined by the above-mentioned models.

Acknowledgements

I am grateful to Dr. C. Juhasz for his help, guidance and encouragement throughout the course of the project. I wish to thank Professor J.C. Anderson for his interest in the project. I am also indebted to Drs. M. Green and M.J. Lee for their helpful advice.

Thanks are also due to the Science Research Council for financial support and to Miss Cynthia Collins for typing the manuscript.

Contents

Page

Page

CHAPTER 1

PROPERTIES OF PbTe

1.1 INTRODUCTION

Lead telluride belongs to the lead chalcogenide family where lead sulphide and lead selenide are its other two members. The reason for continued scientific interest in lead chalcogenides is two-fold. Firstly, since lead chalcogenides have relatively small band gaps (<0.5 eV) they are suitable for infra-red detection and, secondly, the possibility of other devices such as thin film transistor based on lead chalcogenides. Properties of lead telluride, PbTe in conjunction with lead sulphide, PbS and lead selenide, PbSe have been reviewed by Scanlon(S1), Putley (P1) and more recently by Ravich et al.(R1) where all three reviews contain exhaustive lists of earlier work. Therefore the purpose of this chapter is to present, briefly, an overview of properties of PbTe.

1.2 CRYSTAL STRUCTURE

Lead telluride has a sodium chloride type face centred cubic structure with Pb occupying (OOO), (a/2 a/2 O), (a/2 O a/2), (O a/2 a/2) and Te occupying (a/2 a/2 a/2), (OOa/2), (O a/2 O), (a/2 O O) in the unit cell where a is the lattice constant. The value of a given by Dalven (D1) is 6.462Å whereas values given by Scanlon (S1) and Ravich et al. (R1) are 6.46Å and 6.50Å respectively. Bonding in

PbTe is partially ionic and partially covalent, i.e. it is a polar semiconductor.

1.3 BAND STRUCTURE

Since PbTe has face centred cubic structure, the first Brillouin zone is a truncated octahedron (K4), as shown in Fig. 1.1. Investigations of optical absorption show that the extrema of the conduction and valence bands lie at the same point in k-space. The constant energy surfaces for valence and conduction bands are ellipsoids centred at L points and strongly elongated along the <111> direction as shown in Fig. 1.2. Two principal effective masses may be defined with reference to the axes of the ellipsoid of Fig. 1.2.

$$m_\ell = \hbar^2 / \frac{d^2E}{dk^2_\ell} \tag{1.1}$$

$$m_t = \hbar^2 / \frac{d^2E}{dk^2_t} \tag{1.2}$$

where m_ℓ is the longitudinal effective mass and m_t is the transverse effective mass, k_ℓ is a vector perpendicular to k_t and parallel to (111) direction. The mass anisotropy K is related to m_ℓ and m_t by the following equation

$$K = \frac{m_\ell}{m_t} \tag{1.3}$$

Cuff et al. (C1) give the value of K for valence and conduction band to be 14 and 10 respectively at $4^\circ K$. The other two effective masses pertinent to electrical

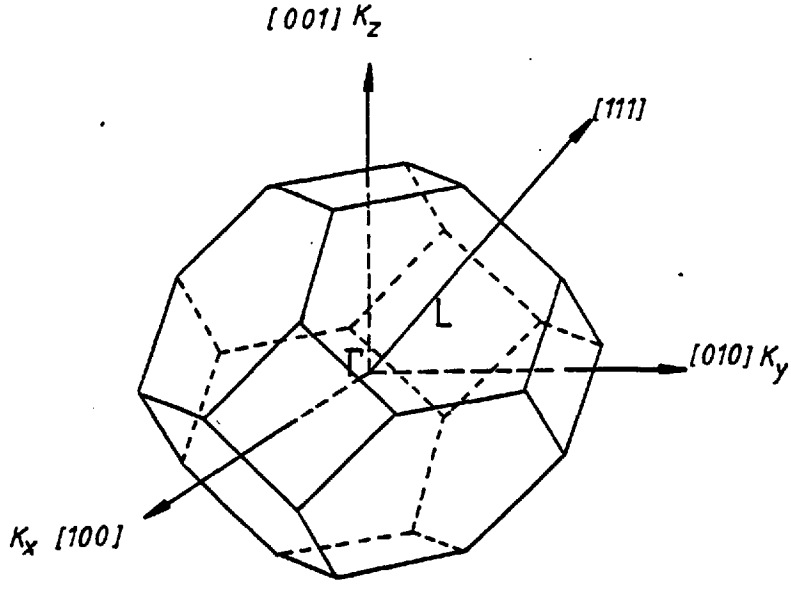

Fig. 1.1 1st Brillouin zone of PbTe

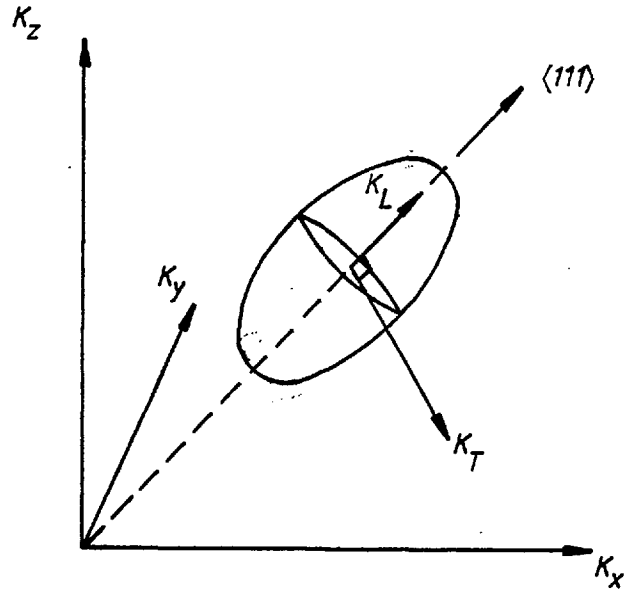

Fig. 1.2 Constant energy surfaces

properties are the conductivity effective mass, m_c, which relates to transport properties and the density of states effective mass, m_d, which relates to the equilibrium statistics of the carriers. The averaged conductivity effective mass m_c is related to m_ℓ and m_t as follows (D1)

$$m_c = \left(\frac{3m_\ell m_t}{2m_\ell + m_t} \right) \tag{1.4}$$

The density of states effective mass, m_d, can also be related to m_ℓ and m_t (C2)

$$m_d = (m_\ell \, m_t^2)^{1/3} \; N_v^{2/3} \tag{1.5}$$

where N_v is the number of equivalent minima and in the case of the conduction band $N_v = 4$. Values of m_d and m_c for PbTe (carrier concentration 10^{18} cm^{-3}) at room temperature given by Egerton (E1) are $m_d = 0.24\ m_o$ and $m_c = 0.09\ m_o$ for conduction band and $m_d = 0.29\ m_o$ and $m_c = 0.11\ m_o$ for valence band where m_o is the mass of free electron.

The band gap deduced from optical absorption experiments performed on epitaxial films of PbTe is 0.31 eV at 300^oK (Z1). It has positive temperature coefficient, $\frac{dEg}{dT}$.

$$Eg = Eg_o + \left(\frac{dEg}{dT}\right) T \tag{1.6}$$

where Eg_o is the band gap at 0^oK and $\frac{dEg}{dT} = (4.5 \pm 0.2) \times 10^{-4}$ eV K^{-1} (P2) in the temperature range 25^oK - 300^oK.

For narrow band gap semiconductor such as PbTe, non-parabolicity is characteristic and consequence of interband interactions (R3). Non-parabolicity of conduction band and valence band of PbTe has been investigated using two models, namely Kane's model and Cohen's model. Kane (K6) developed dispersion relations for non-parabolic isotropic bands of InSb. In the case of conduction band , he gives the following E vs K relationship

$$E(E + Eg) = Eg \left(\frac{\hbar^2 K^2}{2m_{de}}\right) \tag{1.7}$$

where Eg is the energy gap, $\hbar = \frac{h}{2\pi}$, h being Plank's constant, m_{de} is density of states effective mass of electrons and K is the wave number. The density of states function for above dispersion equation is given by the following expression (R3)

$$g_c(E) = \frac{1}{2\pi^2} \left(\frac{2m_{de}}{\hbar^2} \right)^{3/2} E^{\frac{1}{2}} \left(1 + \frac{E}{Eg}\right)^{\frac{1}{2}} \left(1 + \frac{2E}{Eg}\right) \tag{1.8}$$

where energy zero has been taken at the bottom of the conduction band. By replacing E with $(E_v - E)$, a similar expression for valence band can be obtained. Cohen (C8) extended Kane's model to include non-ellipsiodal energy surfaces and non-parabolicity of the bands for Bi. The dispersion relation in this case becomes (R3),

$$E = \frac{\hbar^2 K_t^2}{2m_{te}\left\{1 + \frac{E}{Eg} + \frac{\hbar^2 K_\ell^2}{2m_{\ell é}}\right\}} + \frac{\hbar^2 K_\ell^2}{2m_{\ell e}} \tag{1.9}$$

where K_t and K_ℓ are the transverse and longitudinal wave numbers, m_{te} and $m_{\ell e}$ are the transverse and longitudinal principal valence band edge effective masses, $m_{\ell \acute{e}}$ is the longitudinal conduction band edge effective mass. Density of states function for conduction band is given by equation (1.10)

$$g_c(E) = \frac{1}{2\pi^2} \left(\frac{2m_{de}}{\hbar^2} \right)^{3/2} E^{\frac{1}{2}} \{1 + \frac{5E}{3Eg} (1 + \frac{U}{5})\} \qquad (1.10)$$

where $U = m_{\ell e}/m_{\ell \acute{e}}$. Band (B2) has shown that for lead salts, equations (1.10) and (1.8) may respectively be simplified to the following,

$$g_c(E) \approx \frac{1}{2\pi^2} \left(\frac{2m_{de}}{\hbar^2}\right)^{3/2} E^{\frac{1}{2}} (1 + \frac{2E}{Eg}) \qquad (1.11)$$

and

$$g_c(E) \approx \frac{1}{2\pi^2} \left(\frac{2m_{de}}{\hbar^2}\right)^{3/2} E^{\frac{1}{2}} (1 + \frac{5E}{2Eg}) \qquad (1.12)$$

Since expressions for $g_c(E)$ for non-ellipsoidal energy surfaces and non-parabolic bands and isotropic non-parabolic bands are quite similar, equation (1.8) may be used without incurring a serious error. Equation (1.8) can also be written in reduced energy notation as follows

$$g_c(\varepsilon) = \frac{1}{2\pi^2} \left(\frac{2m_{de}kT}{\hbar^2} \right)^{3/2} \varepsilon^{\frac{1}{2}} (1 + \frac{\varepsilon}{\varepsilon_g})^{\frac{1}{2}} (1 + \frac{2\varepsilon}{\varepsilon_g}) \qquad (1.13)$$

and similarly for holes,

$$g_v(\varepsilon) = \frac{1}{2\pi^2} \left(\frac{2m_{dh}kT}{\hbar^2} \right)^{3/2} (\varepsilon + a\varepsilon)^{\frac{1}{2}} (1 + 2a\varepsilon) \tag{1.14}$$

where

$\varepsilon = \frac{E}{kT}$, non-parabolicity constant $a = \frac{kT}{Eg}$, $\varepsilon_g = \frac{Eg}{kT}$, k is Boltzmann's constant and T is the temperature. Similar expressions for $g_c(\varepsilon)$ and $g_c(\varepsilon)$ are also given by Juhasz (J3) for spherical energy surfaces and non-parabolic bands.

Non-parabolicity of the conduction band of PbTe in the temperature range 77-300°K was investigated by Zhitinskaya et al (Z2) and Dubrovskaya and Ravich (D2) where these investigators measured the transport coefficients like the thermoelectric power, α, the Hall coefficient R_H, electrical conductivity and Nernst-Ettingshausen coefficient as a function of temperature and magnetic field for n-type single crystal PbTe with carrier concentration in the range 10^{18}-10^{20} cm^{-3}. Dubrovskaya and Ravich (D2) found that both models (Kane's model and Cohen's model) described the energy dependence of density of states for carrier concentration less than 5×10^{19} cm^{-3} provided suitable values of m_d and Eg were chosen whereas Zhitinskaya et al (Z2) noted that the dependence of density of states effective mass on carrier density was described by Kane's model. Stavitskaya et al (S2) measured α, R_H and carrier mobility in the temperature range 100-1000°K for n-type PbTe with

carrier density in 10^{18}-10^{20} cm^{-3} range and concluded that the experimental data were in good agreement with Kane's model and acoustic scattering.

Valence bands of PbTe have also been investigated in the temperature range 24-450°K (A1, K1, C3, D6) and like the conduction band, the principal valence band was also found to be non-parabolic. Existence of a second heavy mass valence band has been proposed by Allgaier (A1), Tauber et al (T2) and Chernik et al (C3) but location of the heavy mass valence band is unknown because this band is always unoccupied at very low temperatures (R3).

1.4 ELECTRICAL PROPERTIES OF PbTe

1.4.1 Single Crystals

Allgaier and Scanlon (A2) measured the mobility of electrons and holes of lead chalcogenides between 4.2°K and room temperature where the single crystals were grown by the Bridgman-Stockbargar technique. Some of the earlier work done on the Hall measurements of synthetic crystals of lead chalcogenides is also referenced by Allgaier and Scanlon. In Fig. 1.3, Fig. 1.4 and Fig. 1.5, variation of the Hall coefficient, and the Hall mobility between 4.2°K and 295°K for PbTe is shown where the data are taken from Allgaier and Scanlon. Carrier concentration at room temperature ranged from 10^{17}-10^{18} cm^{-3} and resistivity of the samples ranged from 3 mΩ cm to 24.4 mΩ cm. The Hall coefficient varied by 10-20% over the entire temperature range. Temperature dependence of the Hall mobility was

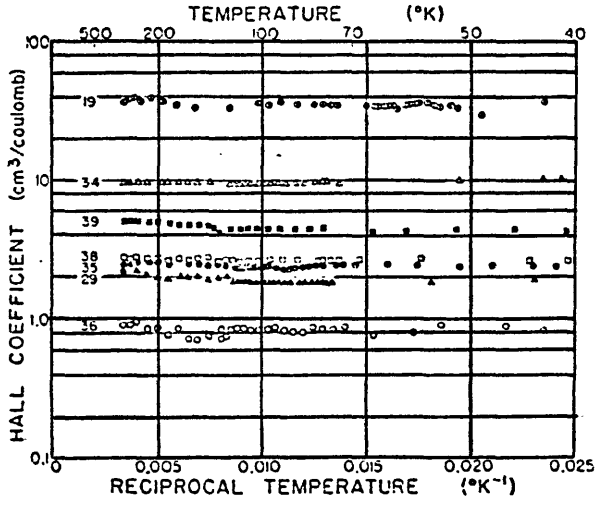

Fig. 1.3 R_H versus Temperature

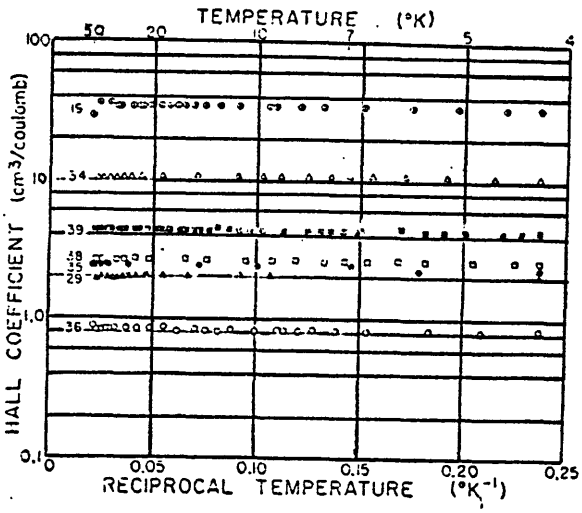

Fig. 1.4 R_H versus Temperature

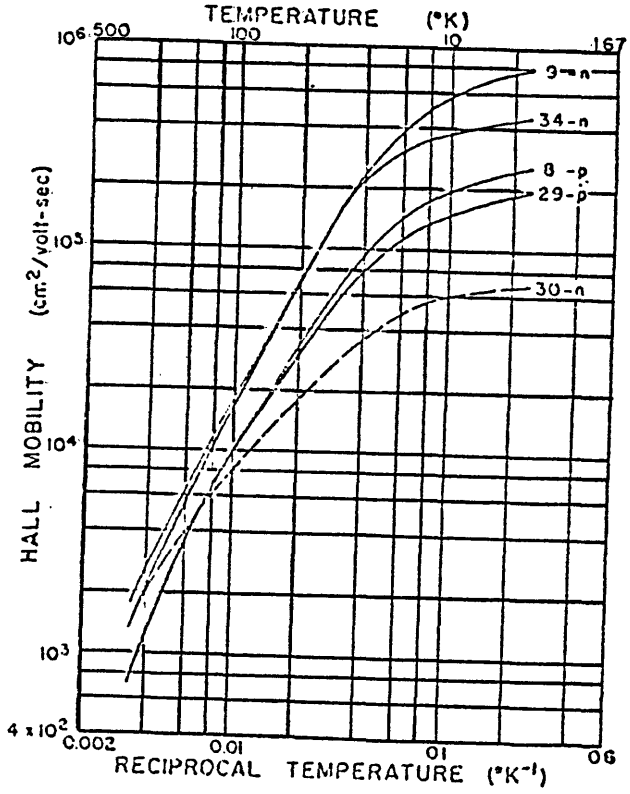

Key

- n-type natural PbS
- n-type PbS
- p-type PbS
- n-type PbSe
- p-type PbSe
- n-type PbTe
- p-type PbTe

Fig. 1.5 μ_H versus Temperature

[Data from Allgaier and Scanlon (A2)]

described by a power law,

$$\mu_H \alpha T^{-s} \tag{1.15}$$

where the averaged value of s between 100°K-295°K was in the range 2.2-2.4. Low temperature mobilities at 4.2°K were sometimes as high as 8 x 10^5 cm^2/vs,where the unimportance of ionised impurity scattering was attributed to high static dielectric constant. (Kanai and Shohno (K2) who measured the capacitance of junction diodes of PbTe suggested a value of static dielectric constant of ∿420 at 77°K.) Furthermore, temperature dependence of μ_H was the same for n-type and p-type single crystals. Putley (P1) when reviewing the transport properties of lead chalcogenides found, (i) complete absence of discrete impurity levels and (ii) no evidence for ionised impurity scattering even in very impure material at 4°K.

An explanation of temperature dependence of mobility was put forward by Allgaier and Houston (A3) where they proposed that the combined effect of one phonon acoustic scattering and a temperature dependent carrier effective mass was responsible for the power law. For classical statistics (D1),

$$\mu \alpha m^{-5/2} T^{-3/2} \tag{1.16}$$

Therefore, $m \alpha T^{0.4}$ for pure samples to give $\mu \alpha T^{-2.5}$.

1.4.2 Thin Films

Electrical properties of epitaxial thin films of lead chalcogenides grown on alkali halides were reviewed by Zemel (Z3). However, glass and mica were also used as substrates during some of the earlier investigations of photoconductivity and electrical properties of lead telluride (S3, M1). Fig. 1.6 and Fig. 1.7 show the temperature dependence of the Hall coefficient and mobility for PbTe films. Two points are worth noting.

(i) High mobilities are maintained even at liquid nitrogen temperatures.

(ii) Around room temperature, the power law $\mu \alpha T^{-s}$ is obeyed where $s \sim 2.5$.

Both of these features are in common with bulk single crystals.

Using mobility as a criterion of film quality, quality of thin film materials is usually much inferior to that of equivalent bulk material especially when the films are grown in a conventional vacuum system (open source, pressure $\sim 10^{-6}$ torr). However, one of the techniques which has contributed significantly to the preparation of thin films with bulk-like properties is the hot wall technique (HWT). A recent reivew of HWT is given by Lopez-Otero (L1) where he defines HWT as the technique of vacuum film deposition, the main characteristic being the growth of epitaxial layers under conditions as near

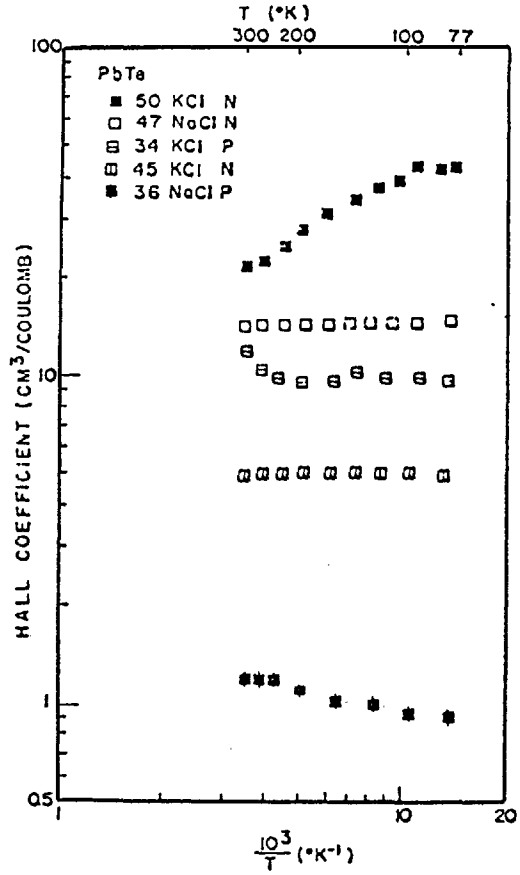

Fig.1.6 R_H *versus Temperature (Z1)*

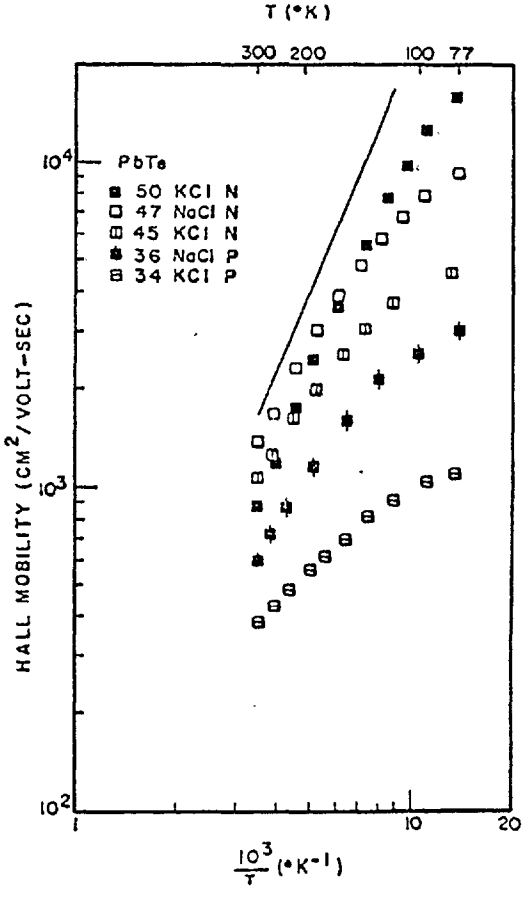

Fig.1.7 μ_H *versus Temperature (Z1)*

as possible to thermodynamic equilibrium. The salient feature of HWT is the use of a hot wall which both encloses and directs the vapour from source to substrate. This also avoids the loss of evaporating material and reduces the difference between substrate and source temperatures to a minimum. In order to illustrate the effectiveness of HWT to produce films with bulk-like properties, in Fig. 1.8 the Hall mobility versus temperature is plotted for PbTe films grown by conventional vacuum system (Egerton (E1)) and HWT (Lopez-Otero (L2) and Dhere (D3)). Also shown on the graph is the plot μ_H vs T for n-type single crystals from Allgaier and Scanlon (A2). Even though Egerton's films were thin ($\sim$3000Å) and grown on mica and films grown by Lopez-Otero and Dhere were thicker and grown on alkali halides, it is clear from Fig. 1.8 that films produced using HWT have essentially bulk-like mobilities. Another advantage of HWT is that it affords control over the carrier concentration which is not possible with a conventional vacuum system.

1.5 GASEOUS AMBIENT EFFECTS

Most of the early work regarding the effect of gases on the electrical properties of lead chalcogenides was concerned with the problem of photoconductivity. For instance, the effect of oxygen on polycrystalline films of PbTe and PbSe grown on glass substrate was investigated by Bode and Levinstein (B1), Jones (J1) and Yasuoka (Y1).

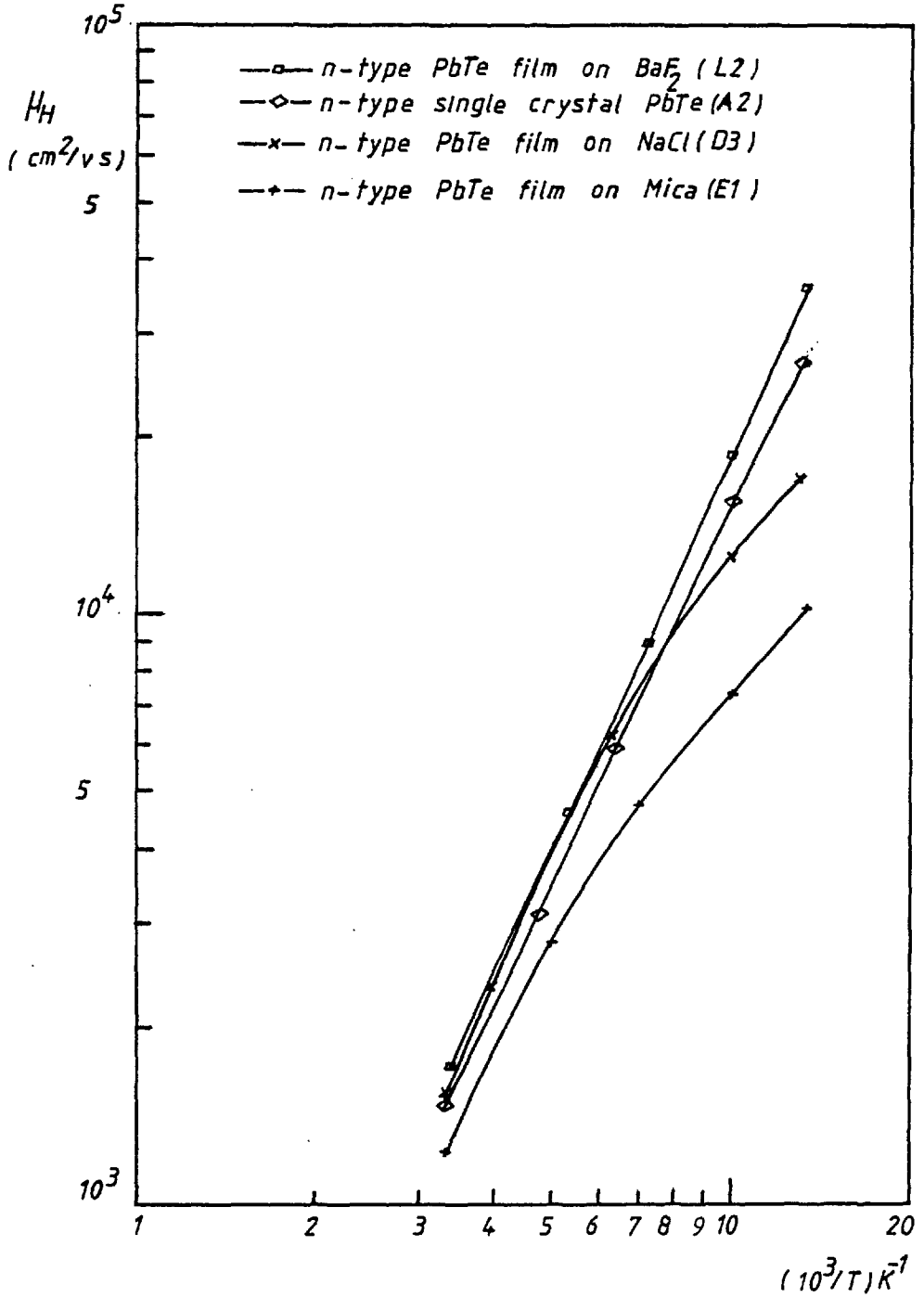

Fig. 1.8 μ_H *versus Temperature*

These workers noted that oxygenated films became photo-conductive.

Interaction of O_2 with epitaxic PbSe films grown on NaCℓ substrate was first investigated by Brodsky and Zemel (B3). The effect of oxygen on epitaxial thin films of lead telluride grown on mica was investigated by Egerton and Juhasz (E2). Later on, Zemel and co-workers (M2, Y2) used alkali halides as substrates for their epitaxial thin films of lead selenide and gaseous ambient experiments. Interaction of oxygen and atomic hydrogen with $Pb_{1-x}\ Sn_xTe$ alloy has also been investigated (B2,H1). A review of gas effects of lead chalcogenides films is given by Zemel (Z4).

Closely allied to the gaseous ambient effects has been the development of hydrogen sensitive MOS, field effect transistor by Lundström et al (L3,L4). They used a thin film of palladium Pd as the gate electrode on an n-channel MOST. With this structure, they were able to detect with ease 40 ppm hydrogen gas in air. Shivaraman (S4) used a similar structure to detect H_2S. In such a structure, Pd-gate acts as a catalyst for the dissociation of H_2 or H_2S and atomic hydrogen thus produced is partially dissolved in Pd and partially adsorbed onto the Pd-SiO_2 interface. This gives rise to changes in the work function difference between the metal and the semiconductor which is equal to a change in threshold voltage of the transistor (S4). Steele and MacIver (S5) used the observation that the height of a Schottky barrier produced at metal and cadmium sulphide, CdS contact was strongly dependent on the metal

work function, to fabricate a hydrogen detector. They evaporated Pd dots (800Å in thickness) onto indium doped single crystal of CdS and measured the dark I-V characteristics of Pd-CdS diodes when exposed to a gas mixture containing hydrogen. In a recent review, Zemel (Z5) has discussed further the possibilities of chemically sensitive semiconductor devices.

1.6 AIM OF PRESENT STUDY AND LAYOUT OF THE THESIS

The aim of the present investigation of interaction of atomic hydrogen and oxygen with epitaxial thin films of PbTe is to gain a clearer insight into the mechanisms of gas uptake. Layout of the thesis is as follows.

In chapter 2, description of the vacuum system used to prepare thin films of PbTe will be given. Results of x-ray diffraction and transmission electron microscopy studies will also be presented. Chapter 3 deals with the Hall measurements and the discussion of temperature dependence of the Hall mobility.

Chapters 4 and 5 are the major chapters of the thesis and these deal with the gaseous ambient experiments. Results are discussed in terms of two theoretical models - surface adsorption model and the diffusion model. Critical examination and extension of these models will be presented in chapter 4. Results of kinetic studies will be presented and discussed in chapter 5. In chapter 6, main conclusions reached during the present study will be given together with some suggestions for future work.

CHAPTER 2

FILM PREPARATION

2.1 INTRODUCTION

A single source evaporation technique was used to produce thin films of lead telluride (E1,B2,H1). Details of the vacuum system employed to produce these films will be described in this chapter. Results of x-ray diffraction and electron microscopy studies will also be presented.

2.2 VACUUM SYSTEM

A glass chamber (12" in diameter, 12" in height) was evacuated by a water-cooled oil diffusion pump. The diffusion pump (6" in diameter and filled with silicone MS 704 oil) was backed by a mechanical rotary pump. A liquid nitrogen trap was inserted in between the diffusion pump and the high vacuum valve (baffle valve) to prevent back streaming of the diffusion pump oil and to reduce the partial pressure of condensible gases. The top end of the glass chamber was sealed by a Viton gasket with a top plate. Similarly, a base plate sealed the lower end of the chamber. Electrical leadthroughs were passed through both plates for supplying current to various heaters. A schematic diagram of the evaporation chamber is shown in Fig. 2.1.

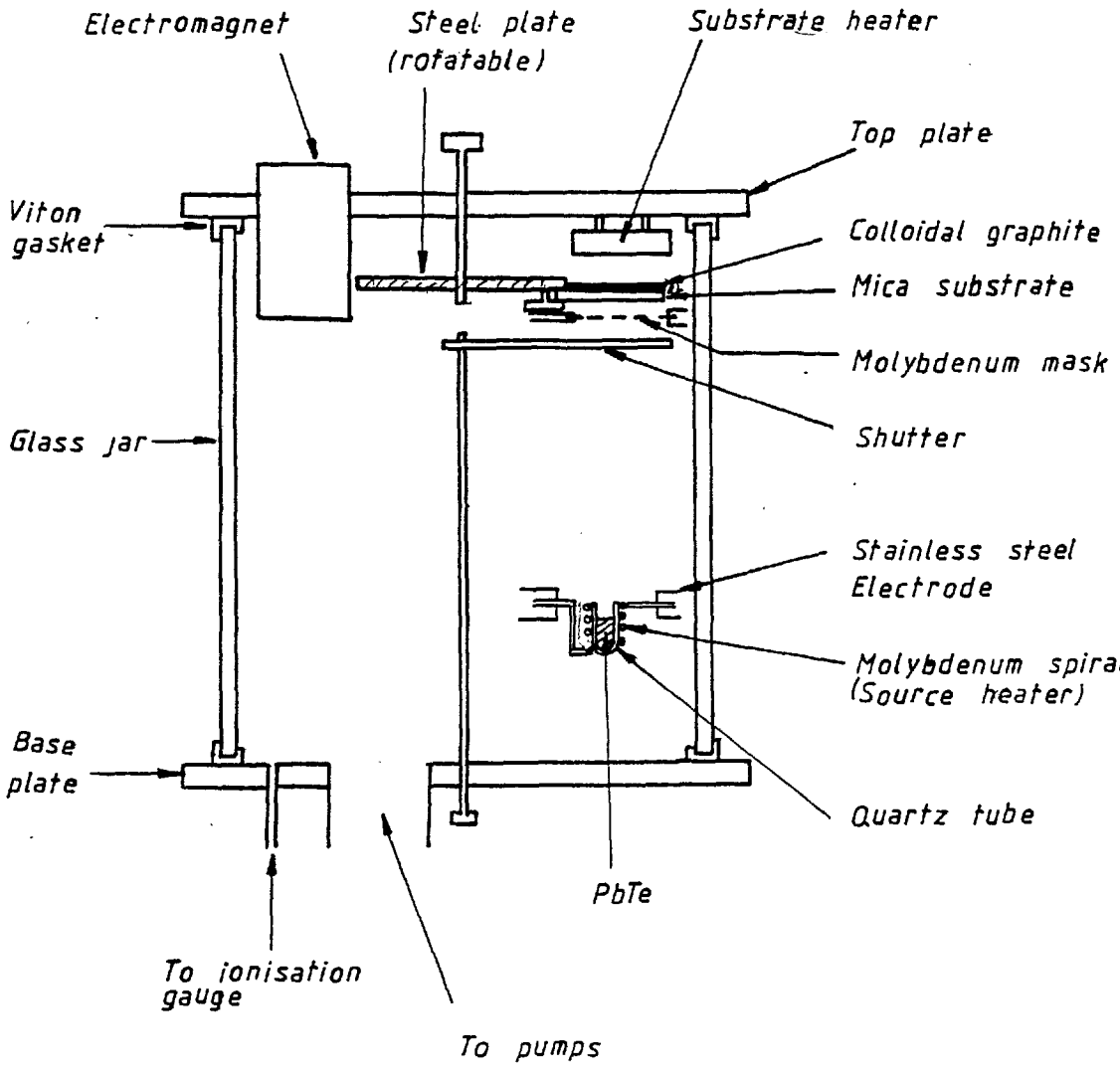

Fig. 2.1 Evaporation Chamber (Schematic)

The top plate consisted of two stainless steel plates where one of the plates could be rotated. A molybdenum mask was used to evaporate the films in standard Hall shape and the pressure contacts were mounted on the fixed plate whereas the substrate was mounted on the rotable plate. The electromagnet and the substrate heater were fixed to the top plate. Fig. 2.2 shows the top plate assembly. The substrate heater consisted of a 5 thou. molybdenum wire threaded through alumina tubes to ensure uniform heating. A double radiation shield of molybdenum sheet was used to prevent upward radiation. The substrate heater was clamped to the top plate so that it was 1 cm above the substrate. The evaporation mask was clamped 5 mm below the substrate. Once the film was deposited, it was allowed to cool down to room temperature and then the film was rotated so that it was situated in between the poles of the electromagnet where pressure contacts to the film were made. In this way, it was possible to carry out the Hall measurements without breaking the vacuum seal.

The source material was contained in a small quartz tube sealed at one end. The tube was 3 cm in length and its outside diameter was 6 mm. It was heated by passing current through a molybdenum wire wound in a spiral around the entire length of the tube. The distance from top of the source assembly to substrate was about 12 cm. Typically, 10-11 amps were passed through the source heater to deposit the film.

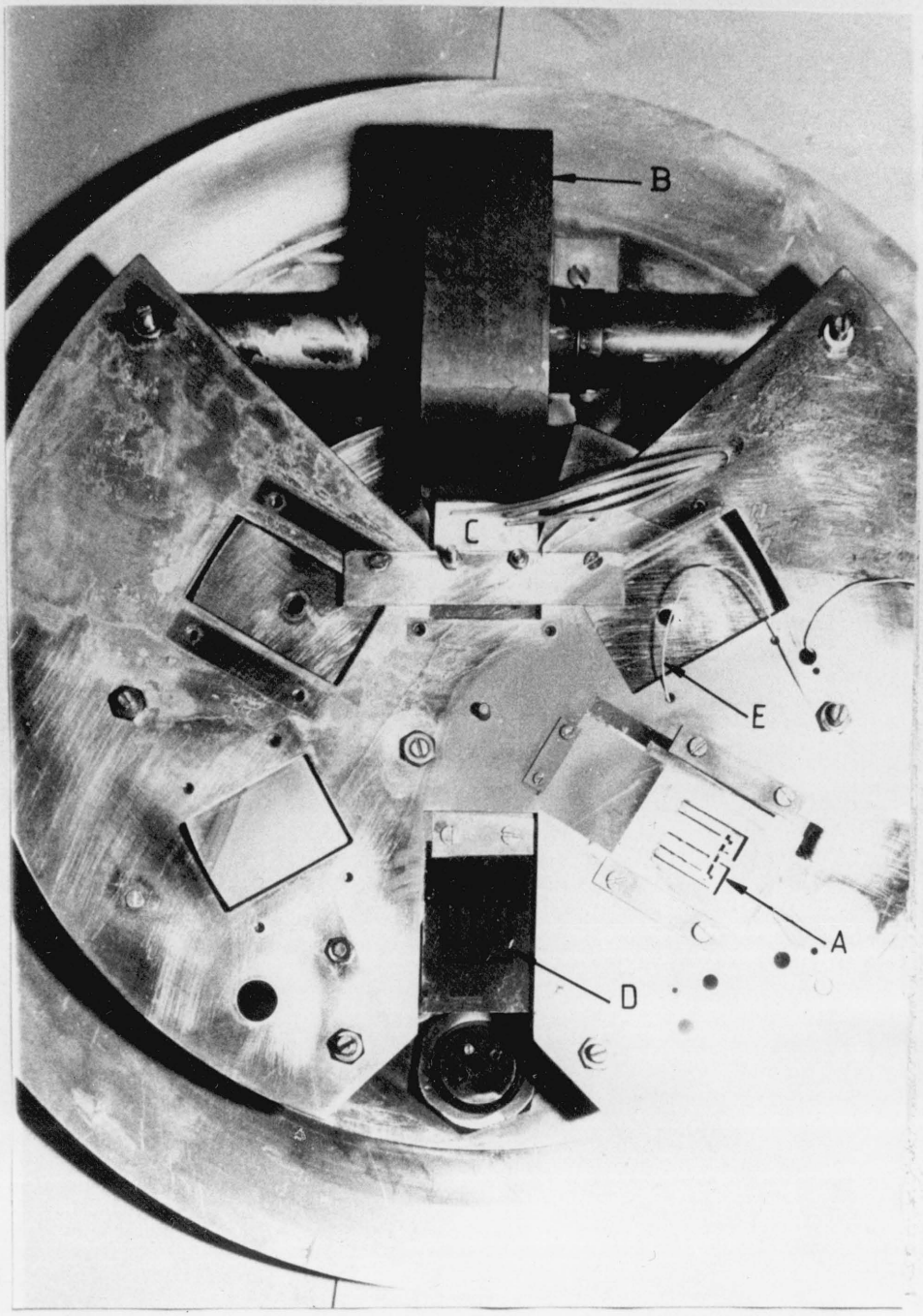

Key

A	Film Mask
B	Electromagnet
C	Pressure Contacts
D	PbTe Film
E	Thermocouple

Fig. 2.2 Top Plate Assembly

To atomise hydrogen for gaseous ambient experiments (chapters 4 and 5), a tungsten filament (8 thou. in diameter) was also incorporated into the vacuum chamber - where the stainless steel electrodes for this heater and the source heater were passed through the base plate. Flexible stainless steel tubing was used to conduct hydrogen gas into the vacuum system where its flow was controlled by a needle leak valve. A separate needle leak valve was used to control the flow of air into the system. Pressure inside the vacuum chamber was measured by a Mullard 10G12 ion gauge.

2.3 EVAPORATION PROCEDURE

Prior to each evaporation, the source tube was etched in concentrated HNO_3 for about one hour and then thoroughly rinsed with distilled water. If the remains of the previous evaporation still persisted, the tube was heated in vacuum until all such remains sublimed. A fresh change of about 400 mgm of crushed source material was placed in the quartz tube. The source material was p-type† single crystal PbTe*. Mass spectrometric analysis (excluding Be, Li, He, D, H) carried out by Analytical Services Laboratory of Imperial College showed that the following impurities were present.

---

*The author is indebted to Dr. Mino Green for supplying the source material.

† $\rho = 6 m\Omega.cm$, Seebeck coefficient at room temp. $= 286 \mu V^{\circ}C^{-1}$.

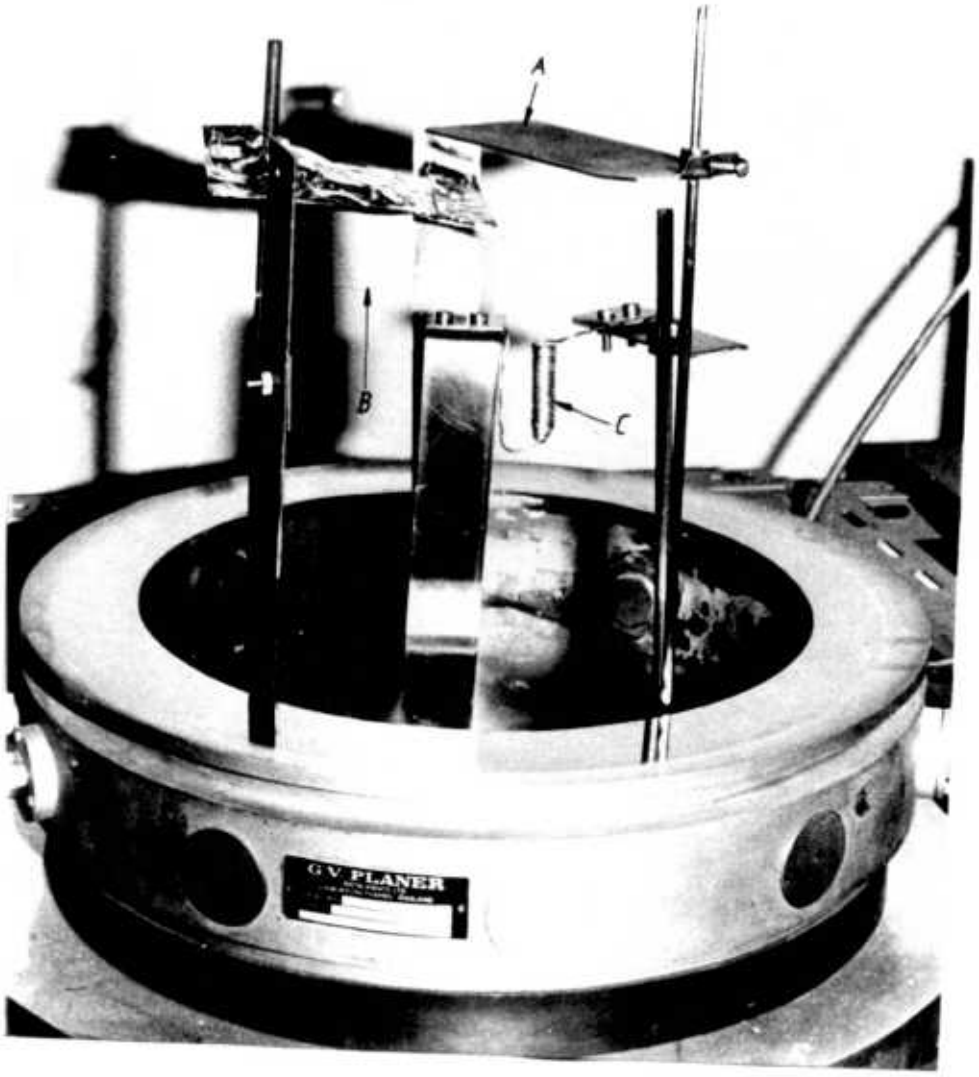

Key

C Source Heater

B Filament For Atomizing Hydrogen

A Shutter

Fig. 2.3

Element	Quantity (ppm wt. for wt.
Au,K,C ,Si, Na	< 1
Fe	1.1
Ca	1.6

Muscovite mica was used as substrate for most of the films because it was a large area single crystal substrate, atomically flat, electrically insulating and chemically inert (G1). Furthermore, it was readily available. One face of mica substrate was coated with colloidal graphite to maximise the absorption of radiation from the substrate heater (B2, P3). The substrate ($1\frac{3}{4}$" x 1) was then cleaved to about 2 thou. thickness and mounted in the top plate with the freshly cleaved face facing the source heater. The glass chamber was evacuated and when the system was left pumping over night, the pressure inside the chamber was $\sim 1 \times 10^{-6}$ torr. The substrate heater was switched on to heat the substrate up to 275°C for one hour before cooling it down to the temperature of film deposition. When the substrate temperature had stabilised, liquid nitrogen was poured into the trap and the system was left pumping for a further 90 minutes. Leaving air-cleaved mica at 200°C in vacuum of $\sim 2 \times 10^{-6}$ torr has been suggested by Ota (O1) as an effective method of cleaning the substrate.

In a separate experiment, the substrate heater was calibrated by embedding an iron-constantan thermocouple in colliidal graphite on the front face (i.e. on the face where PbTe film was to be deposited) of mica. The calibration curve shown in Fig. 2.4 was used to determine the substrate temperature. The films were deposited in the temperature range 150-250°C. When a working pressure of $\sim 1 \times 10^{-6}$ torr was reached, the source heater was switched on making sure that the shutter was covering the substrate. The source tube heated up slowly to typically 700°C and more volatile impurities were sublimed for about 1 minute while the shutter was still masking the substrate. The shutter was then removed and the film was deposited. A typical evaporation run lasted for 15 minutes. The ionisation gauge was kept 'off' during the evaporation run and used sparingly throughout the pump down to prevent production of unwanted atomic hydrogen (see chapter 4). Periodically, all nuts, screws and electrodes inside the vacuum chamber were scrubbed clean, washed in distilled water, washed in dilute HNO_3 and finally rinsed in distilled water.

2.4 FILM THICKNESS MEASUREMENT

The thickness of the film was measured by multiple beam interference method (B12).A sodium lamp was used as a source of monochromatic light ($\lambda/2 = 2946\text{Å}$). A thin film of Aℓ or Ag was evaporated onto PbTe film at room temperature (in a different vacuum system) to obtain a

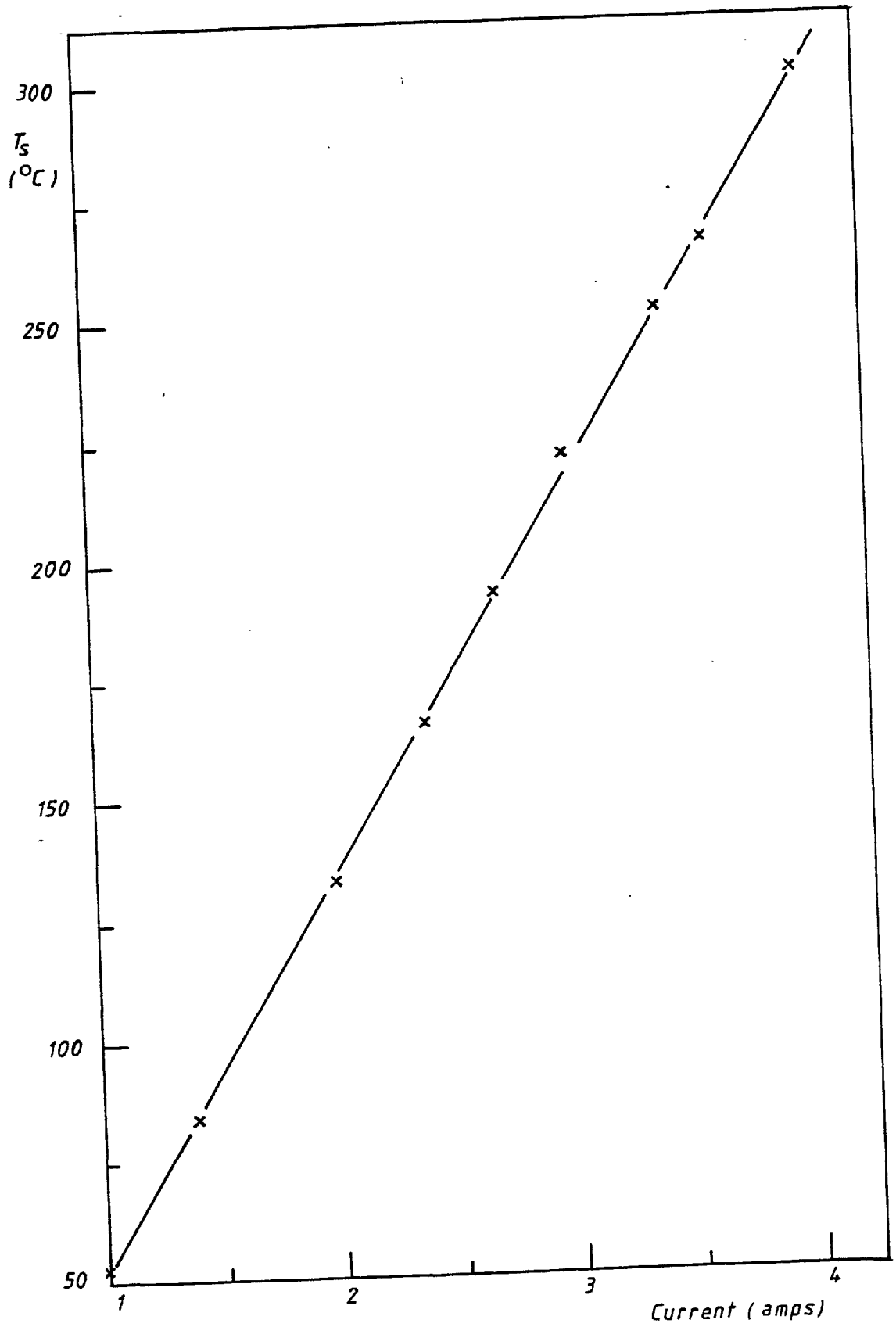

Fig. 2.4 Substrate heater calibration

highly reflective surface. The film surface was pressed against the Fizean plate and by adjusting the contact between the plate and film, interference fringes were produced at right angles to the step. By measuring the fringe spacing,s and the fringe offset, d, the thickness of the film can be calculated as follows (B12),

$$t = \frac{\lambda}{2} \frac{d}{s} \qquad (2.1)$$

where t is the thickness of the film. Values of d and s for several fringes were usually recorded and an average value of t was obtained.* The value of t ranged from 2000-4000Å for films used in the Hall measurements and the gaseous ambient experiments.

2.5 X-RAY DIFFRACTION

Two different x-ray diffraction techniques were used to investigate the source material and the thin films grown from it. Using the Debye-Scherrer powder method (C4), the source material was examined and the cylinderical texture camera (W1) was used to examine the thin films. In both cases, Ni-fitted CuKα raidation was used. Fig. 2.6 shows the photograph of x-ray diffraction pattern of the source material using the Debye-Scherrer method. Following the method of Azaroff and Buerger (A4), interplanar spacings were determined and the lines were indexed. Similarly, the

---

* *to an accuracy of ± 200 Å*

method described by Wallace and Ward (W1) was used to determine the interplanar distances in the case of the x-ray diffraction pattern of the thin film of PbTe grown on a microscope glass slide at 200°C. The indexed pattern is shown in Fig. 2.7. The interplanar spacings determined by the Debye-Scherrer powder method and the cylinderical texture camera agreed closely with those given by A.S.T.M. Using the method of least squares (C4), the corrected value of the lattice constant, a_o was determined for the source material. This value was 6.54Å (2 dec. places) compared with 6.50Å given by Ravich et al (R1) and 6.46Å given by Scanlon (S1).

2.6 TRANSMISSION ELECTRON MICROSCOPY

The films were grown on air-cleaved muscovite mica to an expected thickness of 600Å. Layer of colloidal graphite was floated off by immersing the film gently in distilled water. Several methods were tried to detach the film from mica. When the film was immersed in HNO_3, it dissolved either much too quickly or much too slowly depending on the concentration of the acid. Exposure to HF vapour failed to detach the film from mica substrate as well, whereas Band (B2) used this method successively for his films of $Pb_xSn_{1-x}Te$ grown on mica. Stripping the film off mica using sellotape was also tried, but invariably a thin layer of mica was also peeled off with the film. Diluted HF was used to remove the film from the mica. HF was

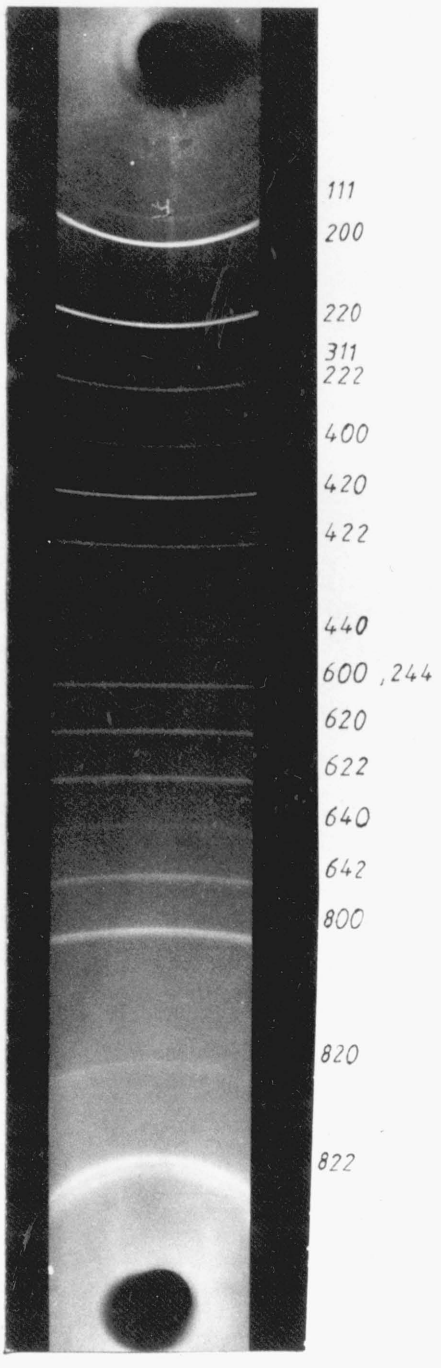

Fig. 2.6 Xray Diffraction Pattern, PbTe (Source Material)

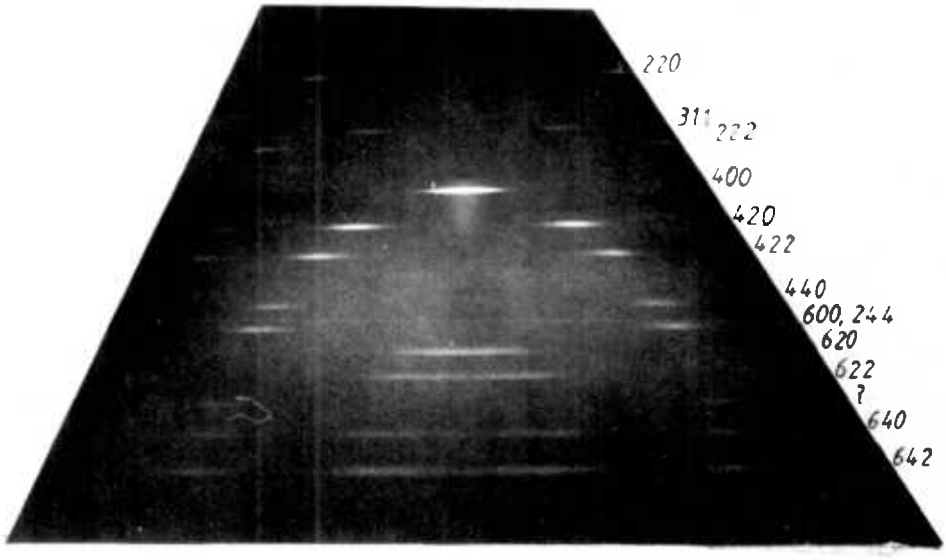

Fig. 2.7 X-ray Diffraction Pattern

PbTe Thin Film On Glass Substrate

diluted to 40% by volume with distilled water. The film was first immersed in HF acid for about 20 minutes and then vigorously shaken in a bath of distilled water. Consequently, the film floated off the mica. Copper grids were used to mount the films and the films were then examined using JEM 100B, a 100 kV transmission electron microscope.

Shown in Fig. 2.8 and Fig. 2.9 are the micrographs considered to be respresentative of this study. These micrographs illustrate some of the common features of structure of a continuous film of PbTe on mica. Fig. 2.8 shows the selected area diffraction pattern and Fig. 2.9 shows the microstructure of a film grown on mica at 225^{o}C. The spot pattern has a six-fold symmetry showing that the deposited material has (111) planes parallel to the substrate surface (E3). In a discontinuous film, triangular nuclei (equilateral) in two orientations are randomly distributed (G1). Coalescence of oppositely oriented triangular nuclei gives rise to double positioning boundaries where the latter become rounded and move out of the $(11\bar{2})$ planes during the film growth (S6). Therefore, a continuous film has a maze-like structure where the like oriented nuclei are bounded in a domain. As the substrate temperature was raised, the domains became larger and the triangular nuclei also grew in size as previously reported (P3, P4).

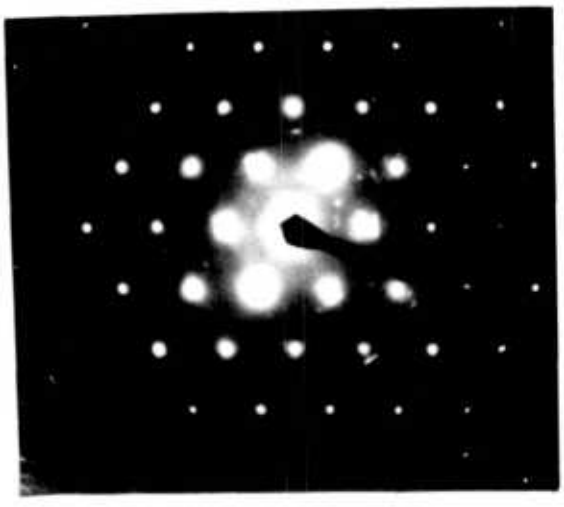

Fig. 2.8 Selected Area Pattern

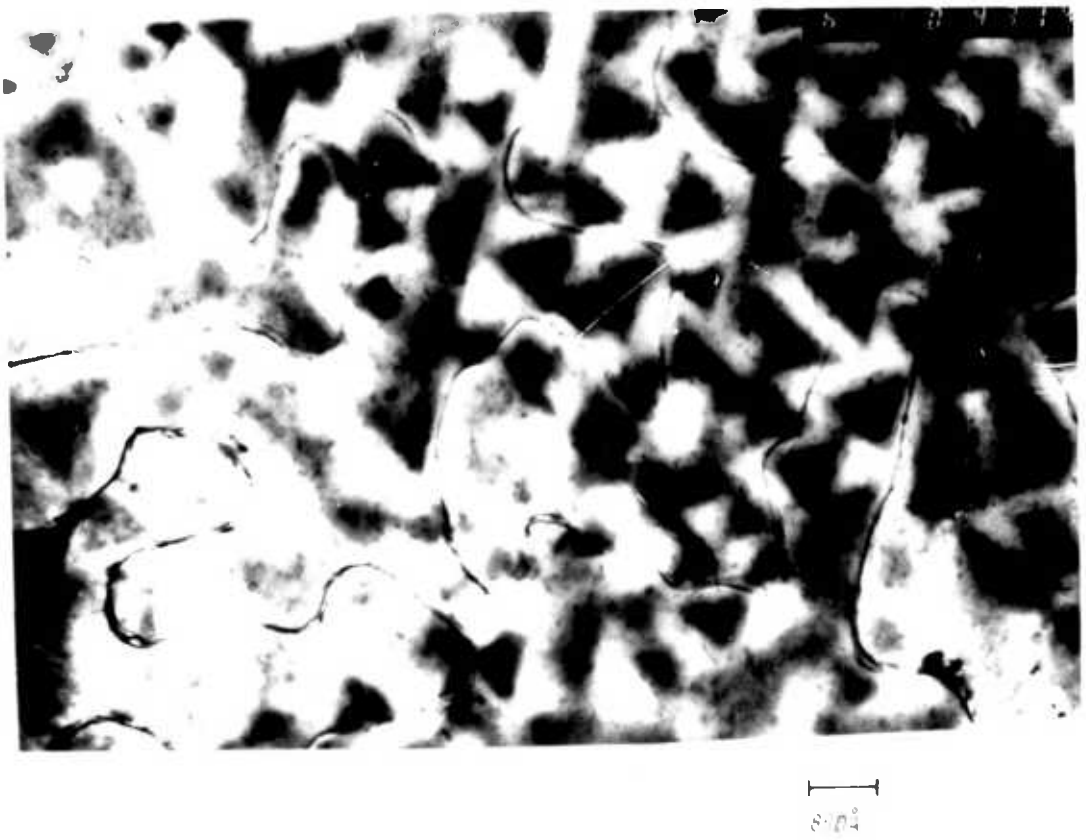

Fig. 2.9 Microstructure Of PbTe On Mica.

CHAPTER 3

HALL EFFECT MEASUREMENTS

3.1 INTRODUCTION

In this chapter, the Hall effect measurements carried out under two different situations are described. In one case, the Hall measurements as a function of temperature were performed for air exposed films. In the second case in situ Hall effect measurements (without breaking the vacuum seal) were carried out at a constant temperature (usually room temperature) as the films were exposed to atomic hydrogen and oxygen. Discussion of results pertaining to the first case will be presented in this chapter, whereas the results for the second case will be discussed in chapters 4 and 5.

3.2 SIMPLE THEORY OF THE HALL EFFECT

Suppose in a p-type semiconductor, current density J_x is produced by the application of an electric field E_x in x-direction and a magnetic field of flux density, B_z is applied in the z-direction. The magnitude of the Lorentz force experienced by holes will be (A5),

$$F_L = ev_{Dx}B_z \qquad (3.1)$$

where v_{Dx} is the average drift velocity. This will create an excess of holes at one face of the semiconductor

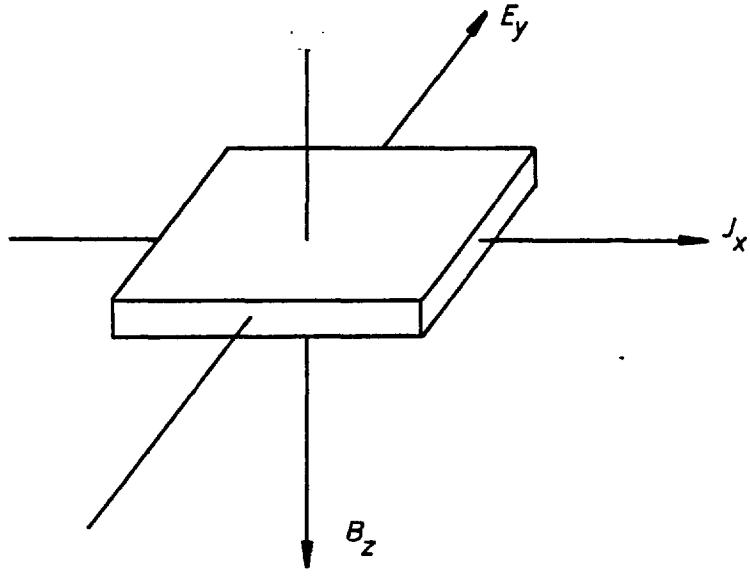

Fig. 3.1 The Hall Effect

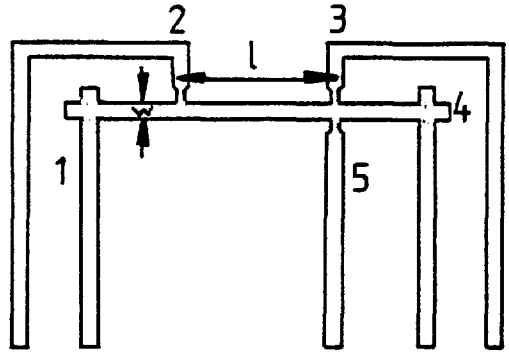

Fig. 3.2 Film Mask

and a deficiency of holes at the opposite face giving rise to a transverse electric field, E_y. In equilibrium, force produced by E_y on holes will balance the Lorentz force.

$$eE_y = ev_{Dx}B_z \tag{3.2}$$

or

$$\frac{E_y}{B_z J_x} = \frac{1}{pe} \tag{3.3}$$

where $J_x = ev_{Dx}p$ and the Hall coefficient R_H is defined by (A5),

$$R_H = \frac{E_y}{B_z J_x} \tag{3.4}$$

When in a semiconductor conduction is due to both electrons and holes, R_H is generally given by (P5),

$$R_H = \frac{R_e\sigma_e^2 + R_h\sigma_h^2 + B^2R_eR_h\sigma_e^2\sigma_h^2\,(R_e + R_h)}{(\sigma_e + \sigma_h)^2 + B^2\sigma_e^2\sigma_h^2\,(R_e + R_h)^2} \tag{3.5}$$

where R_e, σ_e, R_h and σ_h are the Hall coefficient and conductivity of electrons and holes respectively. In the case of low magnetic fields ($\mu B << 1$), equation (3.5) simplifies to the following,

$$R_H = \frac{R_e\sigma_e^2 + R_h\sigma_h^2}{(\sigma_e + \sigma_h)^2} \tag{3.6}$$

Equation (3.6) may also be written in terms of μ_e and μ_h, the mobilities of electrons and holes respectively.

$$R_H = \frac{A_\tau A_K}{e} \left[\frac{p\mu_h^2 - n\mu_e^2}{(p\mu_h + n\mu_e)^2} \right] \qquad (3.7)$$

where p and n are the hole and the electron concentrations respectively and e is the electronic charge. A_K is a numerical factor related to the band structure of the semiconductor. For ellipsoidal constant energy surfaces, A_K is given by the following equation (R1, S7),

$$A_K = \frac{3K(K + 2)}{(2K + 1)^2} \qquad (3.8)$$

where $K = m_\ell/m_t$ is the mass anisotropy ratio (see chapter 1). For conduction band of PbTe, Cuff et al (C1) give $K = 10$ at 4^oK. From equation (3.8), $A_K \approx 0.82$ for $K = 10$.

A_τ is a statistical factor and is related to the relaxation time as follows (S7),

$$A_\tau = \frac{\langle\tau^2\rangle}{\langle\tau\rangle^2} \qquad (3.9)$$

where $\langle\tau\rangle$ is the relaxation time averaged over energy and is given by (R1, A7),

$$\langle\tau^\gamma\rangle = \frac{\int_o^\infty \tau^\gamma \frac{\partial f}{\partial \varepsilon} \varepsilon^{3/2} \, d\varepsilon}{\int_o^\infty \varepsilon^{3/2} \frac{\partial f}{\partial \varepsilon} \, d\varepsilon} \qquad (3.10)$$

where $f = {}^{1}/1 + \exp(\varepsilon-\varepsilon_F)$, is the Fermi-Dirac function, $\varepsilon = E/kT$ and $\varepsilon_F = E_F/kT$, k being Boltzmann's constant.

In the case of classical statistics, from equations (3.9) and (3.10) one obtains,

$$A_\tau = \frac{\Gamma(2r + 5/2)\ \Gamma(5/2)}{\Gamma^2\ (r + 5/2)} \tag{3.11}$$

where $\Gamma(x)$ is the gamma function defined by (S10),

$$\Gamma(x) = \int_o^\infty t^{x-1} e^{-t}\ dt \tag{3.12}$$

The parameter r in equation (3.11) depends on the scattering mechanism and represents the energy dependence of the relaxation time. In the case of acoustical phonon scattering $r = -1/2$ (S7) and from equation (3.11), $A_\tau = \frac{3\pi}{8}$. For a degenerate semiconductor $A_\tau = 1$ (R1). A detailed discussion of scattering mechanisms for non-parabolic energy bands and arbitrary magnetic fields and degeneracy has been given by Harman et al (H8) and Ravich et al (R4).

When $p >> n$, equation (3.7) simplifies further to the following,

$$R_H = \frac{A_\tau A_K}{ep} \tag{3.13}$$

Similarly, for $n >> p$, $R_H = -\frac{A_K A_\tau}{en}$ (3.14)

Under these conditions, corresponding expressions for conductivity become,

$$\sigma_h = ep\mu_h \tag{3.15}$$

and

$$\sigma_e = ne\mu_e \tag{3.16}$$

The Hall mobility μ_H is given by $|R_H|\sigma$. In the present calculations $A_K A_\tau$ has been assumed to be unity. This gives,

$$\mu_H = \mu_e \quad \text{for} \quad n >> p \tag{3.17}$$

and

$$\mu_H = \mu_h \quad \text{for} \quad p >> n \tag{3.18}$$

In terms of experimental quantities, R_H and ρ are given by the following equations,

$$R_H = \frac{V_H t}{BI} \tag{3.19}$$

and

$$\rho = \sigma^{-1} = \frac{V_c tw}{\ell I} \tag{3.20}$$

where V_H is the Hall voltage between contacts 3 and 5 (see Fig. 3.2), V_c is the conductivity voltage between contacts 2 and 3, ℓ, w and t are the length, width and thickness of the sample respectively.

3.3 EXPERIMENTAL PROCEDURE

The mask shown in Fig. 3.2 was used to deposit films in a Hall shape and a standard d.c. technique was used to carry out the Hall effect measurements. The width, w and the length, ℓ of the film were measured using a travelling microscope.

In the case of in situ Hall measurements (i.e. gaseous ambient experiments described in chapter 4), current of typically 300 μA was passed through contacts 1 and 4 (Fig. 3.2) where actual current passing through the sample was determined by measuring the voltage drop across a standard 100Ω resistor connected in series with the sample. The electromagnet was energised by a d.c. power supply unit. The magnetic field was measured by the Hall probe fluxmeter and the fluxmeter was also used to test the uniformity of the field. Using a switch-box, it was possible to change the direction of current flow and magnetic field. The Hall voltage, V_H between contacts 3 and 5 was determined from four readings

	Field	
Current	+B	-B
+I	V_{35}^{++}	V_{35}^{+-}
-I	V_{35}^{-+}	V_{35}^{--}

$$V_H = \frac{1}{4}\left[V_{35}^{++} - V_{35}^{+-} + V_{35}^{-+} - V_{35}^{--}\right] \qquad (3.21)$$

Conductivity voltage V_c between contacts 2 and 3 is given by,

$$V_c = \frac{1}{2}\left[V_{23}^{+} + V_{23}^{-}\right]^{*} \qquad (3.22)$$

where V_{23}^{+} is the value for positive current, i.e. current flowing from contacts 1 to 4.

In the case of the Hall measurements as a function of temperature, the film was removed from the vacuum chamber and mounted in a sample holder shown in Fig. 3.3. Indium, electrodag 915 high conductivity silver paste and an evaporated thin film of gold, were used to make ohmic contacts to the film. All three gave satisfactory results. The sample holder was enclosed in a tight fitting copper can and placed inside a dewar flask. The dewar was then placed between the poles of a permanent magnet of 0.148 T field strength. The circuit used to do the Hall measurements is shown in Fig. 3.4. The sample was rotated through 360° and maximum and minimum values of V_H were recorded. The direction of the current flow was reversed and the sample was rotated through 360° and minimum and maximum values of V_H were recorded again. The two readings were averaged to obtain V_H. V_c was determined from equation (3.22). The sample was cooled to 77°K using liquid nitrogen and when the temperature had stabilised at 77°K, liquid N_2 was poured out. This allowed the film to warm up slowly to room temperature (300°K)

---

* $|V_{23}^{+}|, |V_{23}^{-}|$ were almost identical

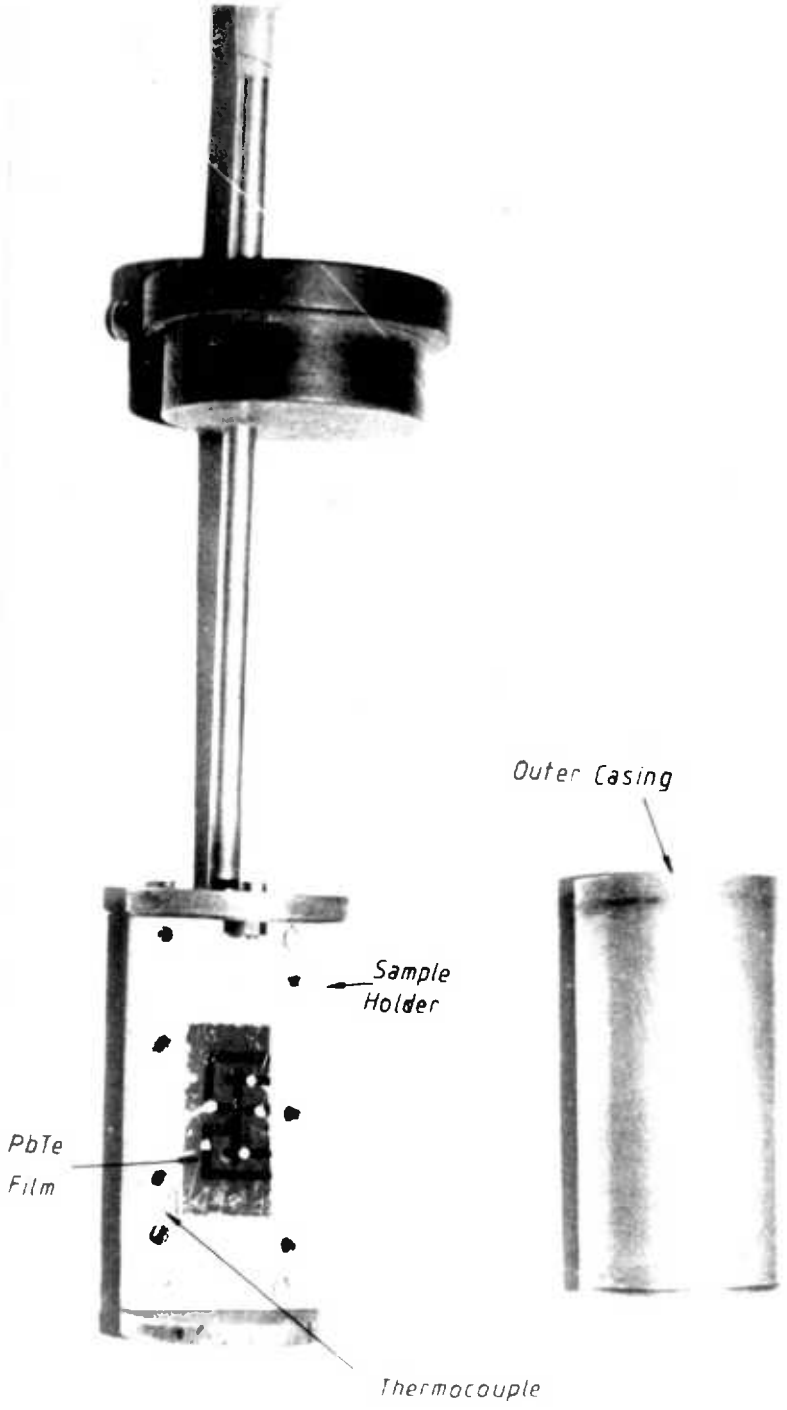

Fig. 3.3

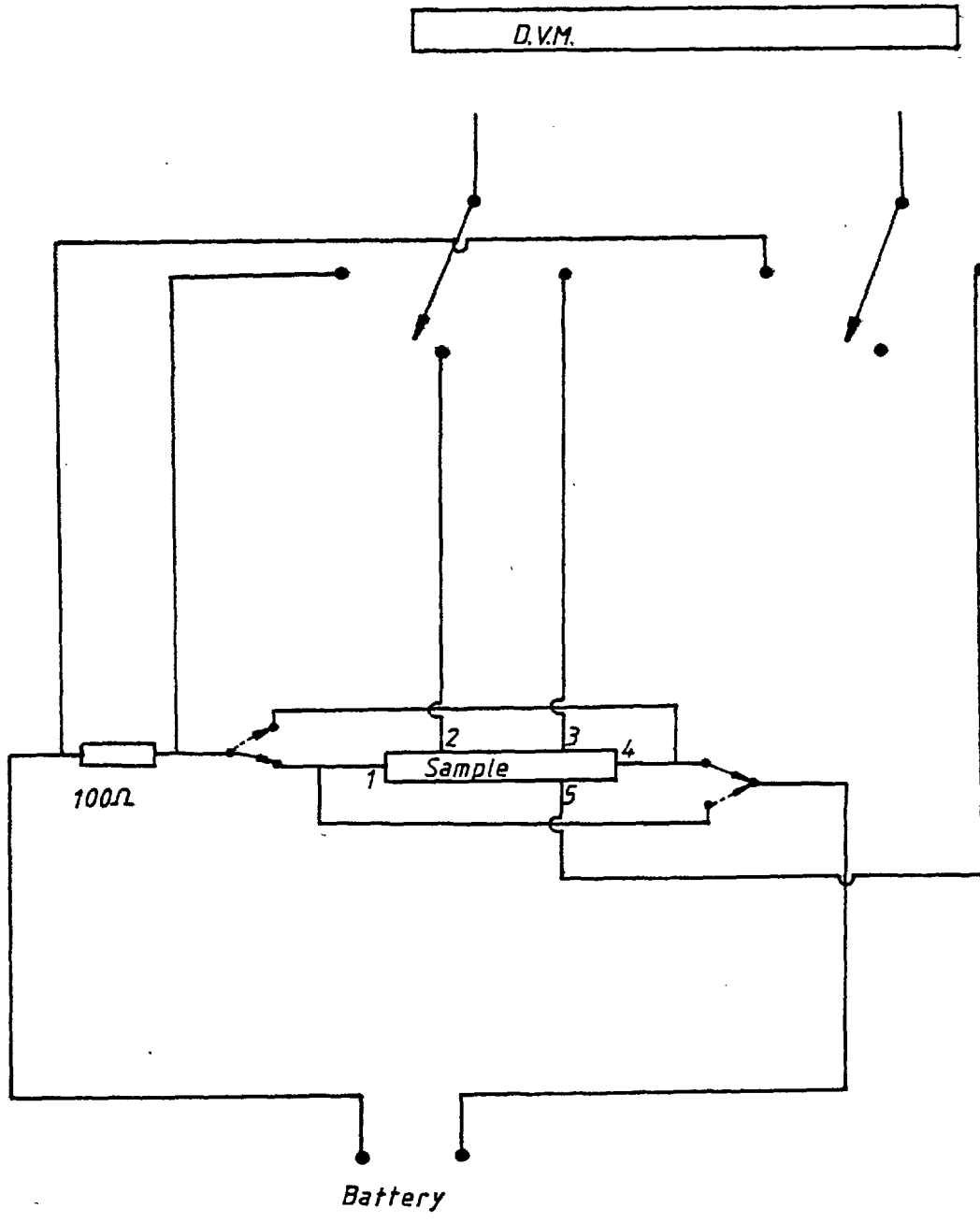

Fig.3.4 Circuit diagram for the Hall measurements

and the Hall measurements were performed. The temperature of the film was monitored by iron-constantan thermocouple placed near the film inside the sample holder. A Solartron LM1420 digital voltmeter which had input impedance of $10^9\Omega$ was used to measure all the voltages.

3.4 RESULTS AND DISCUSSION

The Hall measurements were carried out on eighteen films. Results of four representative films will now be presented. All these films were n-type and grown on mica.

3.4.1 Hall Coefficient, R_H Versus Temperature

Fig. 3.5 shows the temperature dependence of R_H of films S10, S14, S17 and S66. As it may be noted from the figure, R_H has a weak temperature dependence and $|R_H|$ decreases as temperature increases, especially around room temperature. This is in common with other workers (K3, M3, L2, P6) for films grown on mica and NaCℓ. A change of $\sim$18% in R_H may be explained in terms of changing carrier statistics from degenerate to classical when A_τ changes from 1 to $3\pi/8$.

3.4.2 Hall Mobility, μ_H Versus Temperature

Dependence of $\mu_H = R_H/\rho$ on temperature is shown in Fig. 3.6. Also shown in the figure is $\mu \propto T^{-2.5}$ dependence. The following points are worth noting.

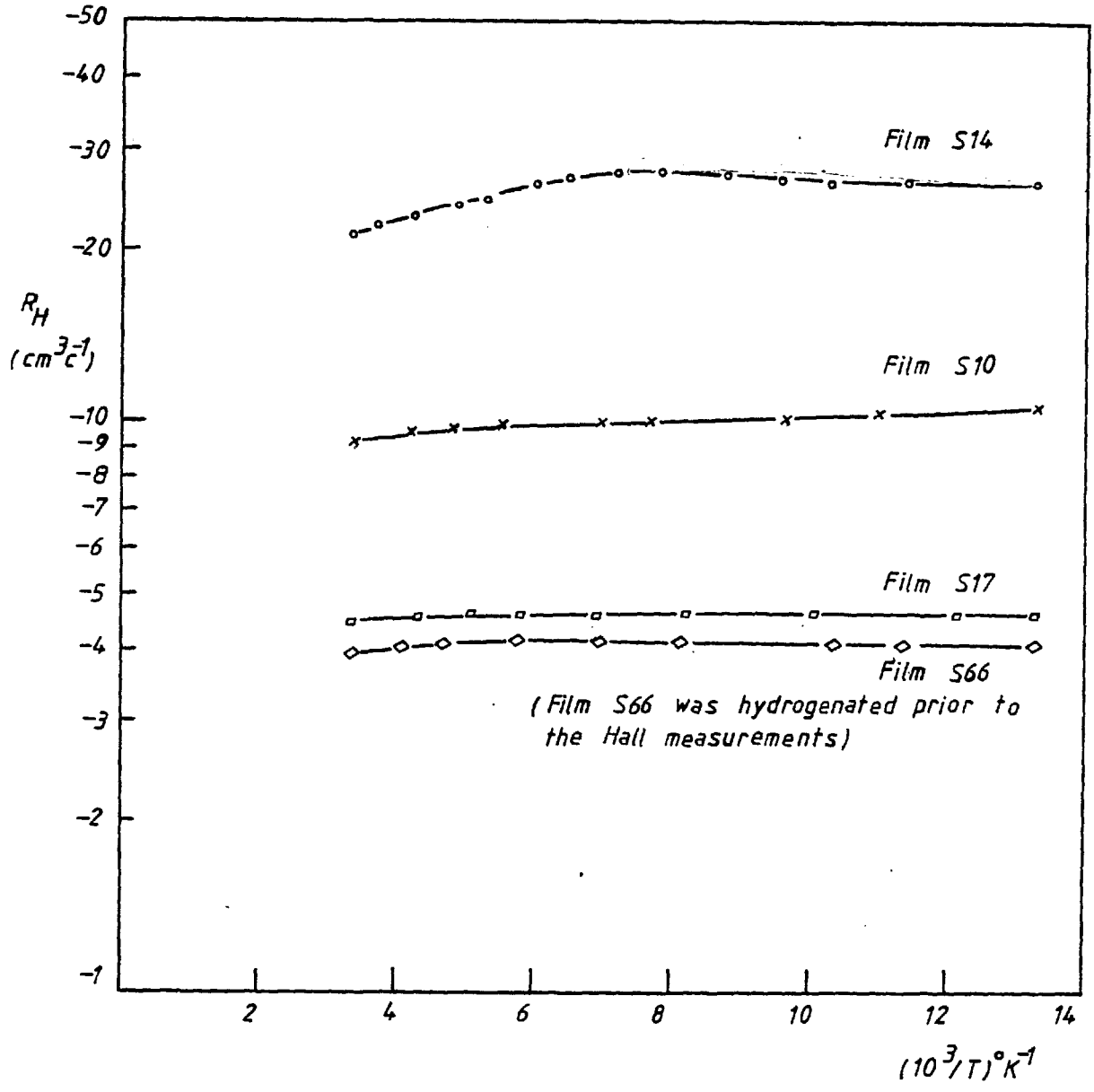

Fig 3.5 R_H versus Temperature

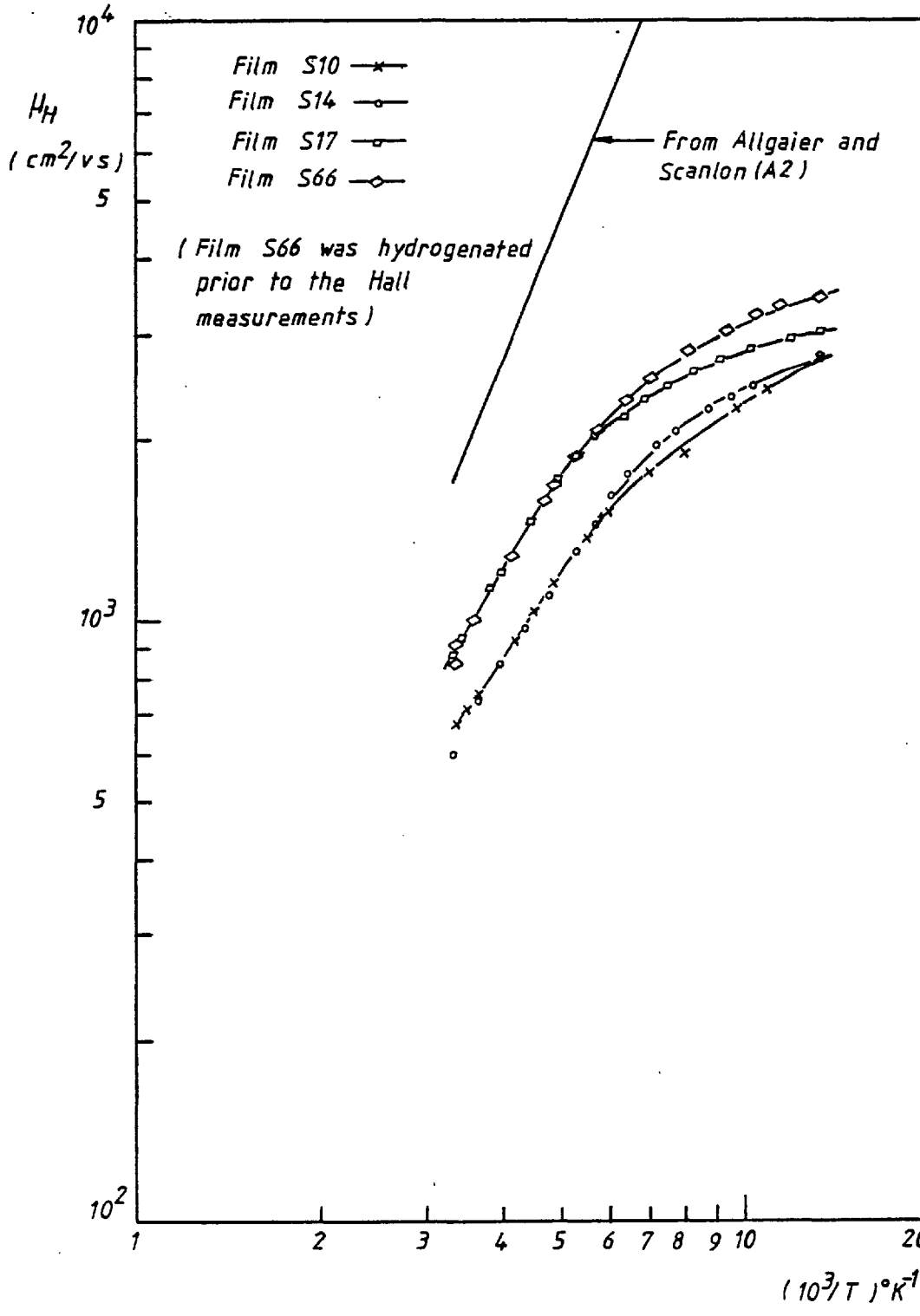

Fig.3.6 μ_H versus Temperature

(i) μ_H increases with decreasing temperature and the rate of increase tends to level off as liquid N_2 temperature is approached. This was particularly true for films with high carrier concentration (X 10^{18} cm^{-3}). This is in common with other workers (K3,G2).

(ii) The temperature dependence of μ_H is weaker than $T^{-2.5}$ dependence observed for good single crystal PbTe and epitaxial films of PbTe grown on BaF_2 and NaCℓ (L2, A2, P1, Z1) where workers in the past have invoked temperature dependence of effective mass in addition to acoustic phonon scattering to account for experimentally observed $T^{-2.5}$ dependence.

In Table 3.1, a summary of Hall measurements of these films is given. Value of s in $\mu_H \alpha T^{-s}$ ranged from 1.4 to 1.8 in temperature range 200-300°K for all the films.

In order to assess the contribution of individual scattering mechanisms in case of strong degeneracy (B11, G2), use of Matthiessen's rule can be made, i.e.

Sample	Deposition Temp. (^{o}C)	Film Thickness ($\mathring{A}$)	Evap. rate ($\mathring{A}$ s^{-1})	'Virgin' μ_H at 300^{o}K ($cm^2 v^{-1} s^{-1}$)	μ_H at 300^{o}K ($cm^2 v^{-1} s^{-1}$)	μ_H at 77^{o}K ($cm^2 v^{-1} s^{-1}$)	s in $\mu \alpha T^{-s}$ in temp. range $\sim$200-300^{o}K	$n_{300^{o}K}$ (cm^{-3})	$n_{77^{o}K}$ (cm^{-3})
S10	175	2900	4.9	882	678	2798	1.45	6.72×10^{17}	6.19×10^{17}
S14	200	4000	3.1	978	591	2792	1.45	2.93×10^{17}	2.39×10^{17}
S17	150	3400	3.5	843	883	3016	1.75	1.4×10^{18}	1.36×10^{18}
S66*	150	3400	2.8	820	845	3483	1.75	1.6×10^{18}	1.55×10^{18}

*S66 was H sat. before Hall measurements

Table 3.1

$$\frac{1}{\mu_H} = \frac{1}{\mu_L} + \frac{1}{\mu_s} + \frac{1}{\mu_d} \qquad (3.23)$$

where μ_H is experimentally determined Hall mobility (assumed equal to μ_e), μ_L is mobility limited by lattice scattering, μ_s is mobility due to surface scattering and μ_d is the defect-scattering mobility. Scattering of carriers due to ionised impurities in the temperature range 77-300°K has been considered to be insignificant in PbTe (C9,P1). It is also assumed in equation (3.23) that the above mentioned scattering mechanisms are operating independently of each other. Equation (3.23) was used to evaluate the contribution due to defect scattering for film S17. Assuming completely diffused surface scattering and flat band conditions (J5, M4),

$$\frac{1}{\mu_H} = \frac{1}{\mu_b}\left(1 + \frac{\lambda}{d}\right) \qquad (3.24)$$

where λ is the mean free path of the carriers, 2d is the film thickness and μ_b is the mobility due to all other scattering processes except surface scattering.

$$\therefore \quad \mu_b^{-1} = \mu_L^{-1} + \mu_d^{-1} \qquad (3.25)$$

From equations (3.23), (3.24) and (3.25),

$$\frac{1}{\mu_s} = \left(\frac{\lambda}{\lambda+d}\right)\frac{1}{\mu_H} \qquad (3.26)$$

For degenerate electron gas, λ is given by (O2, R5),

$$\lambda = \frac{\mu_H h}{e} \left(\frac{3n}{8\pi}\right)^{1/3} \qquad (3.27)$$

where h is Plank's constant, n is the carrier concentration and e is the electronic charge. Since μ_H is known, μ_s can be determined from equations (3.26) and (3.27). μ_d can then be isolated as follows,

$$\frac{1}{\mu_d} = \frac{1}{\mu_H} - \left(\frac{1}{\mu_s} + \frac{1}{\mu_L}\right) \qquad (3.28)$$

By taking μ_L from Allgaier and Scanlon (A2), μ_d was determined from equation (3.28) since both μ_s and μ_H were known.

The result of the above analysis is shown in Fig. 3.7. As it can be seen from Fig. 3.7, μ_s has a weak temperature dependence whereas $\mu_d \alpha T^{-1.47}$ in the temperature range 200-300^{o}K. Before pursuing the analysis any further, the validity of the assumptions pertaining to μ_s must be questioned.

(i) It has been assumed in equation (3.24) that energy bands of the film remain flat right up to the surface. This is not necessarily true. Since oxygen (air) has an acceptor like effect on n-type PbTe films (see chapters 4

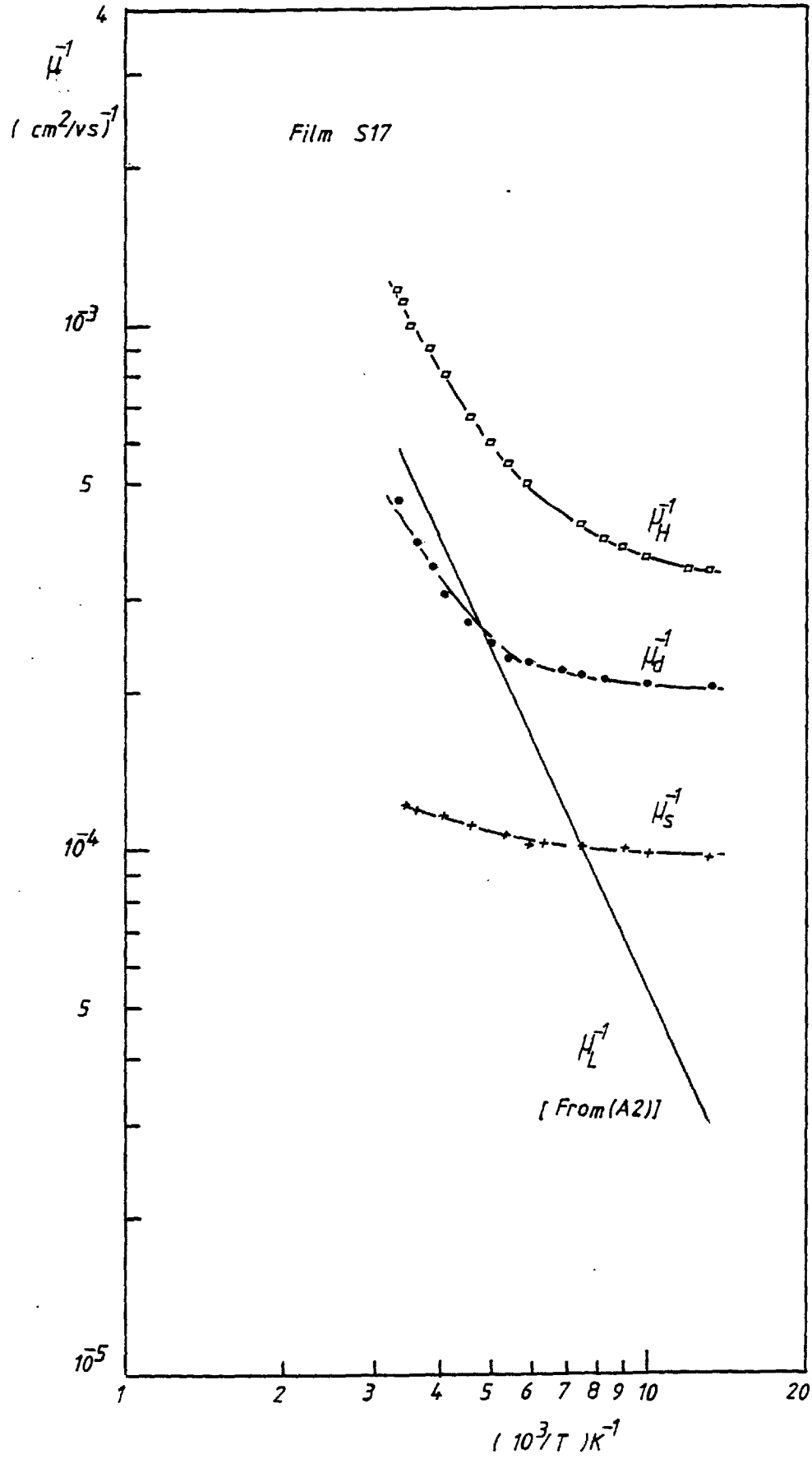

Fig.3.7 μ^{-1} vs. Temperature

and 5), it is possible that there might be some band bending due to, for instance, depletion of the n-type surface.

(ii) Completely diffused surface scattering has also been assumed whereas evidence in the literature (P6, B3) suggests that surface scattering in lead chalcogenides is specular.

In view of these assumptions, the above analysis may at best be described as approximate.

It is difficult to associate $\mu_d \alpha T^{-s}$ where $s = 1.47$ in the case of film S17 (and s ranged from 1.3-1.5 for films S10, S14 and S66) with defect scattering such as dislocation scattering and grain boundary scattering. Dexter and Seitz (D5) give the following temperature dependence of mobility due to unionised dislocations distributed uniformly within the semiconductor.

$$\mu_{dis} \alpha T^{-1} \tag{3.29}$$

Anderson (A6) gives the following expression for grain boundary limited mobility $\mu_{g.b}$,

$$\mu_{g.b} = e\ell \left(\frac{9\pi m_i kT}{8} \right)^{-\frac{1}{2}} \tag{3.30}$$

for classical statistics. For the degenerate case, the expression becomes,

$$\mu_{g.b} = \frac{e\ell}{\hbar} (3\pi^2 n)^{-1/3} \left(\frac{m_d}{m_i}\right)^{\frac{1}{2}} \qquad (3.31)$$

where ℓ is the mean free path*, m_d is the density of states effective mass, m_i is the inertial effective mass, k is Boltzmann's constant, T is the temperature and $\hbar = \frac{h}{2\pi}$, h being Plank's constant.

In the case of PbTe, equations (3.30) and (3.31) become (P6),

$$\mu_{g.b} \alpha T^{-0.7} \qquad (3.32)$$

and

$$\mu_{g.b} \alpha T^{o} \qquad (3.33)$$

Egerton (E1) examined the effect of surface, dislocation and grain boundary scattering on carrier mobility in epitaxial PbTe films. He proposed that the departure from bulk mobility values was due to an additional scattering mechanism. By comparing the theoretical value of ℓ (from equations (3.30) and (3.31) with experimentally determined average spacing, D between grain boundaries, Egerton put forward that carrier mobility in n-type PbTe films was limited by grain boundary scattering in addition to acoustical phonon scattering. Similar comparison was used by

---

* $\ell \approx D/2$

Parker and Williams (P6) for their n-type PbTe films grown on mica and by Myers et al (M3) for their PbTe films grown on NaCℓ, to propose that grain boundary scattering was limiting the carrier mobility.

But as mentioned earlier, the value of s in $\mu_d \alpha T^{-s}$ is incompatible with dislocation and grain boundary scattering in case of present films. Therefore, it seems reasonable to assume that the deviation from $\mu \alpha T^{-2.5}$ dependence in these films is attributable to some other scattering mechanism. For instance, Makino and Hoshina (M5) who carried out in situ Hall effect measurements on n-type PbTe films grown on mica suggested that deviation from $T^{-2.5}$ dependence was due to scattering of carriers by additional defects formed in the films because of the presence of residual oxygen. In the present case, n-type films are exposed to air prior to the Hall measurements. Therefore, the potential barriers introduced by oxygen at grain boundaries could act as scattering centres. In fact, Green and Miles (G3) have suggested that electrical transport behaviour of air-exposed n-type PbTe films is barrier dominated. Dawar et al (D4) also concluded that carrier mobility of their n-type PbTe films was potential barrier limited.

CHAPTER 4

GASEOUS EFFECTS

4.1 INTRODUCTION

It is now well established (G4,B3,M2,E1,E4) that the electrical properties of lead salts (PbS, PbSe, PbTe) can be greatly influenced by their interaction with oxygen and atomic hydrogen. For instance as-grown n-type film can be driven p-type by exposing it to oxygen and as-grown p-type film can be turned n-type by exposing it to atomic hydrogen. However, since the important application of these lead salts is in the manufacture of photoconductive infra-red detectors, early work on lead salts was concerned mainly with enhancing the photo-conductivity of these salts by oxygenation and mechanism of the gas uptake. Before describing the results of the present study, a brief review of the gaseous effects of lead chalcogenides will be given.

Bode and Levinstein (B1) observed that the resistance of the n-type PbTe film grown on glass substrate increased to a maximum when exposed to oxygen before decreasing again and when the oxygenated film was heated to 650^{o}K it returned to its original resistance. They proposed that oxygen, O_2, was adsorbed on the surface eventually rendering the surface p-type followed by the diffusion of O_2 via grain boundaries.

This turned parts of the bulk into p-type giving rise to a series of p-n junctions which were responsible for photovoltaic effects. Jones (J1,J2) investigated the reaction of O_2 with PbSe both in powder form and in thin film form. He observed that conductance of n-type film decreased when exposed to O_2. He also noted that when the oxidised sample was treated with carbon monoxide CO, carbon dioxide CO_2 was evolved. He suggested that O_2 diffuses into the bulk of PbSe to fill Se vacancies. Hillenbrand (H2,H3), studied the reaction of PbS with O_2 and proposed that the adsorbed O_2 exchanged with the lattice to replace S ions and formed PbO phase. The sulphur liberated from the lattice was partially oxidised to SO_2 and slowly desorbed.

Yasuoka et al (Y1) in their study of effects of O_2 on evaporated PbSe films on glass concluded that O_2 was chemisorbed on PbSe at room temperature and diffused into the bulk in the temperature range 100-150°C. Green and Lee (G4) observed that during interaction of O_2 with clean PbTe surfaces in the temperature range 195-303°K, apart from initial rapid reaction a single reaction was operative up to 0.7 monolayer coverage. They further proposed that an adsorption process was consistent with the formation of a peroxide surface complex.

The interaction of O_2 with films of lead salts grown on alkali halides was first studied by Brodsky and Zemel (B3). They noted that the effect of O_2 on epitaxic PbSe films grown on NaCℓ substrate was reversed by a gas generated by the hot filament of the ionisation gauge whereas other gases like N_2, He and Ar had no observable effect. They put forward the idea that an appreciable p-type surface layer existed due to exposure to O_2. However no kinetic studies were carried out to substantiate the proposal. Mclane and Zemel (M2) identified the gas generated by the action of hot filament of the ionisation gauge as atomic hydrogen H. They examined the kinetics of the gas uptake on epitaxial films of PbSe grown on NaCℓ substrate and found that O_2 uptake followed $\log_e t$ dependence whereas H uptake followed $t^{\frac{1}{2}}$ dependence.

Egerton et al (E1,E2) investigated the effect of O_2 on epitaxial films of PbS, PbSe and PbTe grown on mica substrate by performing in situ Hall effect measurements. They noted that N_2 and H_2 had no noticeable effect on electrical properties of PbTe and an effect of pure O_2 and air was identical. In order to explain the observed effect of O_2 on PbTe in terms of surface space charge layer, Egerton and Juhasz (E2) found that the surface band-bending in excess of the band gap was necessary and suggested that diffusion was the mechanism of gas uptake. Zemel and Kaplit (Z6) put forward a model based on the oxide with high defect density of ionised

oxygen. According to this model, oxide of about 20 Å in thickness could account for the surface space charge observed by Brodsky and Zemel (B3) and Egerton (E1). The effect of atomic hydrogen, H on PbTe films was investigated by Egerton and Crocker (E4). They noticed that the sheet conductance of n-type film increased with time when exposed to H and the Hall mobility remained constant. They concluded from the kinetics of the reaction that the mechanism for gas uptake was diffusion after the initial fast uptake due to surface adsorption.

Palatnik et al (P7) worked on the effect of O_2 on single crystal PbS films evaporated onto NaCℓ substrates. They came to the conclusion that an oxide layer was formed at the surface due to diffusion of lead ions from the bulk to the surface. This loss of cation charge from the bulk made the film less n-type and eventually drove it p-type. Galat et al (G5) measured the work function of PbSe (p-type), PbS (p-type) and PbTe (n-type) in the temperature range 100-350°C in oxygen and vacuum and established that oxygen increased the work function of PbSe and PbS and decreased the work function of PbTe. They concluded that initial chemisorption of oxygen at the surface was followed by the formation of heterophase layer where $PbSO_4$, $PbSeO_4$ and $PbTeO_4$ (lead sulphate, selenate, tellurate) were the reaction products. In his investigation of oxygen uptake on PbS films evaporated on NaCℓ substrate in ultra high vacuum, UHV, Lee (L5) carried

out the Hall measurements in situ and suggested a completely new mechanism for the gas uptake. Since the kinetics followed $\log_e t$ dependence, he suggested that O_2 was chemisorbed on the surface. He further suggested that the chemisorbed O_2 changed the surface stoichiometry and consequently changed the number of free carriers in the bulk of the semiconductor.

Parker and Williams (P8) also carried out in situ Hall effect measurements on PbTe films grown on mica substrate in UHV and concluded that there were two distinct mechanisms of O_2 uptake. During the initial stages of O_2 exposure, the gas reacted at the surface with excess interstitial Pb diffusing outside from the bulk to the surface, whereas during the later stages of the exposure, O_2 atoms were weakly bonded to the outside surface. Hagström and Fahlman (H4) and Sun et al. (S8) used the techniques of x-ray photoelectron spectroscopy (XPS) and ultraviolet photoelectron spectroscopy (UPS) to study the interaction of O_2 with epitaxial films of PbSe and PbTe respectively. Hagström and Fahlman (H4) noted that interaction of O_2 with PbSe was a very slow process with O_2 sticking coefficient of 10^{-10} - 10^{-11}. An oxide layer, a monolayer in thickness, was formed and the continued long exposure led to the diffusion of O_2 into the bulk. Sun et al. (S8) came to the conclusion that O_2 uptake on PbTe occurred in two stages. The first stage was fast and characteristic of the adsorption process and the second stage was characteristic of the oxidation

process where Te and Pb ions break their bonds in favour of affiliating with O_2.

In summary, it may be noted that the interaction of O_2 with lead salts (PbS, PbSe, PbTe) has been studied under different experimental conditions using different experimental techniques but clear and consistent explanation of mechanism of gas uptake is still lacking. However, based on the above studies two general remarks can be made about this interaction,

(a) the initial oxygen uptake is rapid and irreversible, and

(b) prolonged exposure of oxygen is reversible due to removal of O_2 either by pumping or by atomic hydrogen.

In the following sections, results of in situ Hall effect measurements carried out on both n- and p-type PbTe films during their exposure to oxygen and atomic hydrogen will be described and discussed.

4.2 EXPERIMENTAL PROCEDURE

The films used in the gaseous experiments were grown on freshly air-cleaved mica by thermal evaporation as described in Chapter 2. The substrate temperature was in the range 150-250°C. The majority of the films grown were n-type (out of about 40 films grown for these experiments only 5 were 'virgin' p-type). When the film had cooled down to room temperature it was placed in

between the poles of an electromagnet using the rotating steel plate. The pressure contacts were then made to the film without breaking the vacuum seal. Since mica substrate (two thou thickness) was not rigid enough to give firm pressure contacts, it was clamped to a clean glass slide. This arrangement gave firm pressure contacts.

The poles of the electromagnet were 1 inch apart and it was energised by passing 3A at 20V through its 3Ω coil. This produced a uniform magnetic field of 0.22T. The coil of the magnet was placed outside the vacuum chamber to avoid outgassing and the flux was conducted through two steel plates. In order to avoid the heating of the coil, the current through it was switched off as soon as a particular set of readings had been taken. It has been established by other workers (B3, E4, H1) that the effect of O_2 and air on the electrical properties of lead salts is indistinguisable, it was decided to use air instead of O_2 in the present experiments. For H experiments hydrogen gas was conducted into the vacuum system by a flexible steel tubing. The flow of H_2 and O_2 (air) was controlled by two separate needle leak valves.

As an initial experiment, both the needle valves were calibrated in terms of respective gas pressures inside the vacuum chamber where the ionisation gauge was used to measure the gas pressure. As mentioned in Section 4.1, Brodsky and Zemel (B3) believed that the electrical properties of PbSe film changed when the

ionisation gauge was switched on and later McLane and Zemel (M2) identified the gas generated by the action of the hot filament of the ionisation gauge as atomic hydrogen and further noted that H was generated only when the vacuum system was pumped by a diffusion pump filled with Octoil-S oil (a hydrocarbon oil). No H was detected when the diffusion pump oil was replaced by Don Coring 704, a silicone oil (a non-hydrocarbon oil). Therefore the interaction of the residual hydrocarbons from the vacuum system with the hot filament of the ionisation gauge was producing atomic hydrogen (M2). Even though the diffusion pump used in the present case was filled with Silicone MS 704 oil, the use of the ionisation gauge was kept to a minimum during an actual experimental run as a precaution.

A tungsten filament was used to atomise H_2 gas. This has proved to be an effective method of producing H in the past (B4, H5, B2). The tungsten filament used was 8 thou in diameter, 20 cm in length and was placed 15 cm below the film. The filament was heated to about 1750^{o}C and the temperature of the filament was measured by an optical pyrometer (Optix No. 10495). An aluminium foil was placed above the tungsten filament to shield the film from the radiative heat. No observable effect on the Hall coefficient R_H and resistivity ρ of the film was found when the tungsten filament was switched on in the absence of H_2 gas in contrast to Egerton's and Crocker's (E4) findings.

In the following section, the description of R_H versus ρ curves for both n- and p-type will be given where the description has been divided into three sub-sections. The first sub-section will deal with the description of R_H vs ρ curves for air-exposed films at room temperature, the second sub-section will deal with the description of unexposed ('virgin') films at room temperature and the third sub-section will deal with the description of air-exposed films not at room temperature. The method of measuring R_H and ρ has been detailed in chapter 3.

4.3 RESULTS (R_H VERSUS ρ CURVES)

4.3.1 Air-exposed Films

During the initial experiments of gaseous effects, some films were grown at 250°C in two different geometric configurations during the same evaporation run. One configuration was the gap configuration achieved by using a molybdenum mask (described in chapter 3) and the other configuration was the sandwich type configuration where the semiconductor film was sandwiched in between two metallic contacts. However, it was necessary to break the vacuum seal to evaporate the contacts for the sandwich configuration and therefore the films grown by this method were all air-exposed prior to carrying out any gaseous effect measurements. All such films remained n-type even after long air-exposure (over one year in some cases). The behaviour of film S6 was typical of these films.

Fig. 4.1 and Fig. 4.2 show the variations of R_H vs ρ and resistance R_D vs time respectively for film S6 during its exposure to atomic hydrogen, H and oxygen O_2. R_H and ρ were monitored for the gap configuration and R_D vs time were monitored for the sandwich configuration. Prior to H exposure, R_H was $-22.1\ cm^3/C$ and ρ was 0.03Ω cm when the film was exposed to H ($pH_2 = 1 \times 10^{-4}$ τ), R_H and ρ decreased until the film was saturated, i.e. no observable changes occurred in R_H and ρ. The saturation values of R_H and ρ were $-2.16\ cm^3/C$ and $0.003\ \Omega$ cm respectively. Throughout the gas exposure, the Hall mobility μ_n given by $R_H \div \rho$ changed by only 2.3% from $\sim 737\ cm^2/V\text{-sec}$ to $720\ cm^2/V\text{-sec}$. The film was then exposed to O_2 ($p_{O_2} = 1 \times 10^{-4}$ τ) and the values of R_H and ρ increased with very small variations in μ_n. Finally when the film was let up to atmospheric pressure, R_H was $-5.25\ cm^3/C$ and ρ was $0.007\ \Omega$ cm. Resistance R_D of film S6 in the sandwich configuration decreased from 49 Ω to 20.3 Ω during the H exposure and increased from 20.3 Ω to 42.7 Ω during the O_2 cycle. As it can be seen from Fig. 4.1, paths traced by R_H vs ρ curves during H and O_2 cycles were almost identical and the film showed no tendency to turn p-type.

4.3.2 'Virgin' Films

Since no additional information other than the reversibility of H effect by O_2 effect was obtained using the sandwich configuration, it was decided to grow the films in gap configuration only. This also meant that

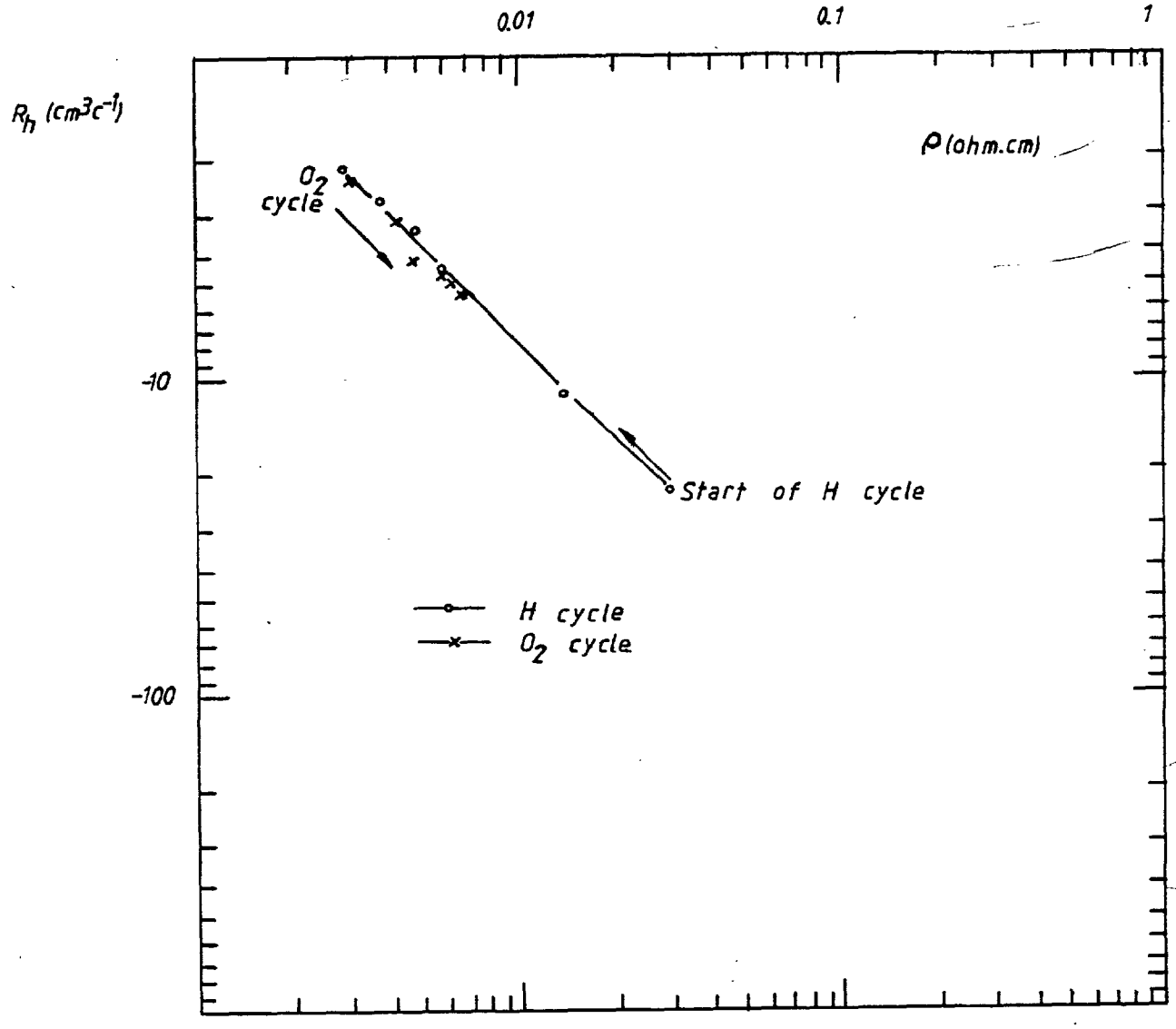

Fig. 4.1 R_h vs. ρ (Film S6)

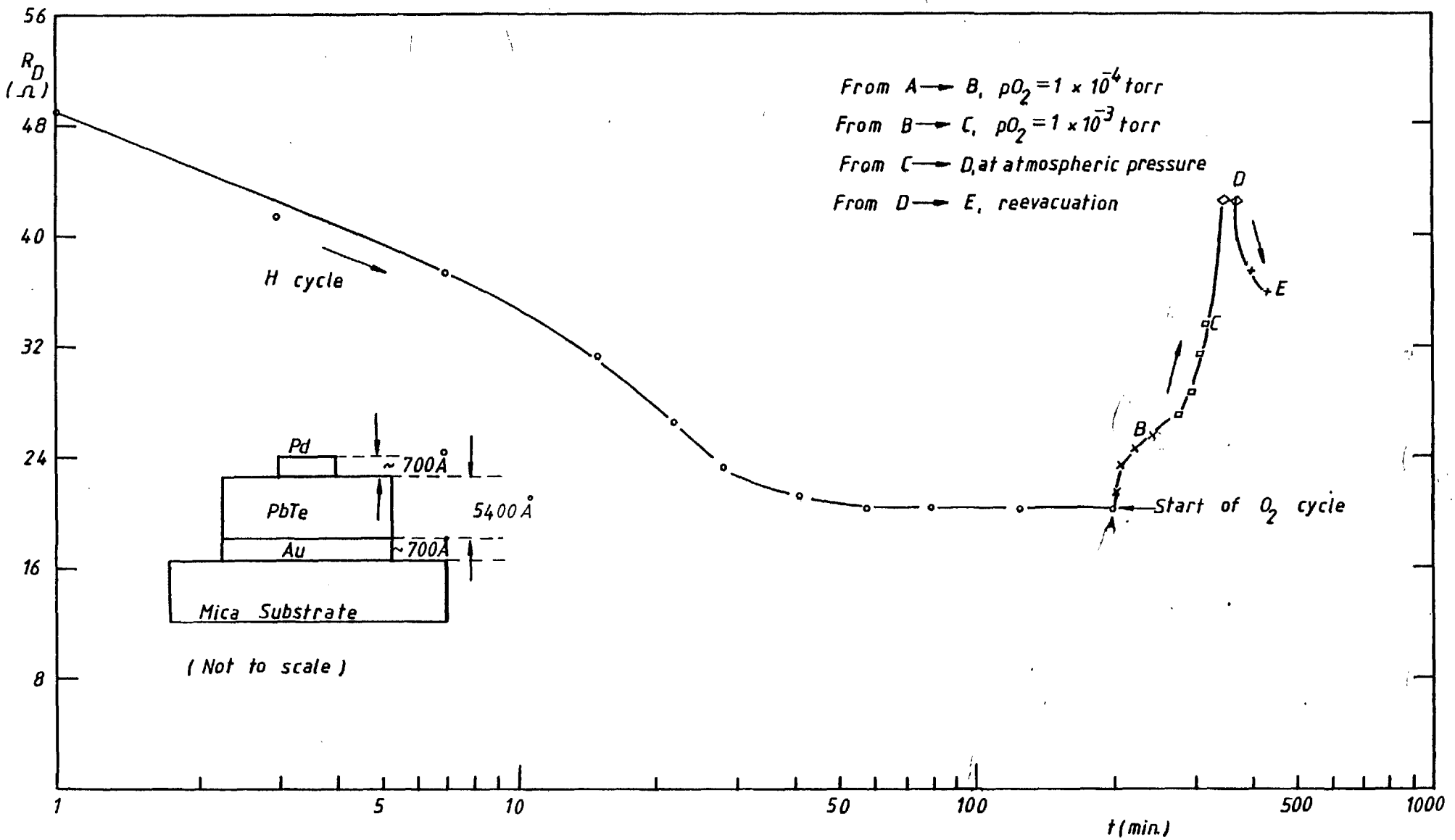

Fig.4.2 R_D versus time for film S6 in sandwich configuration (n-type film)

in situ Hall effect measurements could be carried out as the films were exposed to H and O_2. Because the films typified by S6 were 'stable' n-type, it was decided to evaporate films at lower substrate temperatures (150-250°C) in an attempt to grow both n- and p-type films.

In the following sections, results will be described for three 'virgin' n-type films and three 'virgin' p-type films considered to be representative of the general behaviour of such films.

4.3.2.1 'Virgin' n-type films

Fig. 4.3 shows the changes in R_H and ρ of film S27 grown at 250°C and 2940 Å in thickness. As the film was exposed to H (pH_2 = 2 x 10^{-4} τ), R_H changed from -139.2 cm^3/C to -2.32 cm^3/C and the corresponding change in ρ was from 0.33 Ω cm to 0.0051 Ωcm while the change in μ_n was from 422 cm^2/V-sec to 455 cm^2/V-sec. As expected, H drove the film more n-type and the film was saturated in 96 mins. Film S27 was then exposed to O_2 (p_{O_2} = 2 x 10^{-4} τ) and during the first hour of gas exposure, $|R_H|$ increased from -2.32 cm^3/C to -11.25 cm^3/C and ρ increased from 0.0051 Ω cm to 0.0215 Ω cm indicating that the film was turning less n-type. The film was left at p_{O_2} = 2 x $10^{-4}\tau$ pressure over night and $|R_H|$ increased to -15.2 cm^3/C and when the film was exposed to atmospheric pressure, $|R_H|$ began to decrease slowly and film S27 turned p-type after three days. Film S27 was kept in air for another two days

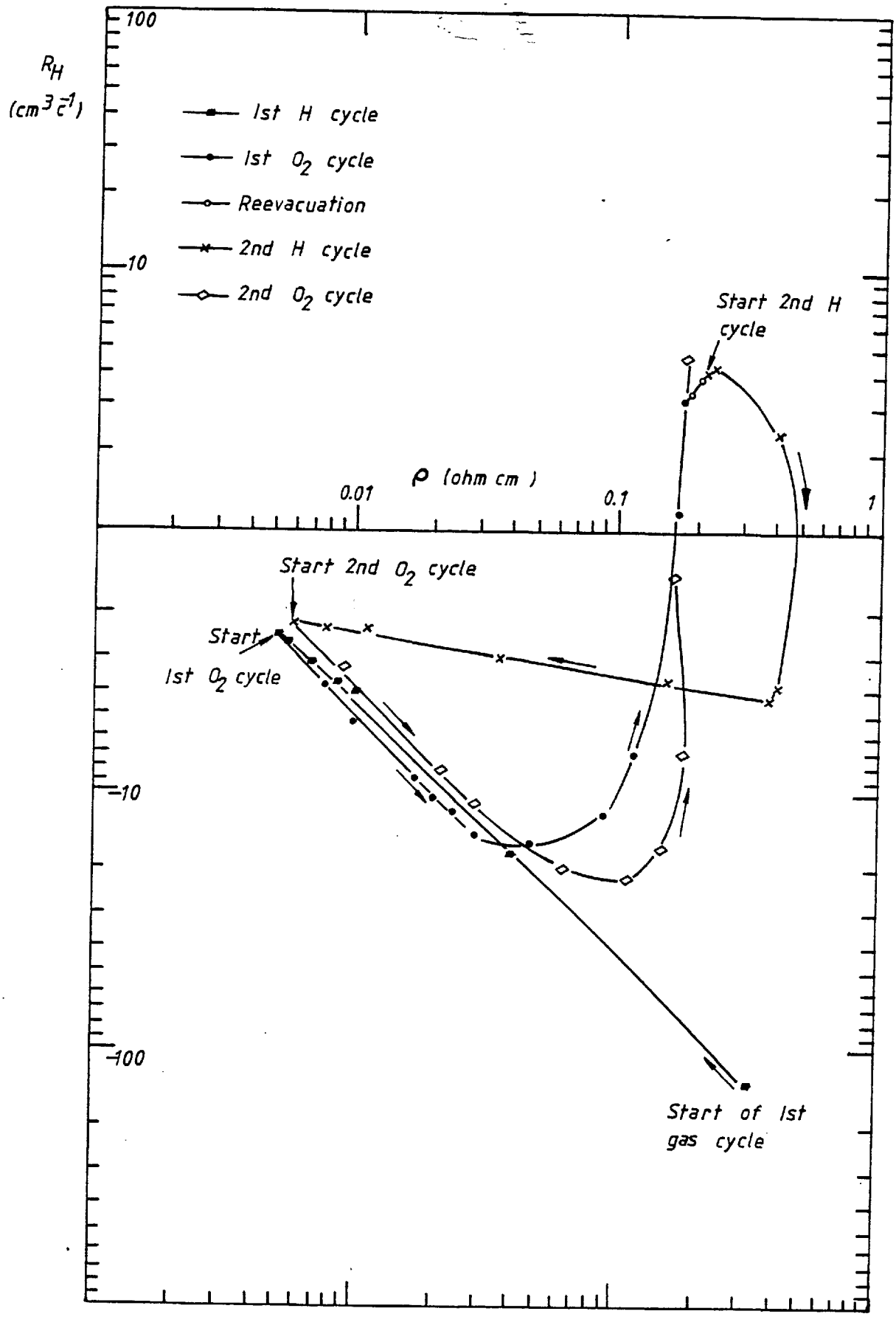

Fig. 4.3 R_H versus ρ for film S27

before re-evacuating the chamber. During re-evacuation, both R_H and ρ increased from 3.2 cm^3/C and 0.183 Ω cm to 4.06 cm^3/C and 0.211 Ω cm respectively, indicating a decrease in surface carrier concentration of $1.21 \times 10^{13} cm^{-2}$. During the second H cycle ($pH_2 = 2 \times 10^{-4}$ τ), the film turned n-type within 10 min. As the film was exposed to O_2 ($p_{O_2} = 2 \times 10^{-4}$ τ) for the second time, $|R_H|$ increased from -2.2 cm^3/C to -22.2 cm^3/C in about three and a half hours before starting to decrease again and the film turned p-type after two days of air exposure at atmospheric pressure. The paths traversed by R_H vs ρ curves during these cycles are shown in Fig. 4.3 where the path traversed during the H cycle is clockwise and the path traversed during O_2 cycle is counter clockwise.

Film S37 (Fig. 4.4) grown at 175°C and 2946 Å in thickness was left in a vacuum of $\sim 1 \times 10^{-6}$ τ for 20 hours. During this period $|R_H|$ increased from -15.1 cm^3/C to -22.3 cm^3/C showing that the carrier concentration had decreased by $\sim 3.9 \times 10^{12}$ cm^{-2}. When the film was exposed to H ($pH_2 = 1 \times 10^{-4}$ τ), it became progressively more n-type and H cycle lasted for 225 mins. When the H saturated film was exposed to O_2 ($p_{O_2} = 2 \times 10^{-4}$ τ), changes in R_H and ρ became slower and slower as time went on. Film S27 turned p-type after six days of air exposure at atmospheric pressure. On re-evacuation, R_H and ρ increased and during this period of pump-down carrier concentration decreased by 3.6×10^{12} cm^{-2}. The second

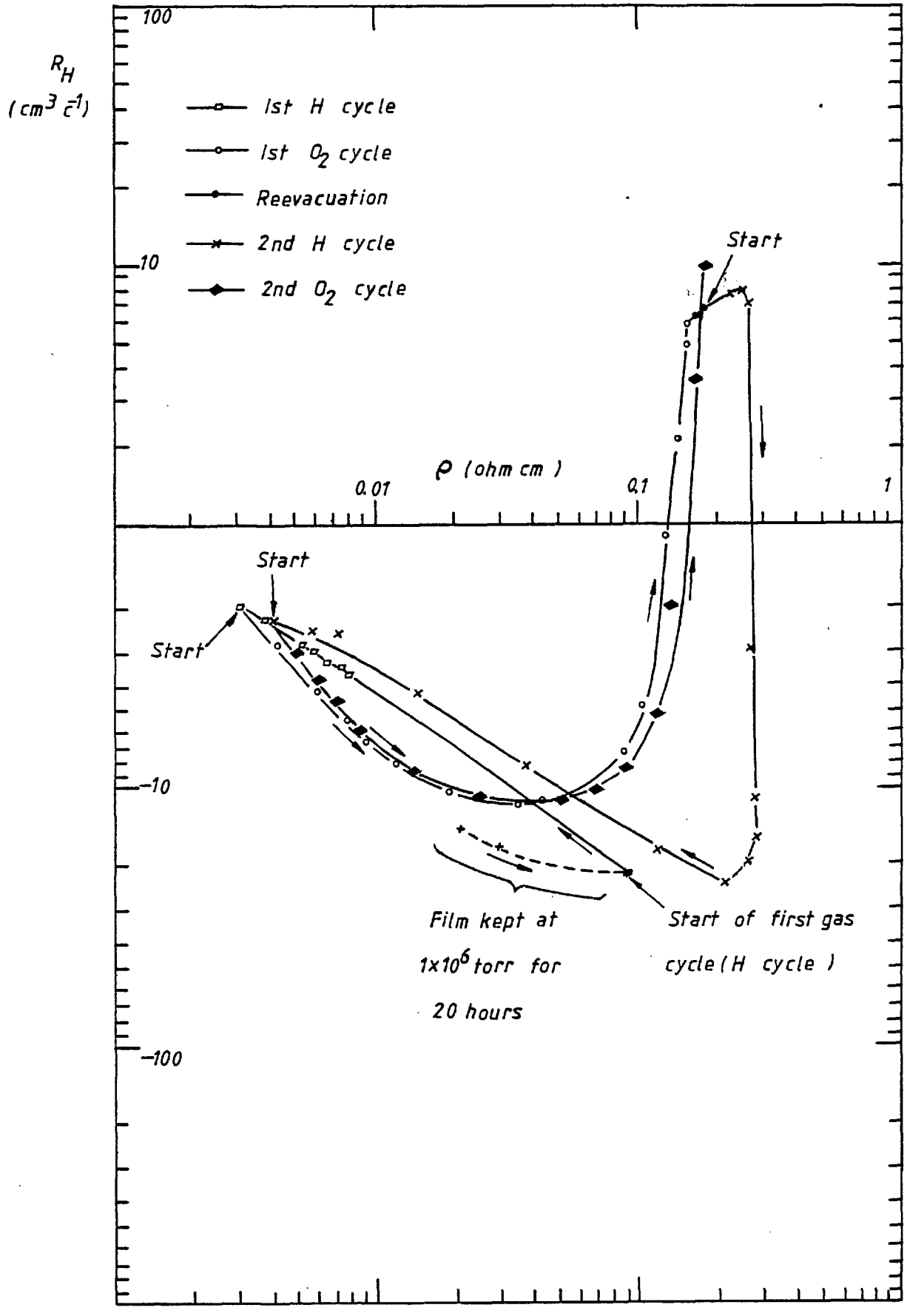

Fig. 4.4 R_H versus ρ for film S37

H cycle drove the film n-type in about 3½ mins whereas it took another six days to turn the film p-type again. Fig. 4.4 shows the paths traversed as the film was exposed to successive H-O_2 cycles.

Film S47 (Fig. 4.5) represents the behaviour of 'virgin' n-type films exposed to O_2 as the first gas cycle. When the film was exposed to O_2 (p_{O_2} = 2 x 10^{-4} τ), R_H changed from -1.17 cm^3/C to +1.48 cm^3/C in ∿4 mins and after a further exposure of three and a half hours R_H rose to 9.8 cm^3/C. The film was kept at this pressure for 48 hours and as a result R_H increased to 73 cm^3/C before decreasing again. When the film was let up to atmospheric pressure, R_H decreased to 14.8 cm^3/C before rising slightly to 15.1 cm^3/C. Corresponding changes in ρ were from 0.516 Ω cm ('virgin' n-type) to 0.106 Ω cm (p-type). In common with the previous films, R_H and ρ rose linearly keeping the Hall mobility almost constant during re-evacuation. During the first H cycle (pH_2 = 4 x 10^{-5} τ), R_H and ρ continued to increase linearly keeping the Hall mobility μ_p constant at ∿180 $cm^2/V\text{-sec}$. As the pressure of H_2 was increased to 1 x 10^{-4}τ, R_H and ρ kept on increasing along the same line and reached a maximum where R_H was 74.7 cm^3/C and ρ was 0.46 Ω cm. The film was driven n-type in 41 mins. During the second O_2 cycle (p_{O_2} = 2 x 10^{-4}τ) $|R_H|$ increased rapidly compared with the previous two films from -3.68 cm^3/C to -155 cm^3/C within 30 mins and then the uptake slowed down. $|R_H|$

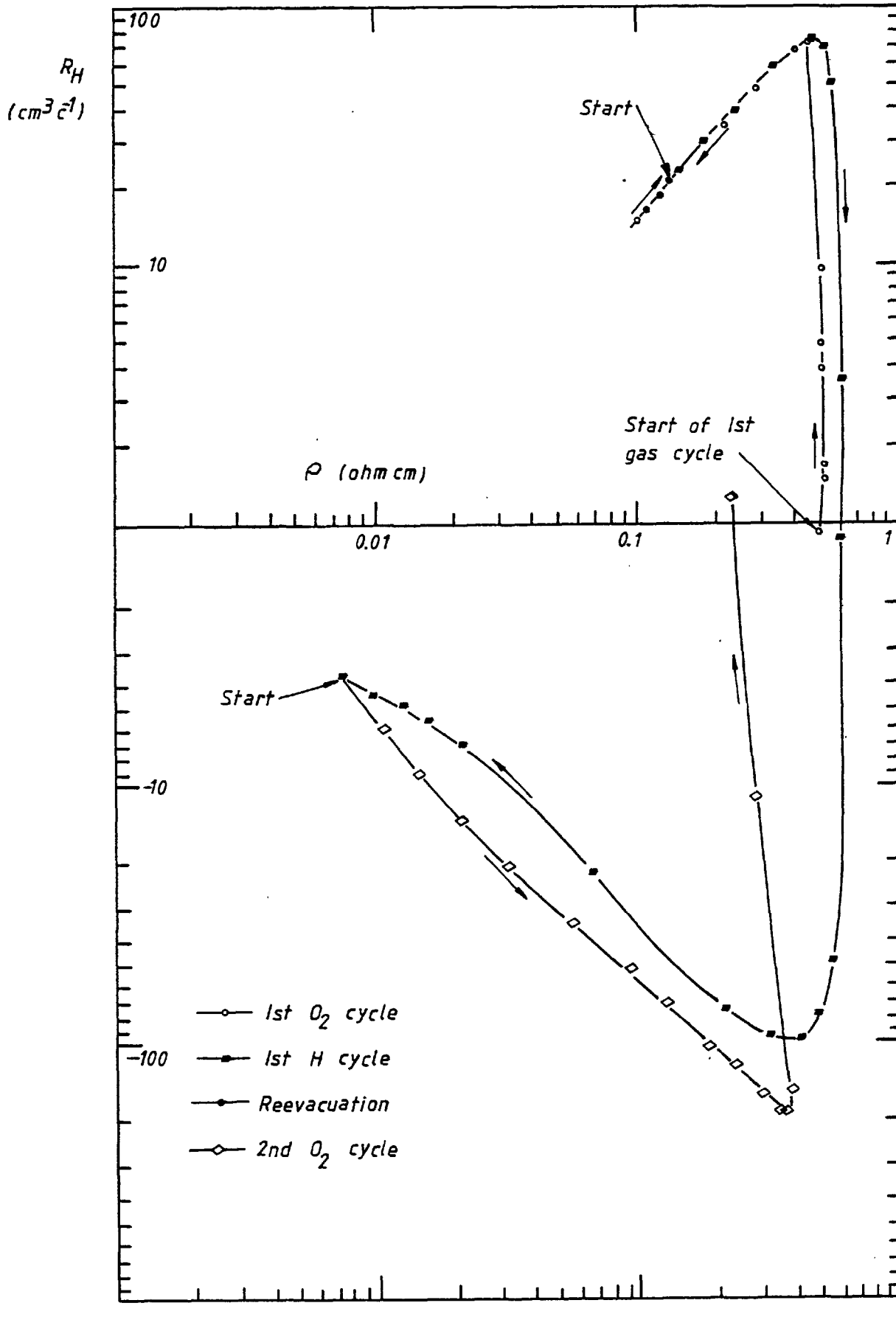

Fig. 4.5 R_H versus ρ for film S47

Film	Virgin Type	Deposition Temp. ^{o}C	Film Thickness (Å)	Cycle No.	Time Elapsed* before Gas Cycle	Effect of Gas Cycle	Time Taken to Reverse Conductivity	Cycle Duration	Carrier Conc. before Gas Cycle (cm^{-3})	Carrier Conc at End of Gas Cycle (cm^{-3})	Fig. No.
S27	n	250	2940	1st H	194 mins	$n \rightarrow n^{+}$	Film became more n-type	96 mins	$n=4.49 \times 10^{16}$	$n=2.69 \times 10^{18}$	4.3
				1st O_2	290 mins	$n \rightarrow p$	3 days	5 days	$n=2.69 \times 10^{18}$	$p=1.95 \times 10^{18}$	
				2nd H	∿5 days	$p \rightarrow n$	10 mins	117 mins	$p=1.54 \times 10^{18}$	$n=2.84 \times 10^{18}$	
				2nd O_2	∿5¼ days	$n \rightarrow p$	2 days	3 days	$n=2.84 \times 10^{18}$	$p=1.3 \times 10^{18}$	
S37	n	175	2946	Film left in vacuum of ∿1×10^{-6} τ for 20 hours		$n \rightarrow n^{-}$	Film became less n-type	20 hours	$n=4.14 \times 10^{17}$	$n=2.8 \times 10^{17}$	4.4
				1st H	20 hours	$n \rightarrow n^{+}$	Film became more n-type	225 mins	$n=2.8 \times 10^{17}$	$n=3 \times 10^{18}$	
				1st O_2	∿24 hours	$n \rightarrow p$	6 days	12 days	$n=3 \times 10^{18}$	$p=1 \times 10^{18}$	
				2nd H	13 days	$p \rightarrow n$	3.5 mins	280 mins	$p=9.11 \times 10^{17}$	$n=2.5 \times 10^{18}$	
				2nd O_2	∿13 days	$n \rightarrow p$	6 days	14 days	$n=2.5 \times 10^{18}$	$p=6.3 \times 10^{17}$	
S47	n	175	2900	1st O_2	19 hours	$n \rightarrow p$	4 mins	2 days	$n=5.34 \times 10^{18}$	$p=4.14 \times 10^{17}$	4.5
				1st H	∿3 days	$p \rightarrow n$	41 mins	204 mins	$p=2.68 \times 10^{17}$	$n=1.7 \times 10^{18}$	
				2nd O_2	∿3 days	$n \rightarrow p$	∿20 hours	24 hours	$n=1.7 \times 10^{18}$	$p=4.81 \times 10^{18}$	

*Time elapsed was measured from the moment the evaporation of the film was completed to starting a particular gas cycle.

TABLE 4.1

reached a maximum at -188 cm^3/C (ρ = 0.38 Ω cm) and started to decrease again. When the film was exposed to atmospheric pressure, it turned p-type where R_H was 1.3 cm^3/C and ρ was 0.231 Ω cm. Curves traced by R_H vs ρ during H-O_2 cycles are shown in Fig. 4.5.

The main points of the gaseous effects of films S27, S37 and S47 are summarised in Table 4.1.

4.3.2.2 'Virgin' p-type films

The curves for R_H vs ρ of film S25 for two H-O_2 cycles are shown in Fig. 4.6 Film S25 had high resistivity (ρ = 0.66 Ω cm) and low carrier concentration ($p = 7.4 \times 10^{16}$ cm^{-3}). As the film was exposed to H ($pH_2 = 1 \times 10^{-4}$ τ), it drove the film n-type within 90 secs and when the H exposure was stopped, R_H was -1.76 cm^3/C and ρ = 0.0036 Ω cm. The film was then exposed to O_2 ($p_{O_2} = 2 \times 10^{-4}$ τ) and $|R_H|$ increased to -14.7 cm^3/C within two hours and after that the changes in R_H and ρ were much slower. When the vacuum chamber was let up to atmospheric pressure, $|R_H|$ increased slowly to -18 cm^3/C and then started to decrease again. The film turned p-type after six days. The film was stored in a dessicator for a period of 20 weeks in the laboratory atmosphere prior to the second H cycle. During the second H cycle, both R_H and ρ increased showing that the film was becoming less p-type and the Hall mobility μ_p remained constant at $\sim$120 cm^2/V-sec. R_H reached a maximum and started to decrease and the film turned n-type

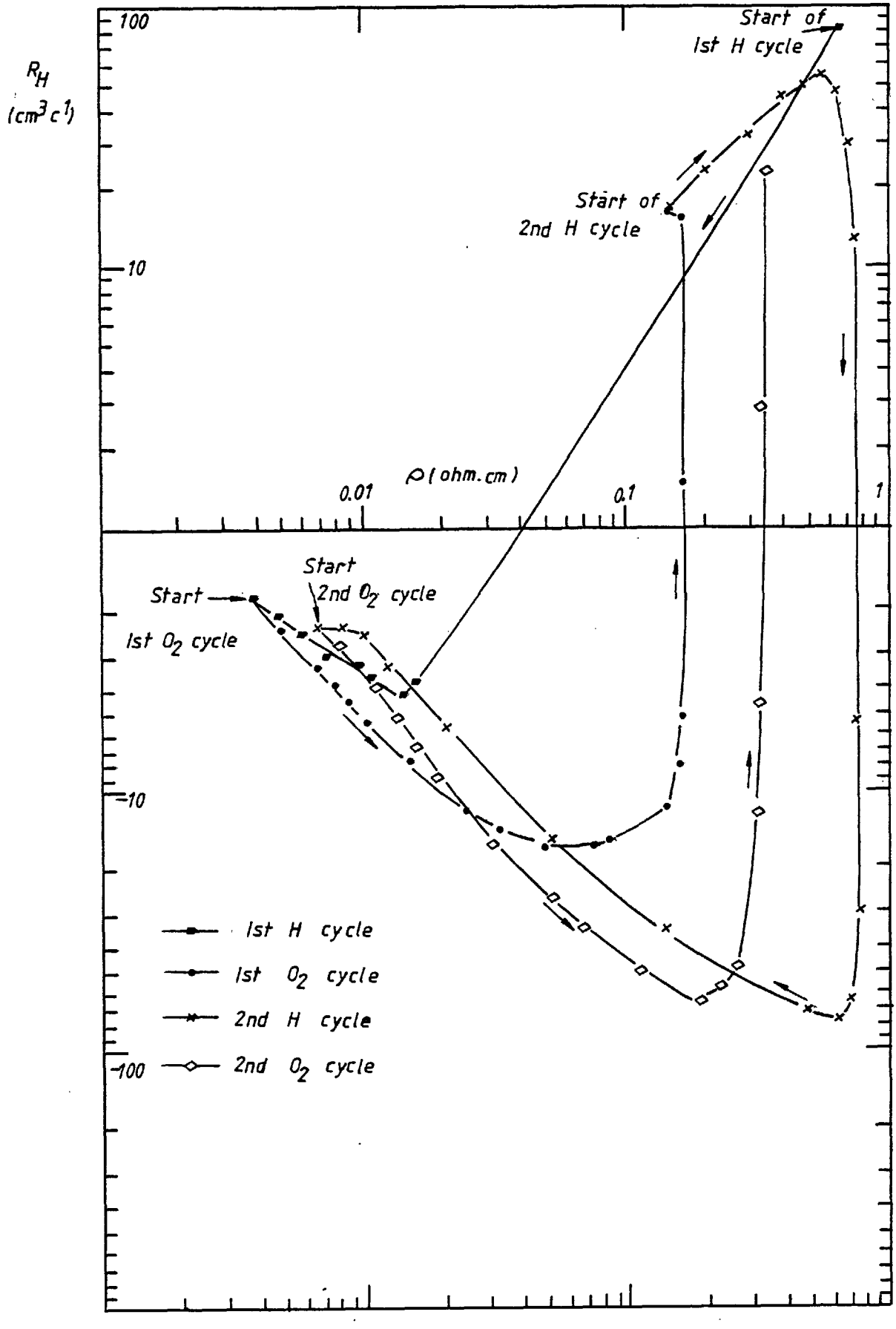

Fig. 4.6 R_H vs. ρ for film S25

after 47 mins. The effect of H was reversed by O_2 when the film was exposed to the gas at $p_{O_2} = 2 \times 10^{-4}\tau$ and the film reverted back to its original type of conductivity after three days.

When film S29 (Fig. 4.7) was left in a vacuum of $\sim 1 \times 10^{-6}\tau$ for 47 hours, R_H decreased slightly from 112 cm^3/C to 109 cm^3/C indicating that surface carrier concentration had risen by 6.81×10^{10} cm^{-2}. As the film was exposed to H ($pH_2 = 1 \times 10^{-4}$ τ), it turned n-type as expected. When O_2 was leaked into the vacuum chamber at $p_{O_2} = 2 \times 10^{-4}$ τ, $|R_H|$ reached a maximum at -129 cm^3/C ($\rho \sim 0.5$ Ω cm) and started to decrease. Film S29 became p-type after 204 mins. As shown in Fig. 4.7, the paths traversed by R_H vs ρ curves during H and O_2 cycles were different.

Fig. 4.8 shows the changes in R_H and ρ as film S51 was exposed to O_2 as the initial gas cycle. Prior to the O_2 cycle, R_H was 71.3 cm^3/C and ρ was 0.52 Ω cm. During the O_2 cycle, both R_H and ρ decreased showing that O_2 was driving the film progressively more p-type as expected. When R_H reached 9.6 cm^3/C, the film was let up to atmospheric pressure and R_H increased to 12.7 cm^3/C. During the re-evacuation, like all other films described, R_H and increased and during the H cycle R_H and ρ continued to increase until R_H reached a maximum at 83 cm^3/C. After reaching this maximum R_H decreased and the film became n-type after 28 mins. The O_2 cycle reversed the effect

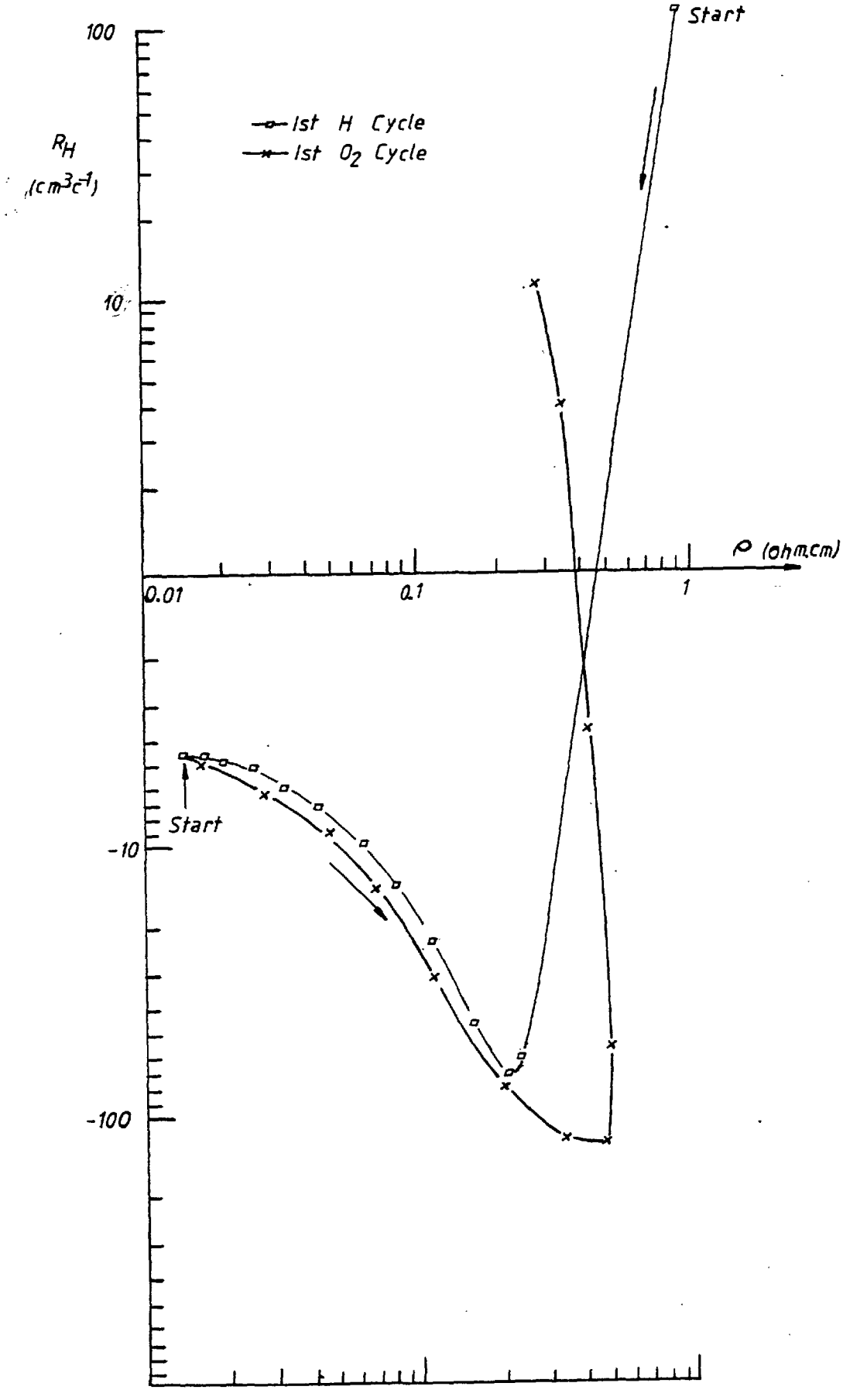

Fig. 4.7 R_H vs. ρ (Film S29)

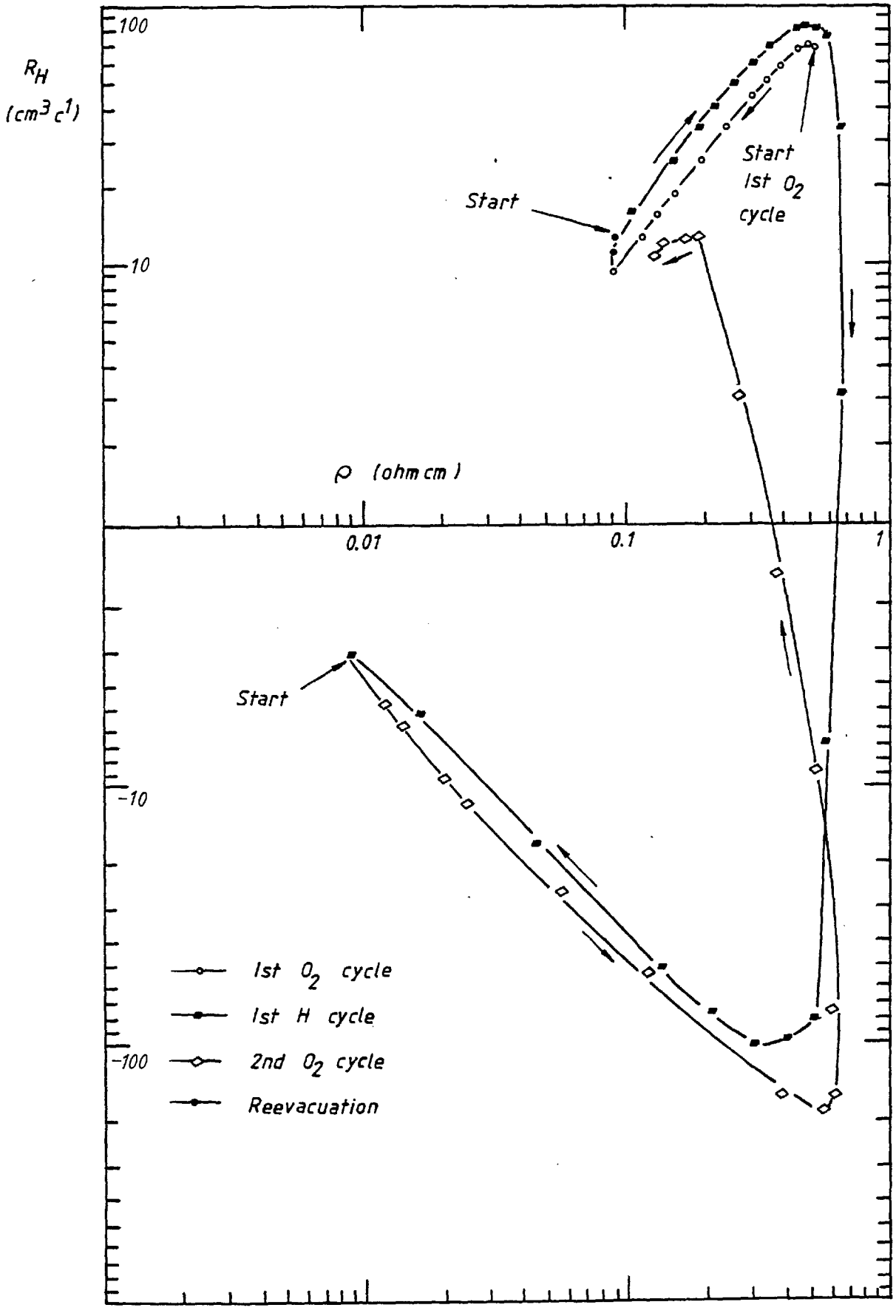

Fig. 4.8 R_H versus ρ for film S51

Film	Virgin Type	Deposition Temp. ^{o}C	Film Thickness (Å)	Cycle No.	Time Elapsed* before Gas Cycle	Effect of Gas Cycle	Time Taken to Reverse Conductivity	Cycle Duration	Carrier Conc. before Gas Cycle (cm^{-3})	Carrier Conc. at End of Gas Cycle (cm^{-3})	Fig.No.
S25	p	170	2038	1st H	138 mins	p → n	∿90 secs	159 mins	$p=7.4 \times 10^{16}$	$n=3.55 \times 10^{18}$	4.6
				1st O_2	297 mins	n → p	6 days	20 weeks	$n=3.55 \times 10^{18}$	$p=3.68 \times 10^{17}$	
				2nd H	20 weeks	p → n	47 mins	230 mins	$p=3.7 \times 10^{17}$	$n=2.31 \times 10^{18}$	
				2nd O_2	∿20 weeks	n → p	3 days	6 days	$n=2.31 \times 10^{18}$	$p=2.6 \times 10^{17}$	
S29	p	150	4438	Film left in vacuum of 1×10^{-6} τ for 47 hours		p → p^{+}	Film became more p-type	47 hours	$p=5.58 \times 10^{16}$	$p=5.73 \times 10^{16}$	4.7
				1st H	47 hours	p → n	∿90 secs	148 mins	$p=5.73 \times 10^{16}$	$n=1.39 \times 10^{18}$	
				2nd O_2	∿49 hours	n → p	204 mins	26 hours	$n=1.39 \times 10^{18}$	$p=5.21 \times 10^{17}$	
S51	p	175	2049	1st O_2	63 mins	p → p^{+}	Film became more p-type	81 mins	$p=8.77 \times 10^{16}$	$p=4.92 \times 10^{17}$	4.8
				1st H	∿20 hours	p → n	28 mins	156 mins	$p=3.93 \times 10^{17}$	$n=2.08 \times 10^{18}$	
				2nd O_2	∿22 hours	n → p	20 hours	24 hours	$n=2.08 \times 10^{18}$	$p=5.95 \times 10^{17}$	

*Time elapsed was measured from the moment the evaporation of the film was completed to starting a particular gas cycle.

TABLE 4.2

of the H cycle and restored the film to its original type of conductivity where $|R_H|$ went through two maxima during the gas cycle.

In Table 4.2, a summary of the H-O_2 cycles is given for films S25, S29 and S51.

4.3.3 Air-exposed Films (not at room temperature)

Up to now, all the results described were for the gas exposures carried out at room temperature. No facility was available to heat the film while it was situated in between the poles of the electromagnet. However, as the film was clamped on the rotating plate therefore by heating the rotating plate radiatively by the substrate heater, the film in turn was heated conductively. This method of heating was inefficient and slow. Seven films were heated to 50-60^{o}C using this method and the changes in R_H and ρ were monitored while the films were exposed to H. In Fig. 4.9, results for two air-exposed p-type films are shown. Film S25 has been discussed previously. Film S36 was grown at 175^{o}C and its thickness was 2900 Å.

In the case of film S25, during the initial pump-down, R_H and ρ increased along path A → B. At this point, the substrate heater was switched on and the temperature of the film was monitored by an iron-constantan thermocouple. As the film was being heated, path B → C was traced where both R_H and ρ decreased. At C, the temperature of the film stabilised at 50^{o}C and the H cycle

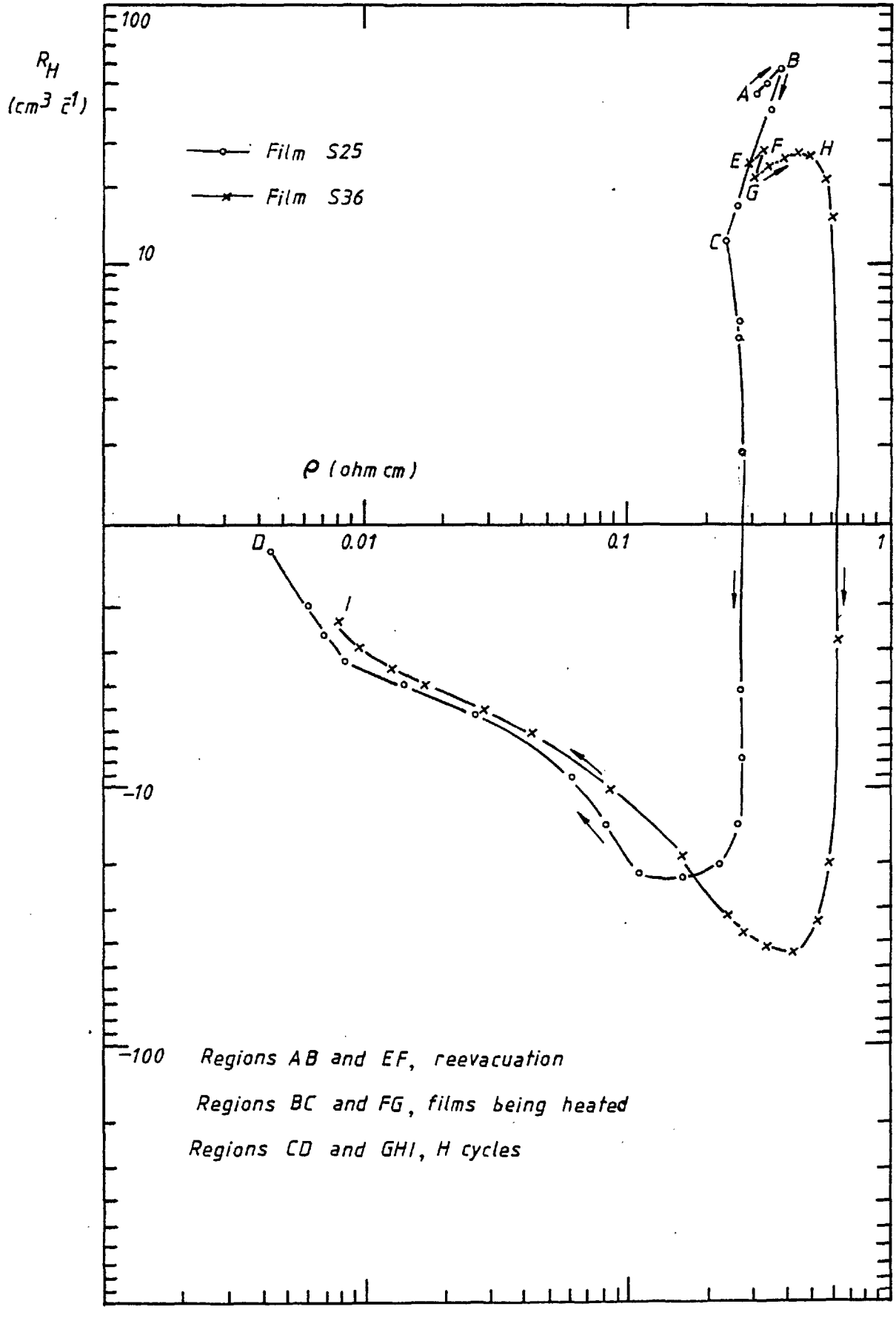

Fig. 4.9 H effect at 50°C

was commenced. During the H cycle, the film turned n-type in 9 mins and path C → D was traversed in a clockwise manner. For film S36, path E → F was traced during re-evacuation, path F → G was traced during the period when the film was being heated and path G → H → I was traced during the H exposure. Film S36 was driven n-type in 21 mins.

It may be noted that the curves shown in Figs. 4.1 through to Fig. 4.9 are drawn to be smooth and continuous and are not the best-fit curves.

4.4 THEORETICAL MODELS

In this section, two major theoretical models will be proposed to analyse the results described in the previous section, namely the surface model (planar form and three-dimensioanl form) and the diffusion model. Both of these models have been used by other workers (E2,H1,B2) with a varying degree of success to explain the gaseous effects of epitaxial films of PbTe and $Pb_{1-x}Sn_xTe$ alloy.

Brodsky and Zemel (B3), in order to explain the changes in R_H vs ρ curves for epitaxial PbSe films deposited on NaCℓ, initially suggested that the existence of the space charge region on the surface of the semiconductor was influencing the transport properties of such films, i.e. the surface model. This surface model will now be examined in detail.

4.4.1 Surface Model (planar form)

Poisson's equation has been used extensively in the past to relate the variation of the electric field to the charge density especially in the study of p-n junctions (M4), but one can also use this equation to formulate the problem of the surface space charge on a semiconductor. It is intended here to develop expressions for R_H and ρ for extrinsic and intrinsic semiconductor-bulks in the presence of surface space charge. For a semi-infinite, homogeneous material under thermal equilibrium the electrostatic potential V can be expressed by Poisson's equation (M4) as follows,

$$\frac{d^2V}{dx^2} = - \frac{\rho}{\varepsilon} \qquad (4.1)$$

where

V is a function of x only

ρ is the charge density

ε is the dielectric constant of the material

x is the distance from the surface of the semiconductor (x = 0)

The space charge region shown in Fig. 4.10 can be classified according to the relative values of the carrier concentrations at the surface. If the bulk majority carrier is still in the majority at the surface, the space charge region can either be an accumulation or depletion region depending on whether the concentration of this carrier is being increased or decreased. If

the minority bulk carrier is in the majority at the surface, then it is called the inversion region (Fl).

The charge density, ρ in equation (4.1) consists of static charge (negative and positive) and charge due to mobile electrons and holes. For a fully ionised p-type semiconductor,

$$\rho = q(p(x) - n(x) - Na) \qquad (4.2)$$

where p(x) and n(x) are the hole and electron concentrations respectively at distance x from the surface. Na is the fixed acceptor density. Using the reduced potential notation of (M4), equation (4.1) can be rewritten as,

$$\frac{d^2v}{dx^2} = - \frac{q^2}{\varepsilon kT} (p(x) - n(x) - Na) \qquad (4.3)$$

where

$$v = \frac{qV}{kT} \qquad (4.4)$$

k is Boltzmann's constant

q is the electronic charge

T is the temperature

Multiplying equation (4.3) by dv/dx and integrating from the bulk (i.e. v = O and dv/dx = O) to the point where the band-bending is v,

$$(\frac{dv}{dx})^2 = - \frac{2q^2}{\varepsilon kT} \int_{v=O}^{y} (p(v) - n(v) - Na)\, dv \qquad (4.5)$$

If n_b and p_b are the bulk electron and hole concentrations respectively, one can define the effective Debye length as,

$$L_D^2 = \frac{\varepsilon kT}{q^2(n_b + p_b)} \tag{4.6}$$

From equations (4.5) and (4.6)

$$\frac{dv}{dx} = \pm \frac{\sqrt{2}}{L_D} \left[\int_{v=0}^{v} \frac{(-p(v)+n(v)+Na)dv}{(n_b+p_b)} \right]^{\frac{1}{2}} \tag{4.7}$$

Defining a surface function F(v) as,

$$F(v) = \sqrt{2} \left[\int_{o}^{v} \frac{(-p(v)+n(v)+Na)dv}{(n_b+p_b)} \right]^{\frac{1}{2}} \tag{4.8}$$

Therefore equation (4.7) becomes,

$$\frac{dv}{dx} = \pm \frac{F(v)}{L_D} \tag{4.9}$$

In equation (4.9), the sign is positive when $v > 0$, i.e. band-bending is downwards (as in Fig. 4.10) and the sign is negative when $v < 0$ (band-bending upwards).

In order to evaluate F(v), expressions for n(v) and p(v) must be developed. This can be done as follows.

In general, total electron concentration in the bulk of a semiconductor can be written as (B5),

$$n = \int_{-\infty}^{\infty} g_c(E)\, F(E)\, dE \tag{4.10}$$

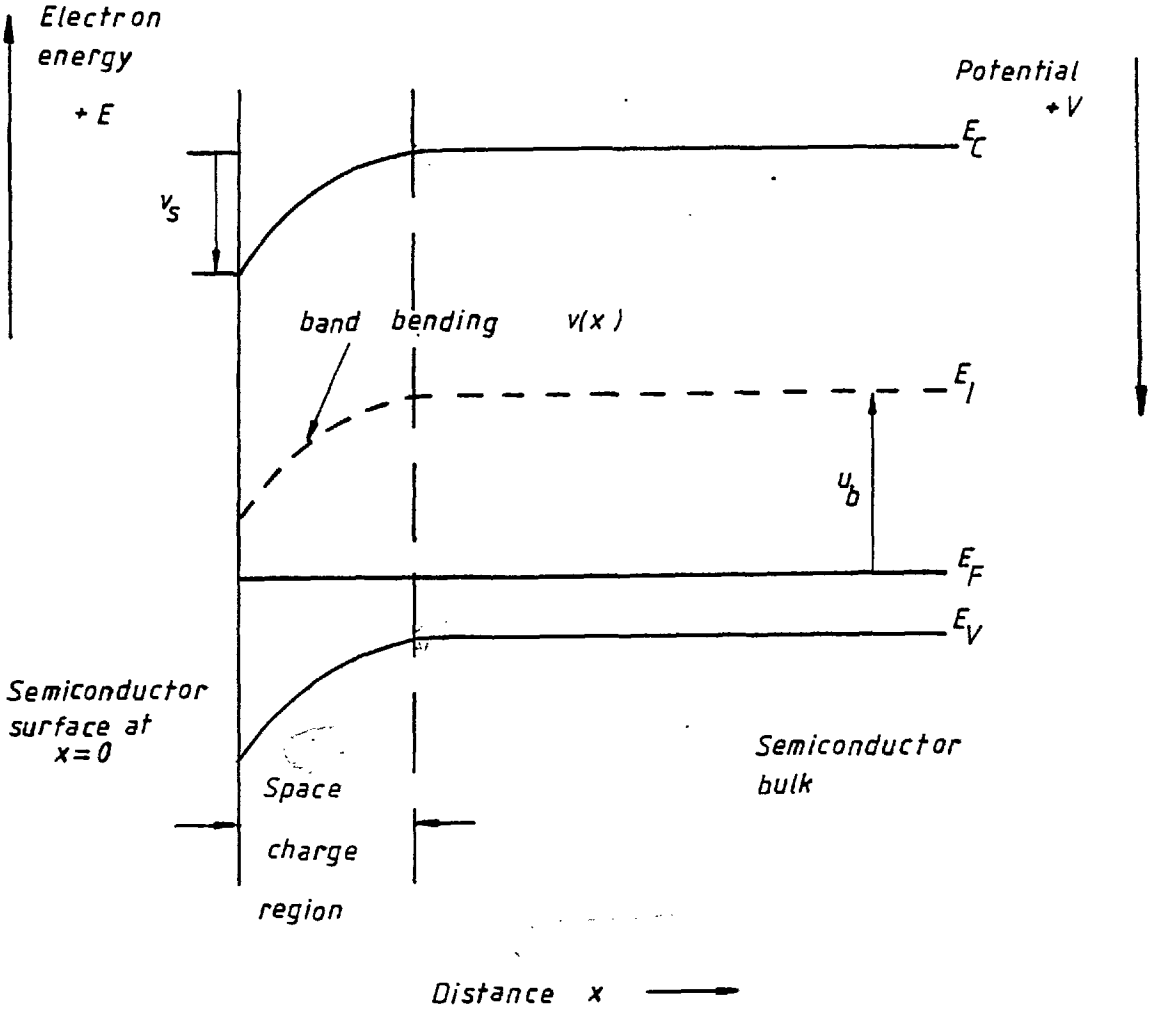

Fig. 4.10 Depleted p-type semiconductor

where $g_c(E)$ is the density of states function for the conduction band and F(E) is the Fermi-Dirac function expressing the probability of an energy level E being occupied by an electron under equilibrium.

$$F(E) = \frac{1}{1 + \exp\left(\frac{E-E_F}{kT}\right)} \tag{4.11}$$

Using equations (4.10) and (4.11), electron concentration can be evaluated at a point in a semiconductor where the band-bending is v.

$$n(v) = \int_o^\infty \frac{g_c(\varepsilon)\, d\varepsilon}{1 + G \exp(\varepsilon - \varepsilon_F - v)} \tag{4.12}$$

where

$$\text{(i)}\ \varepsilon - \varepsilon_F = \frac{E-E_F}{kT}, \quad d\varepsilon = \frac{dE}{kT} \tag{4.13}$$

(ii) G is the degeneracy factor

(iii) lower limit of integration has been taken at the edge of the conduction band

Similarly for holes,

$$p(v) = \int_o^\infty \frac{g_v(\varepsilon)\, d\varepsilon}{1 + G \exp(\varepsilon + \varepsilon_F + v + \varepsilon_g)} \tag{4.14}$$

where $g_v(\varepsilon)$ is the density of states function for the valence band and $\varepsilon_g = E_g/kT$, the forbidden energy gap. Generally in k-space density of states per unit volume

(including the two possibilities for electron spin) is given by,

$$g(E)\,dE = \frac{2}{(2\pi)^3} \int d^3\,\underline{k} \qquad (4.15)$$

The density of states functions for non-parabolic bands and spherical energy surfaces given by Juhasz (J3) were used to evaluate equations (4.12) and (4.14). (These functions have been given in Chapter 1, equations (1.13) and (1.14).) The position of the Fermi level can be determined from the charge neutrality condition in the bulk as follows,

$$p(v) - n(v) - Na = 0 \qquad (4.16)$$

In the space charge region, the excess electrons ΔN and excess holes ΔP with respect to their concentration in the bulk, can be defined as follows,

$$\Delta N = \int_o^\infty (n(x) - n_b)\,dx \qquad (4.17)$$

and

$$\Delta P = \int_o^\infty (p(x) - p_b)\,dx \qquad (4.18)$$

From equations (4.9), (4.17) and (4.18),

$$\Delta N = L_D \int_{v_s}^{o} \frac{(n(v) - n_b)\,dv}{F(v)} \qquad (4.19)$$

$$\Delta P = L_D \int_{v_s}^{o} \frac{(p(v) - p_b)\,dv}{F(v)} \qquad (4.20)$$

where $v = v_s$ at $x = 0$ and at $x \to \infty$, $v = 0$ (flat-bands). It may be noted that for $v_s > 0$, ΔN is positive and ΔP is negative and the converse is true for $v_s < 0$. From (Z4), for a semiconductor of thickness d,

$$\sigma d = \sigma_b d + q(\mu_{ns} \Delta N + \mu_{ps} \Delta P) \tag{4.21}$$

and

$$R_H \sigma^2 d = R_b \sigma_b^2 d + q(\mu_{ps}^2 \Delta P - \mu_{ns}^2 \Delta N) \tag{4.22}$$

where

(i) σ is the conductivity = ρ^{-1}

(ii) subscripts b and s refer to bulk and surface respectively

(iii) μ_{ns} and μ_{ps} are the electron and hole mobilities respectively at the surface

A computer program developed by Juhasz (J3) was used to evaluate R_H and ρ for various assumed values of the surface potential v_s. Firstly, the program evaluates the bulk parameters n_b, p_b, ε_F, ε_{Fi}, U_b etc. and secondly F(v) is calculated. Once F(v) is known ΔN and ΔP can be calculated from equations (4.19) and (4.20). Using these calculated values of ΔN and ΔP in equations (4.21) and (4.22), σd and $R_H \sigma^2 d$ can be evaluated. Finally, ρ and R_H can be determined since the film thickness, d is known. The program requires E_g, m_e, m_h, E_c, E_v, N_a, N_d, dielectric (static) constant, T, μ_{ns}, μ_{ps},

film thickness and the limits of the surface potential v_s as the input data.

Data taken from film S25 (considered to be typical) was used to compare the theoretical R_H vs ρ curve predicted by the computer program with the experimental curve for the second H cycle. Brodsky and Zemel (B3) showed that for PbSe films, surface scattering was specular and assuming the same to be true for PbTe films, $\mu_s = \mu_b$ was used. The values of μ_p and μ_n were deduced from the slopes of the linear parts of the R_H vs ρ curve when the film was considered to be in the single carrier region. Since the film was p-type, N_d was assumed to be zero and N_a was given by $1/R_H e$. The values of E_g, m_h, m_e and static dielectric constant were 0.31 eV, 0.29 m_o, 0.24 m_o and 425 respectively and these values were taken from (E1, B2, Z1). Values of μ_p and μ_n were 114 cm^2/V-sec and 456 cm^2/V-sec respectively and $N_a = 3.7 \times 10^{17}$ cm^{-3}. The thickness of the film was 2038 $\mathring{A}$ and T was the room temperature, 300°K. Fig. 4.11 shows the two curves.

4.4.1.1 R_H and ρ expressions for intrinsic bulk (planar form)

Since 'virgin' p-type films (typified by S29) and some of the 'virgin' n-type films had carrier concentration at room temperature comparable to the intrinsic bulk, expressions for R_H and ρ were developed for intrinsic bulk in the presence of surface space charge region in order to compare the theoretical and experimental data. Unlike the extrinsic bulk case, Poisson's equation for the

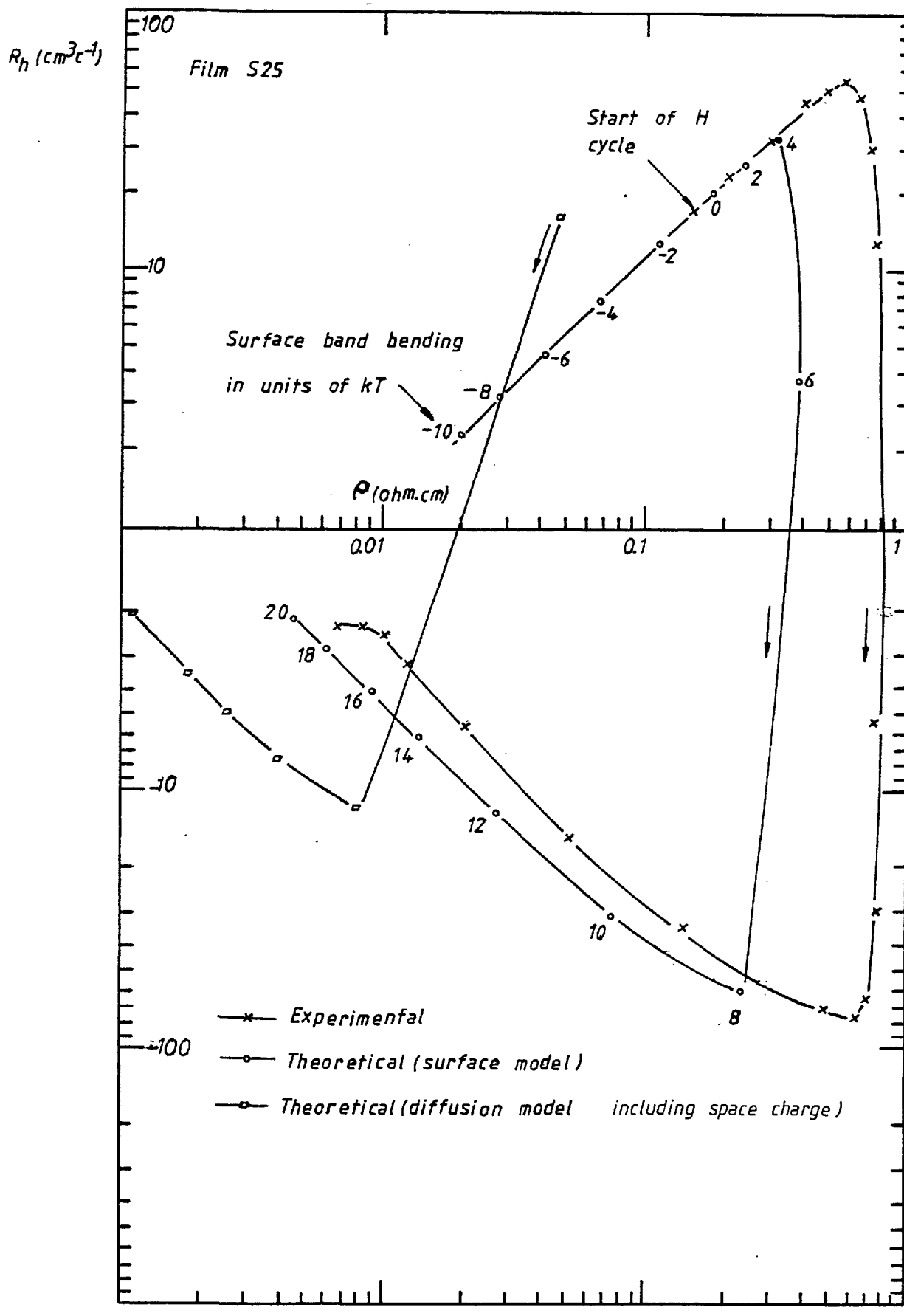

Fig. 4.11 H cycle on O_2 driven p – type film

intrinsic bulk can be solved analytically. This is detailed in Appendix A. From Appendix A,

$$\sigma = \rho^{-1} = \frac{I_1 + I_2}{d} \tag{4.23}$$

and

$$R_H = d\frac{(\mu_p I_2 - \mu_n I_1)}{(I_1 + I_2)} \tag{4.24}$$

where integrals I_1 and I_2 are functions of v_s, the band-bending at the surface and d is the thickness of the film. When $\mu_p I_2 > \mu_n I_1$, the film is p-type and when $\mu_p I_2 < \mu_n I_1$ the films is n-type.

For the sake of completeness, expressions for excess electrons and holes are also given where,

$$\Delta N = 2n_b L\,(\exp(\frac{v_s}{2}) - 1) \tag{4.25}$$

$$\Delta P = 2p_b L\,(\exp(-\frac{v_s}{2}) - 1) \tag{4.26}$$

where the symbols have their usual meaning. In equation (4.25), when $v_s > 0$ (i.e. positive band-bending as in Fig. 4.10), $\exp v_s/2 > 1$ and ΔN is positive whereas in equation (4.26) $\exp - v_s/2 < 1$ for $v_s > 0$ and ΔP is negative. The converse is true when $v_s < 0$ (upwards band-bending).

The model was tested on film S29 for the first H cycle. Fig. 4.12 shows the R_H vs ρ curve predicted by equations (4.23) and (4.24) and the experimental curve.

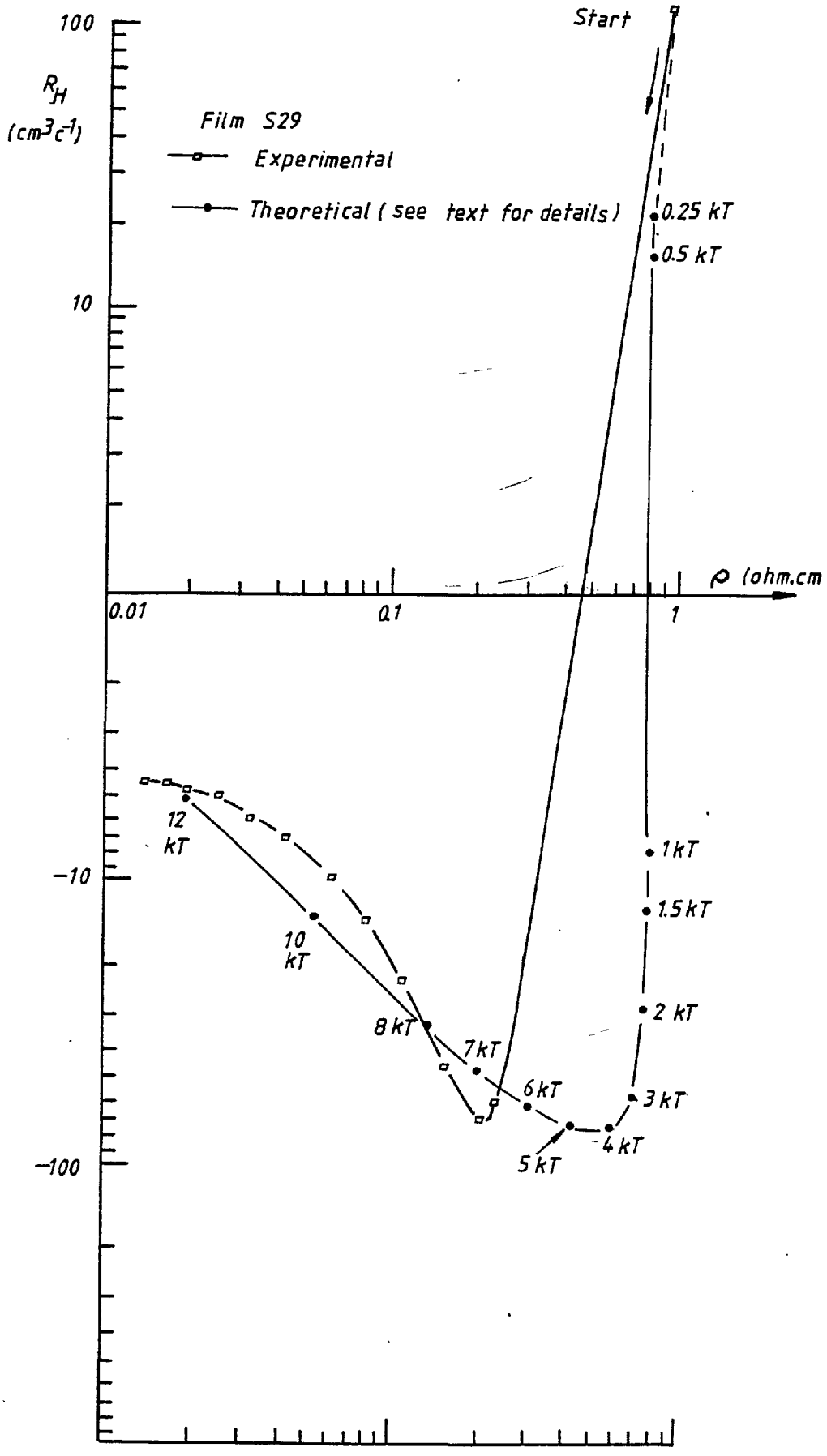

Fig. 4.12 Ist H cycle on a 'virgin' p-type film

As seen from Fig. 4.12, the model appears to predict a satisfactory $\overset{shape}{\wedge}$ to the experimental curve even though it has the following limitations,

(i) the model does not predict the flat-band behaviour because $v_s \neq 0$ when evaluating I_1 and I_2, although v_s can be negative or positive,

(ii) mobility μ was assumed to be independent of x,

(iii) in an intrinsic-like film it was assumed that the carrier mobility is given by the Hall mobility.

4.4.1.2 Three-dimensional surface model

Greene et al (G6) point out that when solving Poisson's equation in planar form, the spatial fluctuations in the potential are not taken into account because a uniform sheet charge is used instead of a more realistic array of point charges at the surface. In order to take into account the spatial fluctuations in the potential, they present a three-dimensional formulation of Poisson's equation for a non-degenerate electron gas with an array of localised charges on or near the semi-conductor surface. The main points of relevance of their paper are presented below.

If an array of point charges described by delta function on the surface of the semiconductor is giving rise to potential V(x,y,z) then Poisson's equation can be written as,

$$\frac{\partial^2 v}{\partial x^2} + \frac{\partial 2_v}{\partial y^2} + \frac{\partial^2 v}{\partial z^2} = \frac{q^2 n_b}{\epsilon kT} (\exp v - 1), \quad z > 0 \tag{4.27}$$

and

$$\frac{\partial^2 v}{\partial x^2} + \frac{\partial^2 v}{\partial y^2} + \frac{\partial^2 v}{\partial z^2} = 0 \qquad z < 0 \tag{4.28}$$

where

(i) semiconductor surface is at z = 0

(ii) $v = q \frac{(V(x,y,z)}{kT}$ (4.29)

(iii) ε= dielectric constant

Defining

$$L^{-2} = \frac{q^2 n_b}{\varepsilon kT} \tag{4.30}$$

equations (4.27) and (4.28) can be rewritten as,

$$\nabla^2 v = \frac{1}{L^2} (e^v - 1) \qquad z > 0 \tag{4.31}$$

$$\nabla^2 v = 0 \qquad z < 0 \tag{4.32}$$

Defining a correction term to the planar band-bending v_p as

$$\delta v(x,y,z) = v(x,y,z) - v_p \qquad (4.33)$$

equation (4.31) can then be rewritten in terms of the correction band-bending and planar band-bending as follows,

$$\nabla^2 \delta v = \frac{1}{L^2} e^{v_p} (e^{\delta v} - 1) \qquad (4.34)$$

Greene et al (G6) have shown that the correction term in equation (4.33) is always negative including at the surface (z = 0). In other words, for the same space charge density, the band-bending in the three-dimensional case is lower than that for the planar case. Commenting further on the inadequacies of the one-dimensional model, Levine (L6) observed that if the surface state density in an accumulation layer is greater than 3×10^{11} cm^{-2} (dielectric constant 5) then the planar potential seriously underestimates the amount of space charge possible. However, one may pose the question that in the context of R_H vs ρ curves, how does the choice between planar model and three-dimensional model influence,

(i) the shape of the R_H vs ρ curve, and

(ii) the magnitudes of R_H and ρ?

Hing (H1) developed an expression for a general function $F_g(v)$ (similar to the one defined by equation (4.8)) for different geometries of the band-bending and noted that

the shape of the band-bending merely modified the surface function defined by equation (4.8) by a constant of proportionality and since $F_g(v)$ did not alter the shape of R_H vs ρ curve, only the magnitudes of R_H and ρ would be affected. In other words, for corresponding values of R_H and ρ in the two cases, the band-bending in the case of the three-dimensional model will be smaller than that for the one-dimensional case, although the shape of R_H vs ρ curve will be similar for both cases.

4.4.2 Diffusion Model

Egerton and Juhasz (E2) first expressed their dissatisfaction with the surface model when explaining the long-term irreversible effect of O_2 on n-type PbTe films grown on mica and they offered the diffusion model as an alternative. The proposed model for O_2 uptake is schematically shown in Fig. 4.13. However, no mathematical formulation of the model was given by them. The diffusion model will now be examined.

As mentioned in the previous section, in the case of the surface model, the formation of the surface space charge region resulted in band-bending and the gas remained on the surface. In the case of diffusion, a shallow space charge region created during the initial stages of gas uptake penetrates further into the film as time goes on and eventually the gas enters into the bulk of the film where the driving force for diffusion of gas is the concentration gradient. Therefore in both

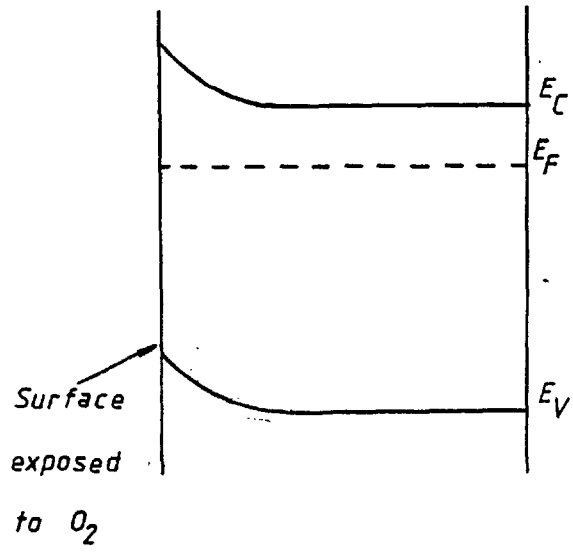

(a)

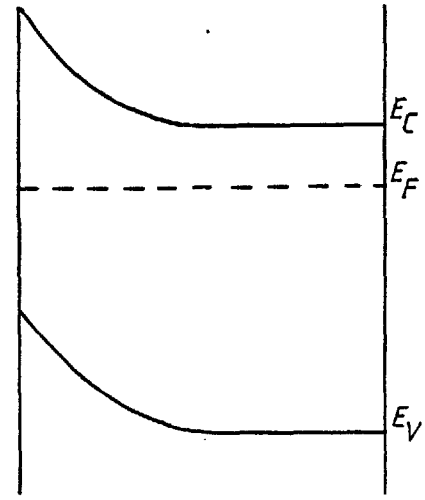

(b)

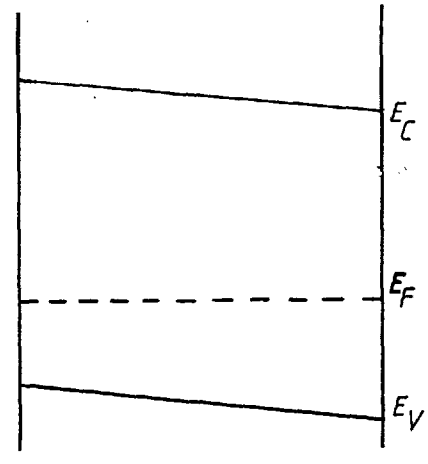

(c)

Fig. 4.13 Band bending due to O_2 effect on an n-type film after Egerton and Juhasz (E2). Progressive oxidation.

cases, there is band-bending at the surface. The diffusion model will now be described qualitatively taking the H effect on a p-type film as an example.

Due to the concentration gradient, H diffuses into the p-type film and acting as a donor neutralises the charge carriers (holes) near the surface giving rise to band-bending at the surface as shown schematically in Fig. 4.14(a). As the diffusion proceeds, H drives the surface of film n-type and the space charge region moves deeper into the p-type film. As the H exposure is continued, the n-type surface grows and penetrates further into the p-type bulk. In other words, the p-type bulk becomes separated from the n-type region by a space charge region as shown schematically in Fig. 4.14(b). This is effectively an advancing p-n junction within the film (J4). Eventually, the film is driven n-type (Fig. 4.14(c)). Therefore, the film which is initially p-type single carrier (Fig. 4.14(a)) becomes a two carrier film (Fig. 4.14(b)) before becoming a single carrier n-type film (Fig. 4.14(c)).

A quantitative description of the diffusion model will now be detailed below.

One may use Fick's Laws to describe a unidirectional diffusion process, i.e.

$$F = - D \frac{dC}{dx} \tag{4.35}$$

and

$$\frac{dC}{dt} = D \frac{d^2C}{dx^2} \tag{4.36}$$

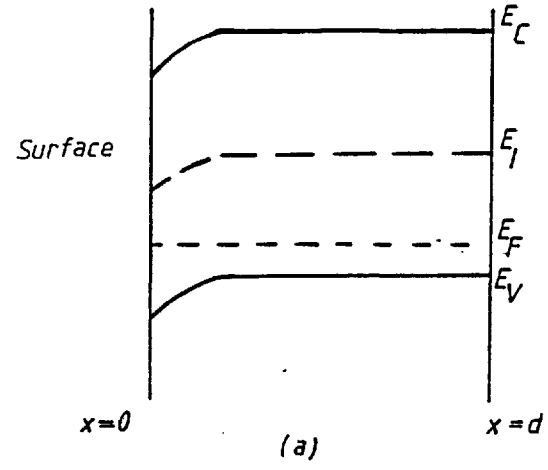

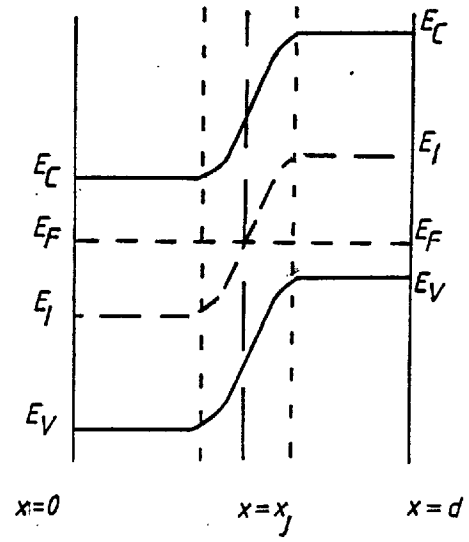

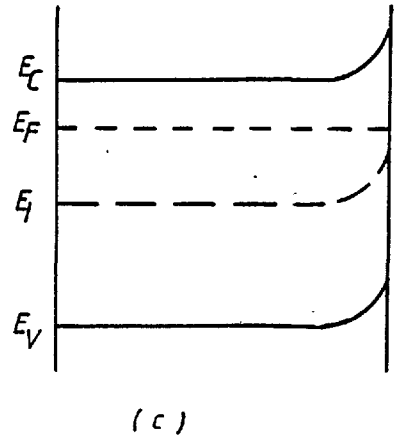

Fig. 4.14 H effect on a p—type film (schematic and idealised)

where

(i) F is the rate of transfer of the diffusant per unit area,

(ii) C is the concentration of the diffusing species,

(iii) D is the constant diffusion coefficient of the diffusant,

(iv) t is the time,

(v) x is the space coordinates along which diffusion is taking place.

The profiles of the diffusing species can be obtained by solving equation (4.36). Crank (C5) has given solutions of equation (4.36) for various practical situations subject to various boundary conditions. In the present case, shown schematically in Fig. 4.15, a film of thickness d is placed in an ambient with constant concentration C_1. Assuming that the initial concentration of the diffusant in the film is zero then the concentration C after time t at distance x within the film is given by (C5),

$$\frac{C}{C_1} = 1 - \frac{4}{\pi} \sum_{n=0}^{\infty} \frac{(-1)^n}{(2n+1)} \exp\left[- D \frac{(2n+1)^2 \pi^2 t}{4d^2} \right] \cos \frac{(2n+1)\pi x}{2d} \qquad (4.37)$$

where n is an integer. Equation (4.37) is plotted (C5) as a function of x and d for various times in Fig. 4.16. Equation (4.37) is rather awkward to handle when, for

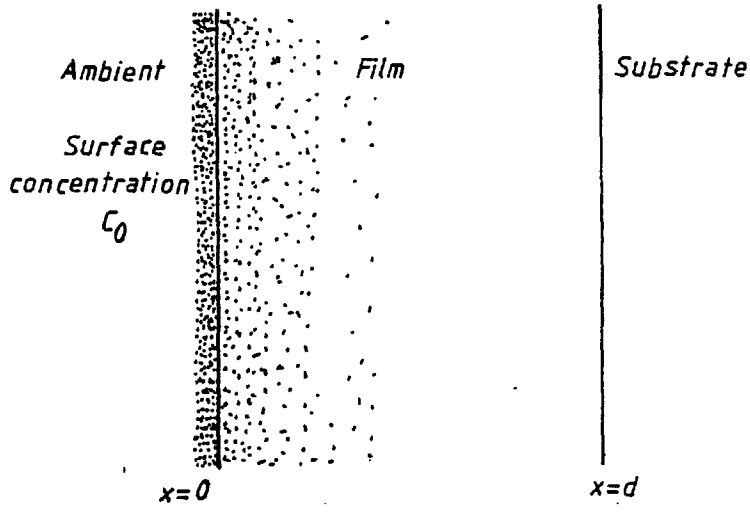

Fig. 4.15 Diffusion Model

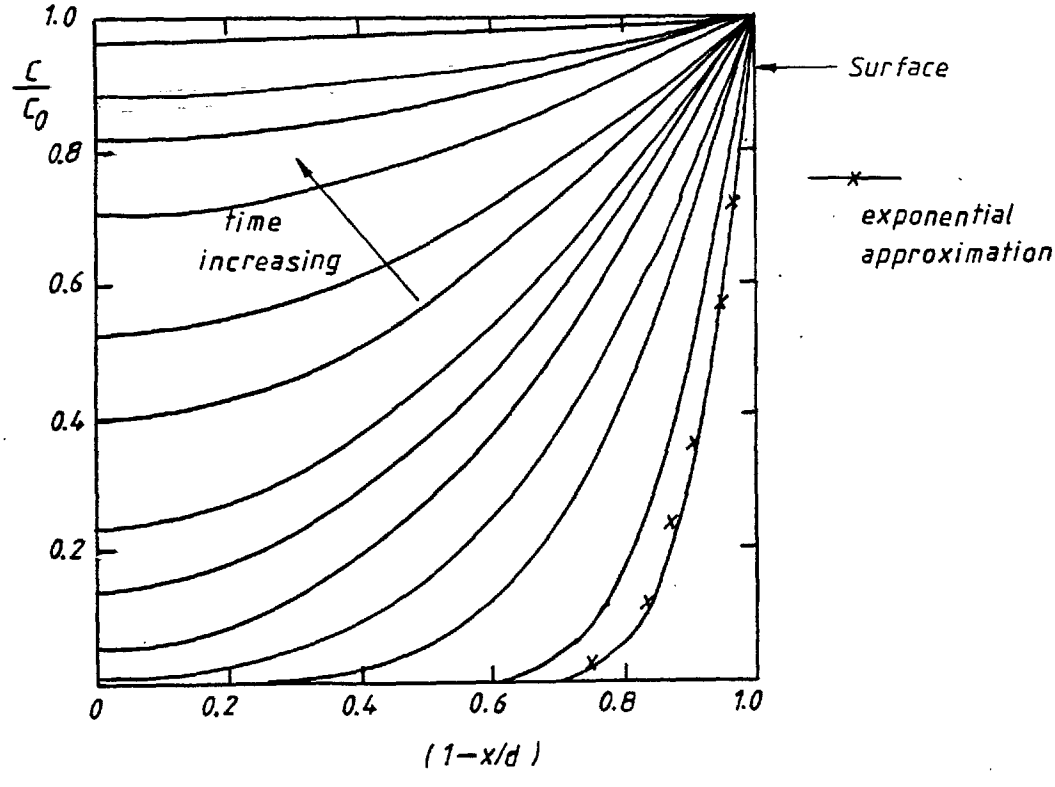

Fig. 4.16 Diffusion profile across the film after Crank (C5)

instance, developing expressions for R_H and ρ. Therefore it is desirable to simplify this equation or use a simpler approximation to it. An exponential approximation given by equation (4.38) was found to agree with equation (4.37).*

$$C(x) = C_o \exp - \frac{x}{\ell} \qquad (4.38)$$

where $\ell = 2\sqrt{Dt}$ and C_o is the surface concentration. Equation (4.38) is also plotted in Fig. 4.16 for comparison and as it can be seen, the approximation holds good especially for small times. Therefore equation (4.38) was used in the subsequent calculations.

The diffusion model will be considered in two parts. In the first part, single carrier films will be treated and the second part will deal with the two carrier films.

4.4.2.1 Single carrier films

In this sub-section, H effect on a p-type film ($p >> n_i$) will be considered as an example. Expressions for R_H and ρ will be developed. The theoretical curve of R_H vs ρ will be compared with the experimental R_H vs ρ curve of film S25.

As explained previously, the profile of the diffusing donors can be described by an exponential, i.e.

$$N_d(x) = N_o \exp - \frac{x}{\ell} \qquad (4.39)$$

---

* Error function approximation is more appropriate.

for a particular value of $\ell = 2\sqrt{Dt}$ where N_o is the surface concentration. The following assumptions are made.

(i) All impurities are fully ionised.

(ii) The acceptor carrier concentration N_a is homogeneously distributed throughout the film, i.e. $N_a(x) = N_a$.

(iii) The minority carrier concentration is negligible.

Since, in the present case, donors are diffusing into a p-type film the surface will be depleted of the charge carriers and the band-bending will be positive (i.e. downwards) - see Fig. 4.14(a).

$$\text{Charge density } \rho(x) = q(N_d(x) - N_a(x)) \qquad (4.40)$$

or

$$\rho(x) = qN_o\left[\exp(-\frac{x}{\ell}) - \frac{N_a}{N_o}\right] \qquad (4.41)$$

In order to develop expressions for R_H and ρ, an expression for band-bending $v(x)$ must be found for a particular value of ℓ. To do this, one may solve Poisson's equation. In the planar form Poisson's equation is,

$$\frac{d^2v}{dx^2} = -\frac{q\rho}{\varepsilon kT} \qquad (4.42)$$

where all the symbols have their usual meanings. From equations (4.41) and (4.42)

$$\frac{d^2v}{dx^2} = -\frac{1}{L_D^2}\left[\exp(-\frac{x}{\ell}) - \frac{N_a}{N_o}\right] \qquad (4.43)$$

where

$$L_D = \left(\frac{\varepsilon kT}{q^2 N_o} \right)^{\frac{1}{2}} \qquad \epsilon = \epsilon_o \epsilon_r \tag{4.44}$$

Equation (4.43) is solved in Appendix B.

From Appendix B,

$$v(x_j) = v(0) \pm A \left(\frac{\ell}{L_D} \right)^2 \tag{4.45}$$

where sign of A depends on the values of N_a and N_o.

Since $v(0) = v_s$ = surface band-bending

$$\therefore \quad v(x_j) = v_s \pm A \left(\frac{\ell}{L_D} \right)^2 \tag{4.46}$$

For a non-degenerate p-type semiconductor, carrier concentration at any point is given by (M4),

$$p = p_b \exp[-v(x)] \tag{4.47}$$

or

$$p = N_a \exp[-v(x_j)] \tag{4.48}$$

Since the film is considered to be single carrier type,

$$\therefore \quad \rho^{-1} = \sigma = e\mu_p p \tag{4.49}$$

and

$$R_H = \frac{1}{ep} \tag{4.50}$$

for particular values of ℓ and v_s.

Therefore, by adjusting ℓ and v_s a best fit curve of R_H vs ρ can be obtained. This has been done for film S25. Reasonable values of ℓ can be estimated provided that H diffusion coefficient, D_H in PbTe films at room temperature is known. The method adopted to evaluate ℓ will now be described.

Young (Y2) gives the following relationship for H diffusion coefficient, D_H in PbSe epitaxial films.

$$D_H = D_o \exp - \frac{E}{kT} \qquad (4.51)$$

where

E is the activation energy for diffusion

D_o is a constant (determined experimentally to be 1.1×10^{-7} cm^2 s^{-1})

Egerton and Crocker (E4) estimated D_H in PbTe epitaxial films to be $\sim 10^{-11}$ cm^2 s^{-1} at 170°C. Using D_H given by (E4) and D_o given by (Y2), E was estimated at 170°C. Using this value of E and D_o given by (Y2) in equation (4.51), D_H was evaluated at room temperature. This was found to be $\sim 6 \times 10^{-14}$ cm^{-2} s^{-1}. The values of ℓ could now be found since both D_H and t were known. For each estimated value of ℓ, v_s was adjusted to give the best fit curve. However, for a film to remain in the single carrier region, $v_s < E_g$ (band gap) was used as a constraint on the values of v_s. The value of N_o, the surface concentration of H, was determined in the following way.

When the film has been saturated with H, this is equivalent to the diffusion condition for $t \longrightarrow \infty$ and $N_d(x) = N_o$ (equation (4.39)). But the saturated donor concentration is determined from the measured Hall coefficient which also includes the concentration of donors neutralised by the initial acceptor concentration.

$$\therefore \quad N_o = N_a + N_\infty \tag{4.52}$$

where N_∞ is the 'saturation' value. The experimental and theoretical curves of R_H vs ρ of film S25 for second H cycle are shown in Fig. 4.17. The value of N_a prior to the H cycle was 3.7×10^{17} cm^{-3} and N_o was equal to 2.87×10^{18} cm^{-3}. μ_p was determined from the slope of the linear (single carrier regime) region of the experimental curve and was found to be 114 cm^2/V-sec. The values of v_s for the best fit curve are also shown in Fig. 4.17.

4.4.2.2 Two carrier films

In the present context, the films are considered to be in two carrier region if the carrier concentration determined by the Hall coefficient is low and comparable to the intrinsic carrier concentration.

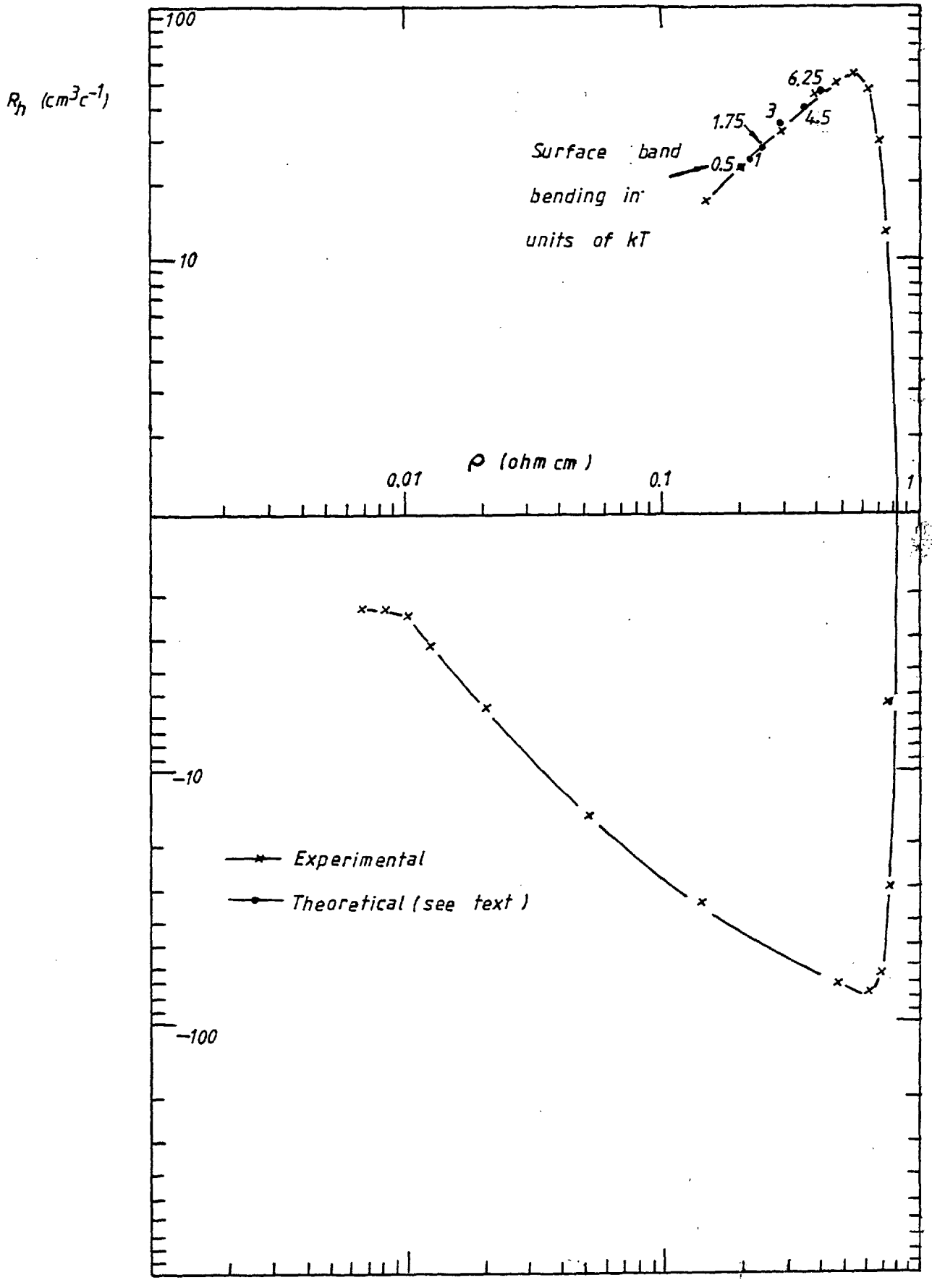

Fig. 4.17 2nd H cycle on film S25

4.4.2.2(a) Two-layer model

This model was proposed by McLane and Zemel (M2) and is shown in Fig. 4.18(a). They proposed that the film consists of a surface layer of thickness d_s and bulk of thickness d_b where the surface layer and the bulk are characterised in terms of R_H, μ and σ. Using Petritz's model (P9),

$$\sigma d = \sigma_b d_b + \sigma_s d_s \tag{4.53}$$

$$= q(C_b \mu_b d_b + C_s \mu_s d_s) \tag{4.54}$$

and

$$R_H \sigma^2 d = R_b \sigma_b^2 d_b + R_s \sigma_s^2 d_s \tag{4.55}$$

$$= q_b C_b \mu_b^2 d_b + q_s C_s \mu_s^2 d_s \tag{4.56}$$

where

(i) σ and R_H are the conductivity and the Hall coefficient of the two-layer (bulk and surface),

(ii) C is the carrier concentration,

(iii) d is the film thickness,

(iv) q is the electronic charge, -q for electrons and +q for holes,

(v) subscripts b and s refer to bulk and surface respectively.

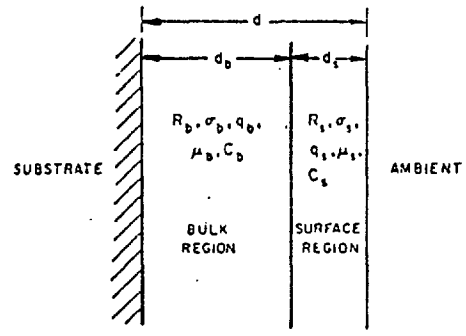

(a)

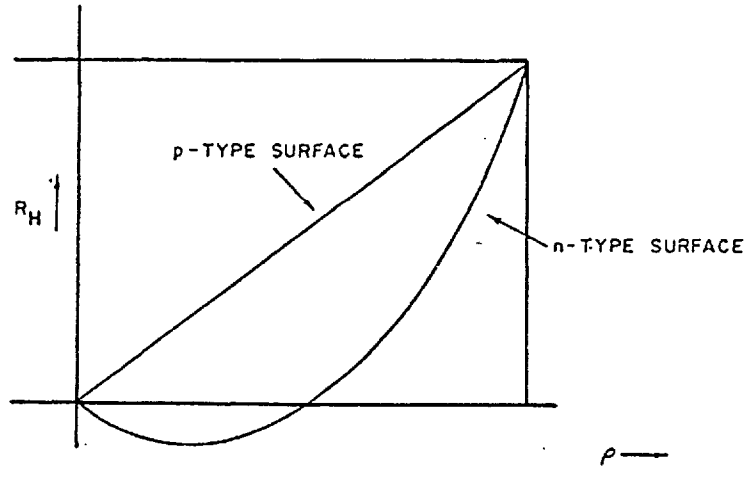

CASE I p-TYPE BULK

(b)

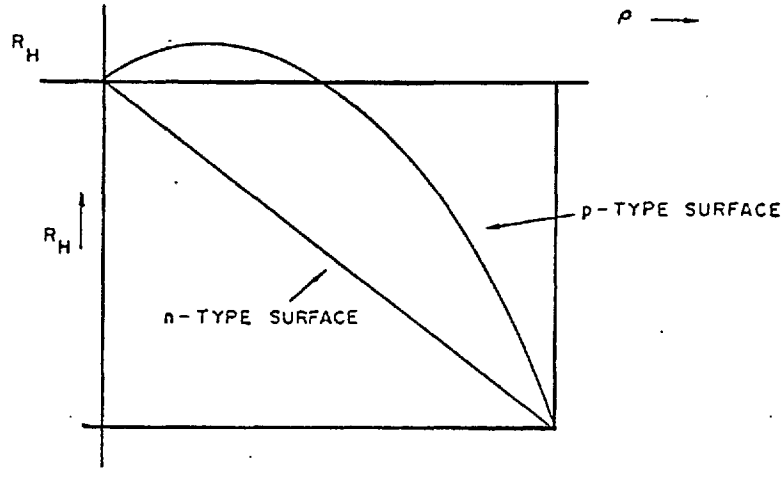

CASE II n-TYPE BULK

(c)

Fig. 4.18 Two layer model after McLane and Zemel (M2)

From equations (4.54) and (4.56)

$$R_H = \frac{q_s \mu_s \rho}{q} + \frac{C_b \mu_b d_b}{d} (q_b \mu_b - q_s \mu_s) \rho^2 \qquad (4.57)$$

Equation (4.57) can be examined for two types of bulk.

Case I - p-type bulk:

$$\therefore \quad q_b = e, \ \mu_b = \mu_p \text{ and } C_b = p_b$$

Therefore for a p-type bulk and p-type surface ($q_s = e$, $\mu_s = \mu_p$) equation (4.57) gives

$$R_H = \mu_p \rho \qquad (4.58)$$

which is a straight line with slope μ_p. However for p-type bulk and n-type surface ($q_s = -e$, $\mu_s = \mu_n$), equation (4.57) gives,

$$R_H = -\mu_n \rho + \frac{e p_b d_b \mu_p}{d} (\mu_n + \mu_p) \rho^2 \qquad (4.59)$$

which is a parabola.

Case II - n-type bulk:

$$\therefore \quad q_b = -e, \ \mu_b = \mu_n, \quad C_b = n_b$$

for a p-type surface ($q_s = e$, $\mu_s = \mu_p$)

$$R_H = \mu_p \rho - \frac{e n_b d_b \mu_n}{d} (\mu_n + \mu_p) \rho^2 \qquad (4.60)$$

and for n-type surface ($q_s = -e$, $\mu_s = \mu_n$)

$$R_H = -\mu_n \rho \qquad (4.61)$$

Fig. 4.18(b) and Fig. 4.18(c) show the schematic plots of R_H vs ρ for p and n-type bulk.

The model predicts rather idealised R_H vs ρ curves because it has the following limitations.

(i) The model assumes that the gas effect is limited to surface region only and the bulk of the film remains unaffected. Furthermore, surface width is considered to remain constant.

(ii) The effect of space charge region is neglected.

However, the model predicts some general features of experimental R_H vs ρ curves.

4.4.2.2.(b) Diffused layer model

The effect of H on p-type film will be considered here to develop the diffused layer model. As usual, expressions for R_H and ρ will be developed so that the experimental and theoretical R_H vs ρ curve could be compared. The following assumptions will be made.

(i) Effect of space charge region is neglected.

(ii) Effect of compensation is neglected.

(iii) μ_n and μ_p are not functions of distance x.

(iv) All impurities are ionised.

(v) All acceptors are homogeneously distributed throughout the film.

The distribution of carriers in the diffused layer is given by,

$$N(x) = N_d(x) - N_a(x) \tag{4.62}$$

and in the p-type bulk,

$$N_a(x) = N_a \tag{4.63}$$

The donor profile is

$$N_d(x) = N_o \exp - \frac{x}{\ell} \tag{4.64}$$

Using Petritz's model (P9),

$$\sigma d = \int_o^{x_j} e \mu_n N(x) \, dx + \int_{x_j}^{d} e \mu_p N_a(x) \, dx \tag{4.65}$$

where it is assumed that the diffused layer extends from $x = 0$ (surface) to $x = x_j$ and the p-type bulk from $x = x_j$ to $x = d$, where d is the film thickness. The value of x_j is given by,

$$x_j = \ell \, \ell n \, \frac{N_o}{N_a} \tag{4.66}$$

$$R_H \sigma^2 d = -\int_{x=0}^{x_j} e \mu_n^2 N_a(x) \, dx + \int_{x_j}^{d} e \mu_p^2 N_a(x) \, dx \tag{4.67}$$

Integration of equations (4.65) and (4.67) is carried out in Appendix C.

From Appendix C,

$$R_H = \frac{\frac{e\mu_p^2 N_a}{d}(d + A\ell) - \frac{e\mu_n^2 N_o}{d}(B\ell)}{\left(\frac{e\mu_p N_a}{d}(d + A\ell) + \frac{e\mu_n N_o B\ell}{d}\right)^2} \tag{4.68}$$

and

$$\sigma(\ell) = \rho^{-1} = \frac{e\mu_p N_a}{d}(d + A\ell) + \frac{e\mu_n N_o B\ell}{d} \tag{4.69}$$

where

$$A = \ell n\, N_a/N_o \text{ and } B = \left(1 - N_a/N_o + \frac{N_a}{N_o}\ell n\, \frac{N_a}{N_o}\right) \tag{4.70}$$

All other symbols in equations (4.68) and (4.69) have their usual meanings. From equations (4.68) and (4.69), R_H and ρ can be evaluated as functions of $\ell = 2\sqrt{Dt}$ and R_H vs ρ can be plotted. The model was tested for film S29 where μ_p was 121 cm^2/V-sec, μ_n = 274 cm^2/V-sec, $N_a = 5.69 \times 10^{16}$ cm^{-3}, N_o was 1.45×10^{18} cm^{-3} and d = 4438 Å. The theoretical and experimental curves of R_H vs ρ for film S29 are shown in Fig. 4.19. As it can be seen from Fig. 4.19, there is satisfactory agreement between the two curves.

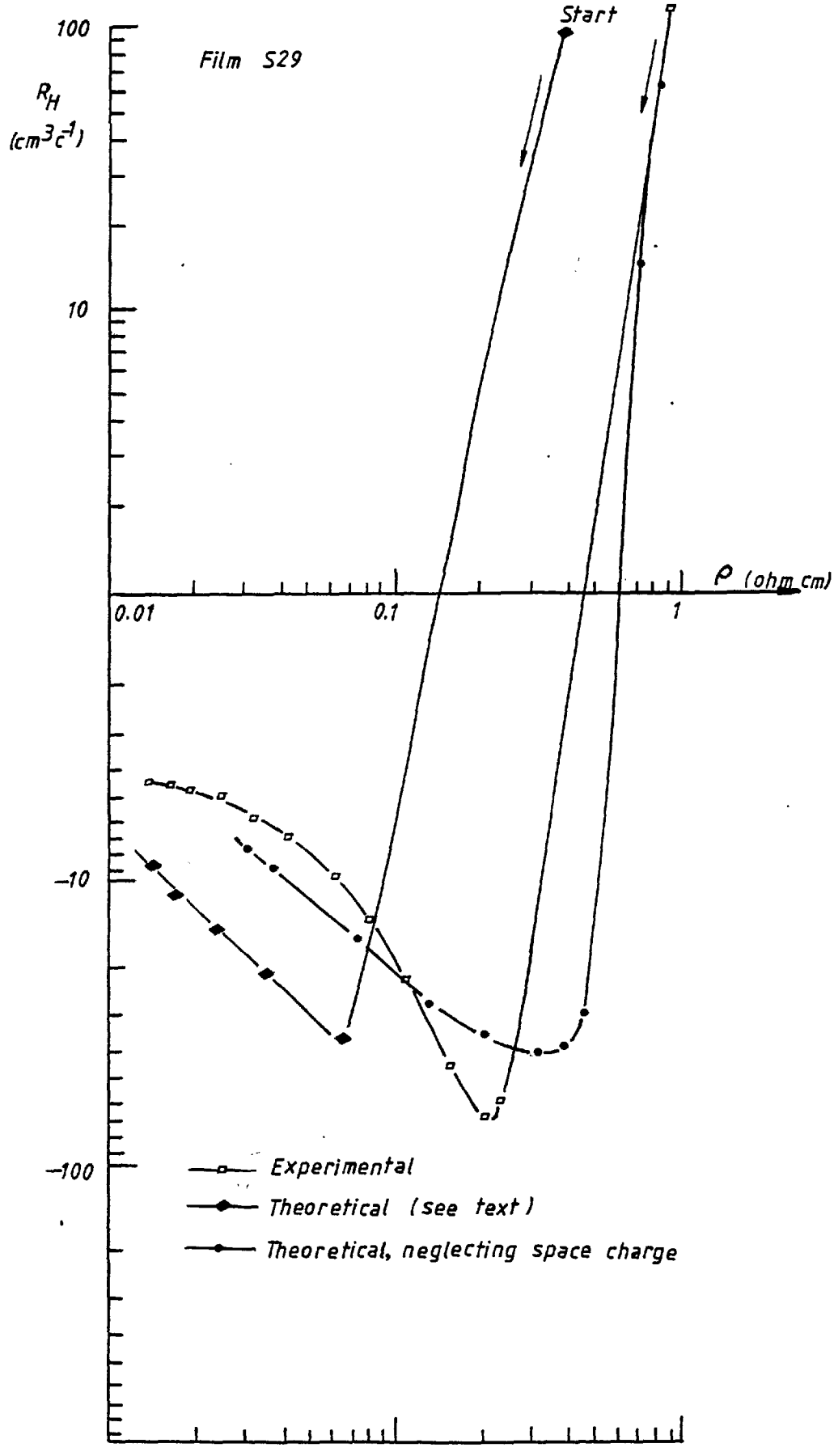

Fig. 4.19 Ist H cycle on film S29

4.4.2.2(c) Mobile p-n junction model

The major objection to the two models considered previously is that the space charge region which exists when donors diffuse into a p-type film is not taken into consideration. A model will now be discussed which takes into account the space charge region.

As mentioned in section 4.4.2, for prolonged diffusion of donors into a p-type film, the bulk of the film becomes separated from the n-type surface by a space charge region. This is similar to a moving p-n junction within the film. (See Fig. 4.14.) In common with the other models, expressions for R_H and ρ will now be developed for this model. The assumptions made are as follows.

(i) The diffusion coefficient D is constant.

(ii) p-n junction formed due to diffusion is approximated by a linearly graded junction of width W.

(iii) Charge neutrality exists on either side of the p-n junction.

(iv) Non-degeneracy is assumed and at equilibrium $pn = n_i^2$.

(v) All impurities are ionised.

(vi) μ_n and μ_p are independent of x.

(vii) Homogeneous distribution of all acceptors is assumed.

Consider the effect of H diffusion described by equation (4.39) into a p-type film. For charge neutrality to exist,

$$\rho(x) = 0 \tag{4.71}$$

or

$$p(x) - n(x) + N_d(x) - N_a(x) = 0 \tag{4.72}$$

where $N_a(x)$ is calculated from the measured Hall coefficient of the p-type film.

$$p(x)\, n(x) = n_i^2 \tag{4.73}$$

Eliminating p(x) by means of equations (4.72) and (4.73),

$$n(x) = \frac{1}{2}\left[N_d(x) - N_a\right] + \frac{1}{2}\left[(N_d(x) - N_a)^2 + 4n_i^2\right]^{\frac{1}{2}} \tag{4.74}$$

Eliminating n(x), gives

$$p(x) = \frac{1}{2}\left[N_a - N_d(x)\right] + \frac{1}{2}\left[(N_d(x) - N_a)^2 + 4n_i^2\right]^{\frac{1}{2}} \tag{4.75}$$

Using Petritz's model (P9) once again,

$$\sigma d' = \int_o^{d'} \sigma(x)\, dx = q\mu_n \int_o^{d'} n(x)\, dx + q\mu_p \int_o^{d'} p(x)\, dx \tag{4.76}$$

and

$$R_H \sigma^2 d' = q\mu_p^2 \int_o^{d'} p(x)\, dx - q\mu_n^2 \int_o^{d'} n(x)\, dx \tag{4.77}$$

where d´ is the effective film thickness given by equation (4.78)

$$d' = d-w \tag{4.78}$$

where d = actual film thickness

w = width of the depletion region

For a linearly graded junction, the depletion width w is given by (G7),

$$w = \left(\frac{12\ \varepsilon_r \varepsilon_o\ \phi}{qa} \right)^{1/3} \tag{4.79}$$

where

(i) ε_o is the permittivity of free space

(ii) a is the concentration gradient at the junction $x = x_j$

(iii) ϕ is the built-in voltage

All the other symbols have their usual meanings. From *(G7)*,

$$\phi = \frac{kT}{q}\ \ln\ \frac{N_a N_d}{n_i^2} \tag{4.80}$$

If the donor concentration on the n-side of junction is N_{dn} then a is given by,

$$a = \frac{N_{dn} - N_{dp}}{w} \tag{4.81}$$

Since no mobile charge carriers exist in the depletion width, one may account for the effect of the depletion width by subtracting it from the film thickness, i.e. $d' = d-w$. Therefore, in order to evaluate equations (4.76) and (4.77), effective thickness, d' of the film must be found. In other words, w must be evaluated as a first step. The following procedure was used to evaluate equations (4.76) and (4.77).

For an assumed value of the junction depth x_j, ℓ was calculated using equation (4.66) and for this value of ℓ, N_{dn} and N_{dp} were evaluated. ϕ and a were found from equations (4.80) and (4.81). Using these values of ϕ and a in equation (4.79), the depletion width w was evaluated for that particular value of the junction depth. Once w was known, d' was calculated from equation (4.78). Since d' was known, $\sigma d'$ and $R_H \sigma^2 d'$ could now be determined. This process was repeated for a series of increasing values of x_j. A computer program written by Hing (H1) was used to evaluate R_H and ρ.

The model was tested on film S29 and as it can be seen from Fig. 4.19, there is satisfactory fit between the shape of the theoretical and the experimental curve. To illustrate the inadequacy of the model in the single carrier regime, it was used to predict the theoretical R_H vs ρ curve for film S25 during second H cycle when the film was in single carrier region. This is shown in Fig. 4.11. It may be noted from Fig. 4.11 that no fit between the theoretical and the experimental curve exists.

A brief discussion of some of the assumptions made will now be presented.

(a) Ionisation of Impurities

For monovalent donors and acceptors, the degree of ionisation may be expressed as (B5),

$$N_a^- = \frac{N_a}{1 + \frac{1}{2}\exp\left(\frac{E_a - E_F}{kT}\right)} \tag{4.82}$$

and

$$N_d^+ = \frac{N_d}{1 + \frac{1}{2}\exp-\left(\frac{E_d - E_F}{kT}\right)} \tag{4.83}$$

where N_a and N_a^- are the densities of acceptors and ionised acceptors with energy level E_a in the forbidden band gap. Similarly N_d and N_d^+ are the densities of donors and ionised donors where E_d is the donor energy level. E_F is the Fermi level and $\frac{1}{2}$ is the spin degeneracy factor. Since no carrier freeze-out has been evident from the Hall effect measurements (C6) and the static dielectric constant of PbTe is high anyway, therefore it is reasonable to assume that all impurities are ionised at room temperature

$$\therefore \quad N_a \approx N_a^- \qquad N_d \approx N_d^+ \tag{4.84}$$

and charge neutrality gives

$$p + N_d^+ = n + N_a^- \tag{4.85}$$

$$\therefore \quad \text{for a p-type film } p = N_a^- = N_a \quad \left.\right) \text{ at}$$
$$\text{and} \qquad\qquad \left.\right) \text{ room}$$
$$\text{for an n-type film } n = N_d^+ = N_d \quad \left.\right) \text{ temperature} \qquad (4.86)$$

(b) Constant Diffusion Coefficient D

The temperature dependence of D has already been mentioned but this dependence is not crucial in the present case since the comparison between the theoretical and the experimental data was carried out at only one temperature (room temperature). However, D can also be dependent on the concentration of the diffusing impurities in addition to being field assisted where the electric field is due to the diffusion of ionised impurities and in the case of non-homogeneous materials, D may also vary with distance x.

When, for example, the diffusing impurities are donors, simultaneous diffusion of ionised donors and electrons must be considered. Since the mobilities of the two diffusing species are different, this will result in a built-in electric field where the field assists the diffusion of the slower species (Tl). Lehovec and Slobodskoy (L7) give an expression for effective diffusion coefficient, D_{eff} for the diffusion of a singly charged impurity into an intrinsic semiconductor. (In the present context, films in two-carrier regime.)

$$D_{eff} = D(1 + f) \qquad (4.87)$$

where

$$f = \frac{C/n_i}{\left[(C/n_i)^2 + 4\right]^{\frac{1}{2}}} \qquad (4.88)$$

D = field independent diffusion coefficient

C = concentration of the diffusing impurities

n_i = intrinsic carrier concentration (at diffusing temperature)

If $C \ll n_i$, $f \to 0$ and $D_{eff} \approx D$

If $C \gg n_i$, $f \to 1$ and $D_{eff} \approx 2D$

In other words, in the extreme case, the built-in field can effectively double the diffusion coefficient. Since neither C is known explicitly nor the dependence of D on the concentration of the diffusing donors (H) in the present case, it is difficult to make allowances for these factors affecting D. However, if D is known as a function of concentration then equation (4.36) can be written as (for unidirectional diffusion),

$$\frac{dc}{dt} = \frac{d}{dx}\left(D \frac{dc}{dx}\right) \qquad (4.89)$$

(c) Compensation Effect

If a semiconductor contains both donor and acceptor impurities it behaves as if only the difference between the two types of impurities were effective in an otherwise pure crystal. For example, a fully ionised p-type semiconductor, N_a may be compensated by donors, N_d giving an effective carrier concentration of $N_a - N_d$. It is likely that films may have been doped inadvertently during growth to give compensated films. Hing (H1)

considered the compensation effect for H diffusion into $Pb_{1-x}Sn_xTe$ thin films. For a p-type film with carrier concentration N_a^* compensated by donors N_{do}, the measured carrier concentration (N_a) from the Hall coefficient is given by,

$$N_a = N_a^* - N_{do} \tag{4.90}$$

For H diffusion into such a film, total donor concentration at any point x within the film will be,

$$N_d(x) = N_{do} + N_o^* \exp - \frac{x}{\ell} \tag{4.91}$$

where $N_o^* = N_a^* + N\infty$ (4.92)

and N_∞ is the 'saturation' donor concentration.

For an assumed donor compensation N_{do}, N_a^* can be calculated from equation (4.90) and then using N_a^* in equation (4.92), N_o^* can be determined. Using this value of N_o^* in equation (4.91), $N_d(x)$ can be evaluated. Equations (4.74), (4.75), (4.76) and (4.79) can be used to determine σ and R_H. Hing (H1) found that the theoretical curves were not significantly different from the curves where compensation effect was neglected and furthermore the shape of R_H vs ρ curves remained unaltered.

The diffusion model is shown schematically in Fig. 4.20 for different stages of diffusion. Distribution of the charge density is shown in Fig. 4.20(a) and the corresponding energy distribution diagrams and R_H vs ρ curves are shown in Fig. 4.20(b) and Fig. 4.20(c) respectively. During the initial stages of diffusion, the charge density distribution was as shown in Fig. 4.20(a,i) and the corresponding energy distribution diagram and R_H vs ρ curve was as shown in Fig. 4.20(b,i) and Fig. 4.20(c,i) respectively.

4.5 IONISATION OF H

The effect of H entering the PbTe lattice can be examined in terms of Parada-Pratt model (P10) where they considered the effect of introducing Pb and Te vacancies in PbTe. In their model, they consider the perturbing potential due to the vacancy (of Pb and Te) to be approximately the negative of the highly localised potential normally associated with the site. Since Pb has four valence electrons (the outer shell of Pb is $6s^2 6p^2$), it has the perturbing potential corresponding to a charge of -4 electrons. Therefore, introduction of a Pb vacancy into a perfect lattice will result in the loss of four valence electrons and two valence states and production of two holes in the valence band (P10). Similarly, for a Te vacancy ($5s^2 5p^4$), eight valence states

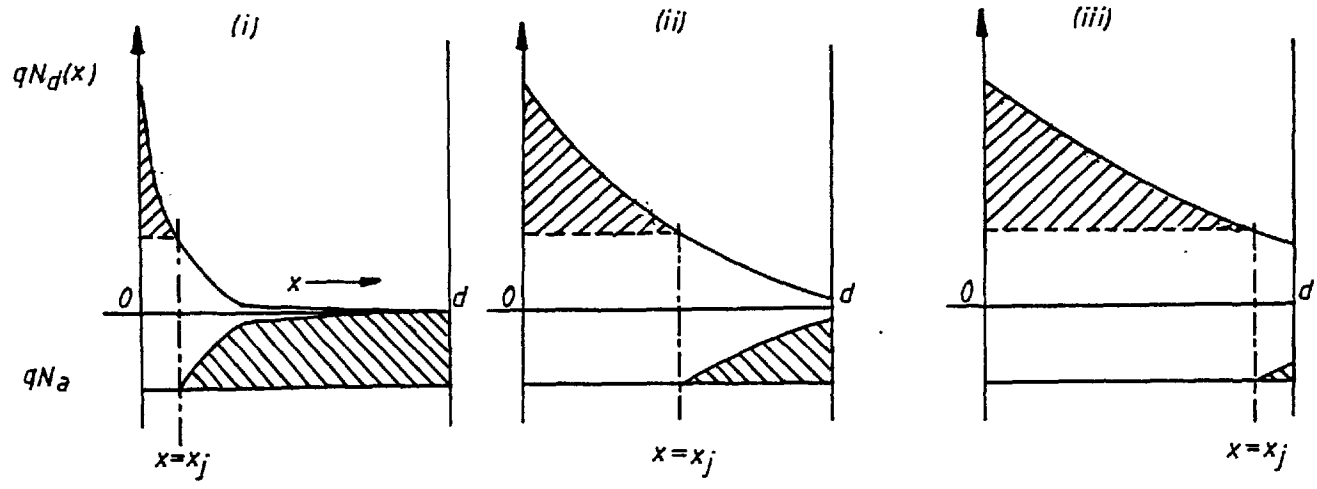

Charge – density distribution (a)

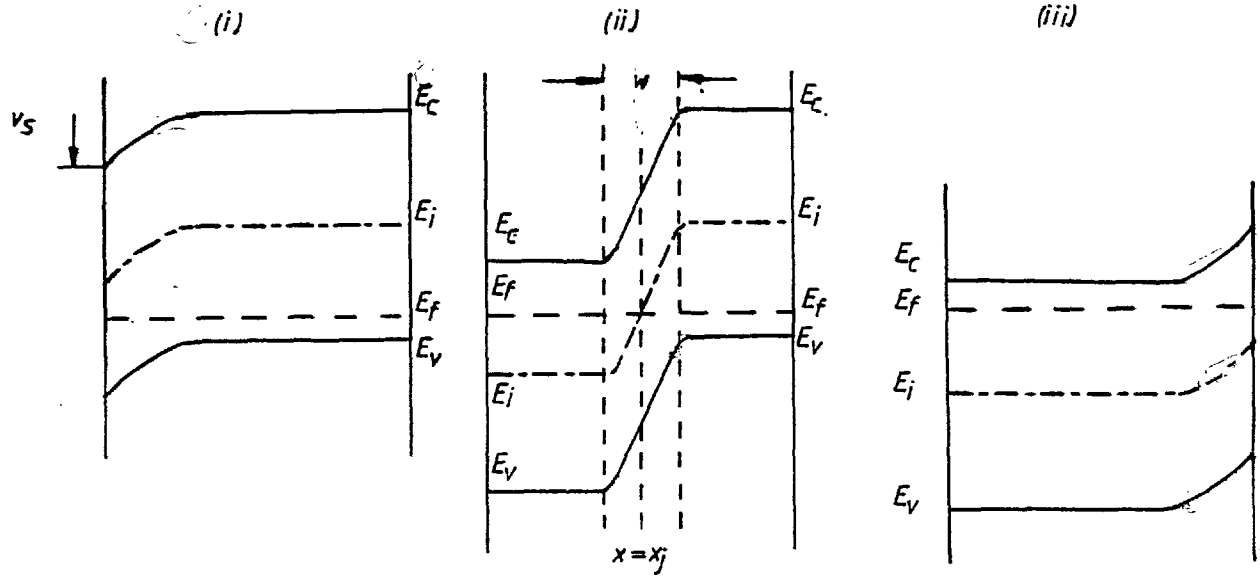

Energy distribution (b)

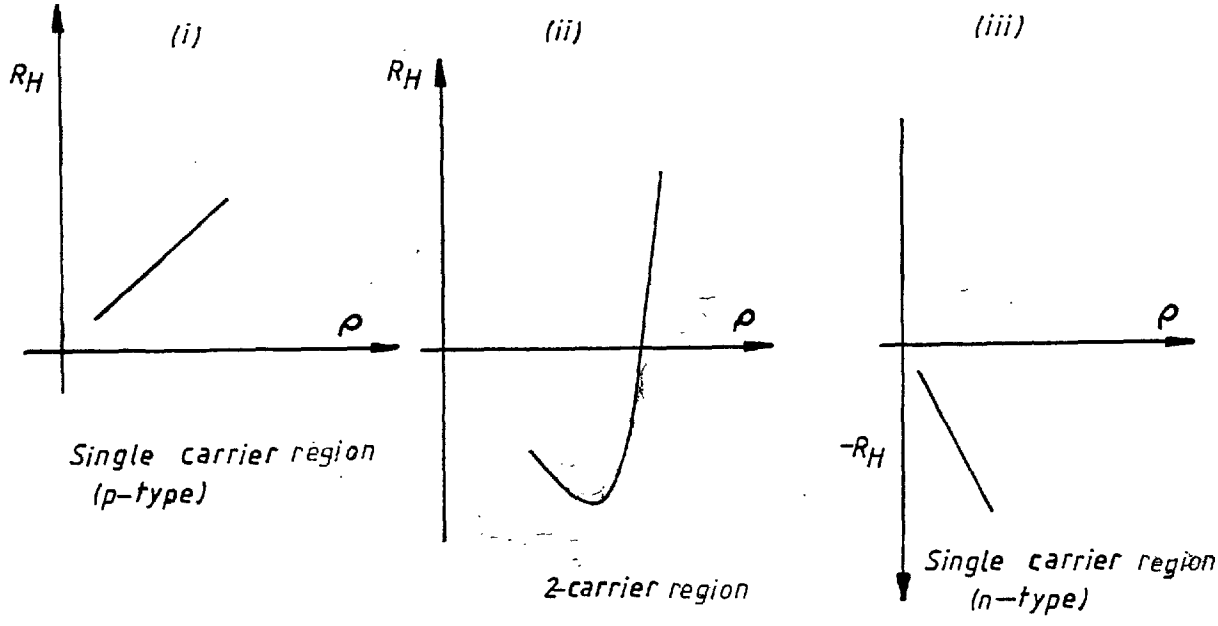

R_H vs. ρ (c)

Fig.4.20 Diffusion model (schematic). H effect on p-type film.

and six electrons are lost and two electrons are produced in the conduction band where the ionisation of Pb vacancy V_{pb}, and that of Te vacancy V_{Te} can be written as,

$$V_{pb} \rightarrow V_{pb}^{Z-} + Zh \qquad (4.93)$$

$$V_{Te} \rightarrow V_{Te}^{Z+} + Ze \qquad (4.94)$$

where Z is the level of ionisation (i.e. Z = 1, 2 etc.). Therefore ionised native defects can make PbTe n or p-type.

McLane and Zemel (M2) first considered the Parada-Pratt model to explain the ionisation of H in PbSe epitaxial films. If H atom occupies a V_{pb}, it produces a perturbing potential of -3e. This results in the removal of two valence states and three valence electrons and production of one hole. Therefore occupation of V_{pb} by H has resulted in the reduction of holes due to V_{pb} from 2 to 1 in the valence band which explains the donor-like effect of H in PbSe. Occupation of V_{Te} by an oxygen atom can be treated similarly. Since Te and oxygen belong to the same chalcogen family (outer shell of the form s^2p^4), the electrical effect of introducing an oxygen atom on to a Te vacancy is equivalent to reintroducing a Te atom and producing two holes in the valence band. Therefore, the vacancy model assumes that H and O_2 affect the electrical properties of lead salts when H and O_2 occupy V_{pb} and

V_{Te} respectively.

Re-examination of the vacancy occupation model was done by Zemel (Z4). He also considered the possibility of H entering the interstitial sites but rejected the idea on the basis that the changes introduced in the carrier concentration of lead salts would be far higher than experimentally observed. He concluded that H atom can only influence the carrier concentration when it occupies a V_{pb}. Further evidence of this model was produced by the mobility-temperature dependence observed for a film before and after the H effect. If H were an ordinary ionised impurity, it would have introduced an additional scattering factor for the H saturated film. However, the temperature dependence of mobility in both cases was identical which was understandable if H was destroying a hole by occupying a V_{pb} (Z4).

Consider the effect of H entering PbTe film. If the concentration of Pb vacancies is V_{pb} and C_H^+ is the concentration of ionised H at any point in the film, then the probability of H finding a V_{pb} is proportional to V_{pb} (i.e. $K V_{pb}$) and the probability of finding H on V_{pb} is C_H^+/V_{pb}. (This treatment is based on McLane-Zemel (M2) formulation.) This gives,

$$C_H^+ = C_H K V_{pb} \left(1 - \frac{C_H^+}{V_{pb}}\right) \qquad (4.95)$$

where C_H is the total concentration of H (both ionised and unionised) and $(1 - C_H^+/V_{pb})$ is the probability of V_{pb}

being unoccupied by H. From equation (4.95),

$$\frac{C_H^+}{V_{pb}} = \text{probability of finding H on } V_{pb} = \frac{KC_H}{1 + KC_H} \tag{4.96}$$

where K is a constant

when $KC_H << 1$, $\frac{C_H^+}{V_{pb}} \approx KC_H << 1$ (4.97)

i.e. most V_{pb} are unoccupied by H and C_H^+ is proportional C_H.

However, for H to turn an extrinsic p-type film n-type, there must be sufficient number of V_{pb} to compensate the hole concentration. Therefore, for a p-type film,

$$p = \frac{1}{R_H e} = 2 (V_{pb} - V_{Te}) \tag{4.98}$$

where Z = 2 has been assumed in equations (4.93) and (4.94) when H is introduced,

$$\frac{1}{R_H e} = 2V_{pb} - 2V_{Te} - C_H^+ \tag{4.99}$$

when all V_{pb} are occupied by H, (i.e. $C_H^+ = V_{pb}$)

$$\frac{1}{R_H e} = V_{pb} - 2V_{Te} \tag{4.100}$$

Therefore for a film to be n-type, R_H must be negative.

$$\therefore \quad V_{Te} > \frac{1}{2} V_{pb} \tag{4.101}$$

Since typical hole concentration was 10^{17}-10^{18} cm^{-3} in the present case and $V_{pb} \sim 10^{19}$ cm^{-3}*, equation (4.101) is easily satisfied.

In summary, the following points may be noted.

(i) It is reasonable to assume that when H occupies V_{pb}, it releases one of the two electrons trapped at the vacant site which as a result would increase the concentration of electrons in the conduction band by one or annihilate a hole in the valence band. Furthermore, if the vacancy-impurity interaction model is to be believed then H will affect the electrical properties of lead salts only if H occupies a V_{pb}.

(ii) When most V_{pb} are unoccupied by H (i.e. during the initial period of H exposure), C_H^+ is proportional to C_H.

(iii) Based on the above model, H can drive a p-type film n-type if the film is highly compensated.

---

* From (L8), Schottky constant $K_s = [V_{Pb}^{2-}][V_{Te}^{2+}] \simeq 10^{38}$ cm^{-6} at 1023K

4.6 DISCUSSION OF RESULTS

In this section, an attempt will be made to reconcile the experimental results with the theoretical models described in the previous sections.

4.6.1 (a) H Effect on O_2-driven P-type Films

Before discussing the mechanism of H-uptake, one may note the following general features of H effect on these films.

(i) H makes p-type film less p-type and drives n-type film more n-type. In other words, H has a donor-like effect on PbTe films.

(ii) The H effect and the desorption of O_2 from the surface of PbTe films is undistinguishable since R_H vs ρ dependence during re-evacuation and H cycle is the same provided the film remains in the single carrier region.

As explained in the previous section, when H occupies a lead vacancy V_{pb} it releases one of two electrons trapped at the site and H has effectively been ionised. Since H_2 had no effect on the electrical properties of PbTe films, it is reasonable to assume that only one hydrogen atom can occupy V_{pb} where the energy to dissociate H_2 into H atoms has been provided by the tungsten filament. The interaction between H and

tellurium to form H_2Te was suggested by Egerton and Crocker (E4).

$$2H + Te^{x}_{Te} \rightarrow H_2Te + V^{\cdot}_{Te} + e \qquad (4.102)$$

where $V^{\cdot}_{Te}$ is a singly charged tellurium vacancy. But they rejected this possibility since the loss of volatile H_2Te would make the process irreversible and no desorption should be evident.

The surface model for H-uptake was tested on film S25 (Fig. 4.11) and it gave a very good fit for the linear portion of the R_H vs ρ curve and the fit became poor as the film moved into the two carrier region. The diffusion model developed in section 4.4.2.1 also gave a very good fit for the linear region (Fig. 4.17). Therefore, during the initial stages of H exposure it is difficult to distinguish between the two models. However, it is more reasonable to believe that the surface model applies during the initial stages of H exposure and the diffusion model during the latter stages.

4.6.1 (b) H Effect on P-Type 'Virgin' Films

Unfortunately, it was not possible to grow single carrier 'virgin' p-type films and all the 'virgin' p-type films had low carrier concentrations comparable to the intrinsic carrier concentration, i.e. the films were two-carrier type. When such films were exposed to H, there was no initial increase in R_H and ρ values

(Fig. 4.7) and the films turned n-type rather quickly (see Table 4.2). This is expected since the excess hole concentration to be neutralised by H is much smaller (compared to the single carrier case) due to much smaller difference between the concentrations of ionised V_{pb} and V_{Te}. But it is difficult to explain such a quick change-over from p-type to n-type by surface model or even the diffusion of H down short circuit paths such as grain boundaries and dislocations because in the latter case the mechanism of H ionisation remains unclear.

Leaving the kinetics aside for the moment, the diffusion model incorporating the mobile p-n junction does predict the correct shape for the experimental R_H vs ρ curve. There is a discrepancy between the theoretical and the experimental values of ρ where the theoretical values are underestimated.* This may be so because the width of the depletion region has been subtracted from the actual film thickness to evaluate ρ, i.e.

$$\rho_c = \rho_e \left(\frac{d-w}{d}\right) = \rho_e \left(1 - \frac{w}{d}\right) \qquad (4.103)$$

where ρ_c is the calculated value, ρ_e is the experimental value, w is the width of the depletion region and d is the film thickness. Since (1-w/d) is less than unity, $\rho_c < \rho_e$.

---

* *Suitable adjustment of parameters like w should give a better fit.*

4.6.1 (c) H Effect on 'Virgin' N-type Films

All such films were driven more n-type when exposed to H where R_H and ρ decreased linearly keeping the Hall mobility almost constant. This is consistent with the donor effect of H on PbTe films. Once again, the surface model is expected to apply during the initial stages where an accumulation layer is formed on n-type bulk followed by some in-diffusion of H. Films are considered saturated with H when all the lead vacancies have been occupied.

4.6.1 (d) H Effect on O_2-driven P-type Films at 50°C

Both films S25 and S36 were put through H-O_2 cycles at room temperature before H cycle at 50°C was carried out. Therefore, it was possible that when these films were heated up to 50°C (prior to H cycle) in a vacuum of $\sim 10^{-6}$ τ, some out-diffusion of H previously incorporated into the films had occurred. This made the films more p-type as evidenced by the decrease in values of R_H and ρ (regions BC and FG in Fig. 4.9).

4.6.2 (a) O_2 Effect on N-type Films (H Saturated)

Even though the paths traversed by R_H vs ρ curves are not the same during the H and O_2 exposures and the duration of the gas exposure to turn a p-type film n-type and vice versa is different, the effect of O_2 on H saturated film can essentially be described as the reversal of H effect especially during the initial stages of

O_2 cycle. When a H saturated film was left in vacuum ($\sim 10^{-6}\tau$) at room temperature both R_H and ρ started to increase showing that carrier concentration was decreasing. In other words, some desorption of H was occurring where the desorption of H could take place in the form of either H_2 (Z4) or H_2O (E4). The possibility of H recombining with O_2 on the surface to form H_2O which would then be desorbed was confirmed by Young (Y2). Therefore, it is reasonable to suggest that when H saturated films are exposed to O_2, H is removed from the film in the form H_2O which is desorbed at the surface. This has the effect of making such films less n-type. During the initial stages the O_2-uptake is fast and irreversible. During the latter stages of the gas cycle, the rate of O_2 uptake was slower. When the films became p-type on exposure to O_2 at atmospheric pressure, some of the O_2-uptake was reversible by re-evacuation of the vacuum system.

4.6.2 (b) O_2 Effect on 'Virgin' N-type Films

As it can be seen from Table 4.1, when a 'virgin' n-type film was left in vacuum ($\sim 10^{-6}\tau$), it became less n-type. This can be explained by the formation of the space charge region on the surface of the film. In this case, the surface region was being depleted of the mobile carriers.

When film S47 (Fig. 4.5) was exposed to O_2, $|R_H|$ began to decrease instantly whereas ρ was almost constant. Since the film is in two carrier region, it is difficult to say whether changes in R_H are due to changes in the carrier concentration or carrier mobility. Once the film was driven p-type and into the single carrier region, both R_H and ρ decreased linearly to keep the Hall mobility almost constant. When the film was exposed to O_2 at atmospheric pressure and re-evacuated, some desorption of O_2 from the surface occurred as evidenced by the increase in R_H and ρ values.

4.6.2 (c) O_2 Effect on 'Virgin' P-type Films

Film S51 (Fig. 4.8) illustrates this case. As expected, an originally p-type film became more p-type when exposed to O_2. In terms of the surface model, an accumulation region was being formed on the surface of the p-type film.

A further discussion of these results will be presented in the next chapter.

CHAPTER 5

KINETICS STUDIES

5.1 INTRODUCTION

The variation of the Hall coefficient as a function of resistivity was discussed in the previous chapter. In order to gain further insight into the mechanism of gas-uptake, the changes in the Hall coefficient and resistivity as a function of time were also studied. The results of these kinetic studies will be presented in this chapter. Once again, an attempt will be made to interpret the experimental data in terms of the two models discussed in the previous chapter, namely surface adsorption model and diffusion model.

5.2 RESULTS AND CALCULATIONS

Before describing the results, some general characteristics of the R_H vs ρ curve will be discussed first.

Fig. 5.1 shows a schematic R_H vs ρ curve. Regions AB and ED are the single carrier regions (p-type and n-type respectively). In these regions, the R_H vs ρ dependence is linear and from the slopes of AB and ED the Hall mobility of holes and electrons respectively can be deduced. The measure of gas-uptake in these regions is reflected in the changes of the respective carrier

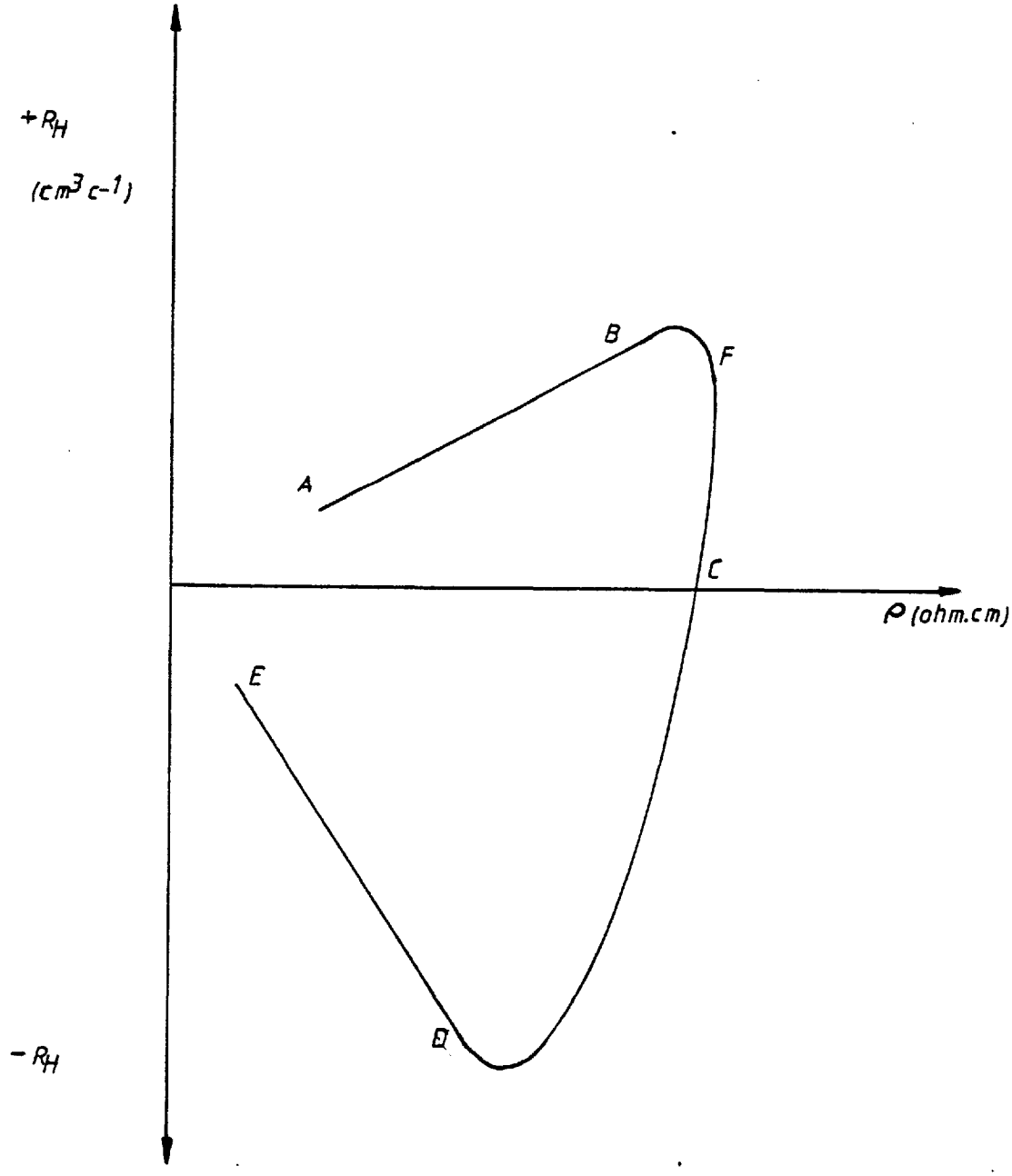

Fig. 5.1 Schematic R_H vs. ρ Curve

concentrations. In the regions BC and CD, it is a two carrier film (p-type and n-type respectively) and the measure of gas-uptake can no longer be interpreted in terms of the changes in carrier concentration because the Rσ product also varies in these regions. Therefore, the kinetic studies in the present case were restricted to the linear regions of the R_H vs ρ curve.

Let us consider the effect of H cycle starting at A (Fig. 5.1). Since H effectively reduces the carrier concentration of a p-type film, both R_H and ρ will increase.

$$\therefore \quad \text{at time } t = t_1 \ , \quad p_1 = \frac{1}{R_{H_1} e} \tag{5.1}$$

$$\text{and} \quad \text{at time } t = t_2 \ , \quad p_2 = \frac{1}{R_{H_2} e} \quad \text{where } t_2 > t_1 \tag{5.2}$$

$$\therefore \quad \Delta P = p_2 - p_1 = \frac{1}{e}\left[\frac{1}{R_{H_2}} - \frac{1}{R_{H_1}} \right] \tag{5.3}$$

Writing R_H in the planar form,

$$\Delta P = \frac{d}{e}\left[\frac{R_{H_1} - R_{H_2}}{R_{H_1} R_{H_2}} \right] \text{cm}^{-2} \tag{5.4}$$

where d is the film thickness in cm and e is the electronic charge.

Since $R_{H_2} > R_{H_1}$, ΔP is negative. Therefore, for H effect on single carrier p-type films, -ΔP vs time will be plotted.

When considering the H effect on 'virgin' n-type films, the relevant part of the R_H vs ρ curve is ED. Since H has a donor-like effect, both $|R_H|$ and ρ will decrease.

$\therefore$ equation (5.4) becomes

$$\Delta N = \frac{d}{e}\left[\frac{R_{H_1} - R_{H_2}}{R_{H_1} R_{H_2}}\right] \qquad (5.5)$$

In this case $R_{H_2} < R_{H_1}$ $\therefore$ ΔN is positive.

Therefore, for H effect on 'virgin' films ΔN vs time will be plotted.

Let us now consider the effect of O_2 on H saturated n-type films. In this case the cycle will commence at E (Fig. 5.1). As observed in the previous chapter, O_2 makes n-type film less n-type and both $|R_H|$ and ρ increase during the initial stages of the gas exposure.

$\therefore$ from equation (5.5)

$$\Delta N = \frac{d}{e}\left[\frac{R_{H_1} - R_{H_2}}{R_{H_1} R_{H_2}}\right]$$

where $R_{H_2} > R_{H_1}$ and $\therefore$ ΔN is negative.

Therefore, for O_2 effect on H saturated n-type films $-\Delta N$ vs time will be plotted. However, for O_2 effect on 'virgin' p-type films, ΔP will be positive.

$$\therefore \quad P = \frac{d}{e}\left[\frac{R_{H_1} - R_{H_2}}{R_{H_1} R_{H_2}}\right]$$

and $R_{H_2} < R_{H_1}$ in the present case.

For a unidirectional diffusion in the x-direction,

$$\frac{dC}{dt} = D \frac{d^2C}{dx^2} \tag{5.6}$$

where D is the diffusion coefficient (assumed to be concentration independent) of the diffusing species, C is the concentration of the diffusant and t is the time. Solutions of equation (5.6) exist for various practical situations. For diffusion from a constant source into a semi-infinite medium equation (5.6) has the solution (B6),

$$C(x,t) = C_o \text{ erfc } \frac{x}{2\sqrt{Dt}} \tag{5.7}$$

where C_o is the constant surface concentration and erfc is the complementary error function. The area under the curve defined by equation (5.7) gives the amount of the diffused species after time, t.

$$Q(t) = \int_o^\infty C(x,t)dx \tag{5.8}$$

$$\therefore \quad Q(t) = 2C_o \left(\frac{Dt}{\pi}\right)^{\frac{1}{2}} \tag{5.9}$$

Therefore, amount of diffused impurity is proportional to $t^{\frac{1}{2}}$. In order to see whether H uptake was a diffusion limited process, kinetics of the gas-uptake were plotted using $t^{\frac{1}{2}}$ dependence. Oxygen kinetics were plotted using

a $\ell n(t)$ dependence[M2,Z4]. H and O_2 kinetics will now be described for both n- and p-type films, including the films discussed in chapter 4.

5.2.1 H Kinetics

Fig. 5.2 shows the kinetics of H-uptake when 'virgin' n-type films were exposed to it. As can be seen from the figure, $t^{\frac{1}{2}}$ dependence is followed by all the films after the initial faster rate of uptake which implies that the mechanism of gas-uptake is diffusion limited. An estimate of the diffusion coefficient can be made as follows.

Rewriting equation (5.9) in the present context,

$$\Delta N = 2N_o \left(\frac{Dt}{\pi}\right)^{\frac{1}{2}} \qquad (5.10)$$

$$\therefore \text{ Slope of } \Delta N \text{ vs } t^{\frac{1}{2}} = 2N_o\left(\frac{D}{\pi}\right)^{\frac{1}{2}} \qquad (5.11)$$

$$\text{or} \qquad D = \pi\left(\frac{\text{Slope}}{2N_o}\right)^2 \qquad (5.12)$$

where N_o is the value when $t \to \infty$, i.e. the 'saturation' value which can be determined experimentally.

Estimated values of D are shown in Table 5.1.

H-uptake was investigated for some films at temperatures higher than the room temperature. This was not an exhaustive investigation since (as mentioned in chapter 4) no adequate facility was available to heat the films while situated in between the poles of the electromagnet. Fig. 5.3 shows the H-uptake at 50^oC

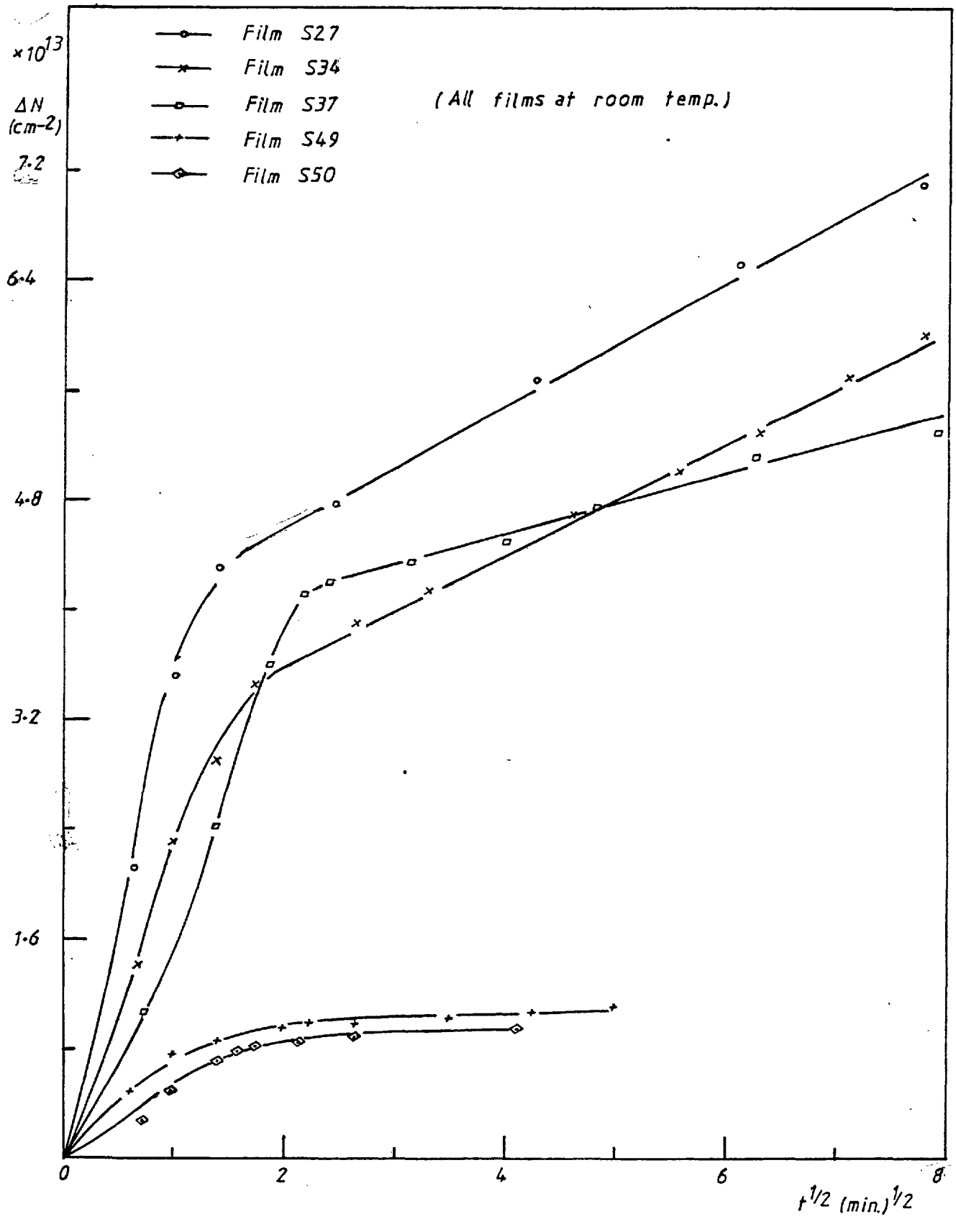

Fig.5.2 H-kinetics of 'virgin' n-type films.

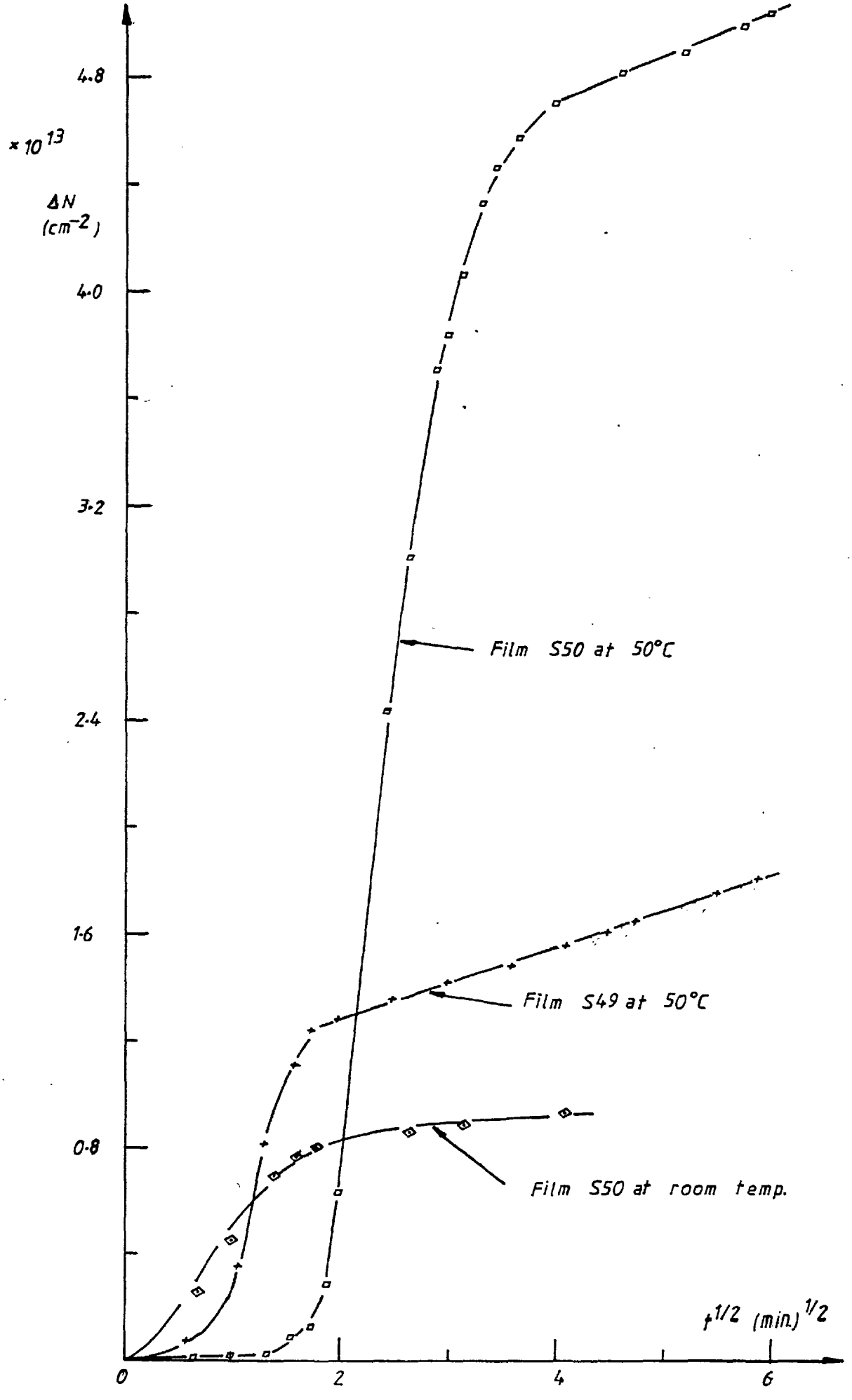

Fig. 5.3 H-kinetics of n-type films

for two n-type films (S49 and S50). Films S49 and S50 were 'virgin' n-type. These films were first exposed to H at room temperature. After 'saturation' had been reached, the films were exposed to O_2 and eventually let up to air at atmospheric pressure. Both films remained n-type. The system was pumped down and the second H exposure was carried out at 50°C. As can be noted from Fig. 5.3, the initial gas-uptake at 50°C is slower but during the latter stages of the gas exposure, both the amount of H-uptake and its rate of uptake is higher than that for room temperature. The estimated values of D at 50°C were 9.9×10^{-15} cm^2s^{-1} and 1.14×10^{-14} cm^2s^{-1} for S49 and S50 respectively (see Table 5.1 for room temperature values of D). Invoking an exponential temperature dependence of D,

$$D = D_o \exp - \frac{E_a}{kT} \qquad (5.13)$$

value of effective activation energy E_a can be calculated. In the case of S49, E_a was 0.34 eV whereas for S50 it was 0.4 eV.

Fig. 5.4 shows the effect of interrupting H cycle in the case of a 'virgin' n-type film, S66. When the tungsten filament was switched on to atomise H_2, $|R_H|$ decreased rapidly initially but more slowly as time progressed. When the filament was switched off, $|R_H|$ increased. However, the rate of increase of $|R_H|$ during the 'off' period was slower than the rate of decrease of

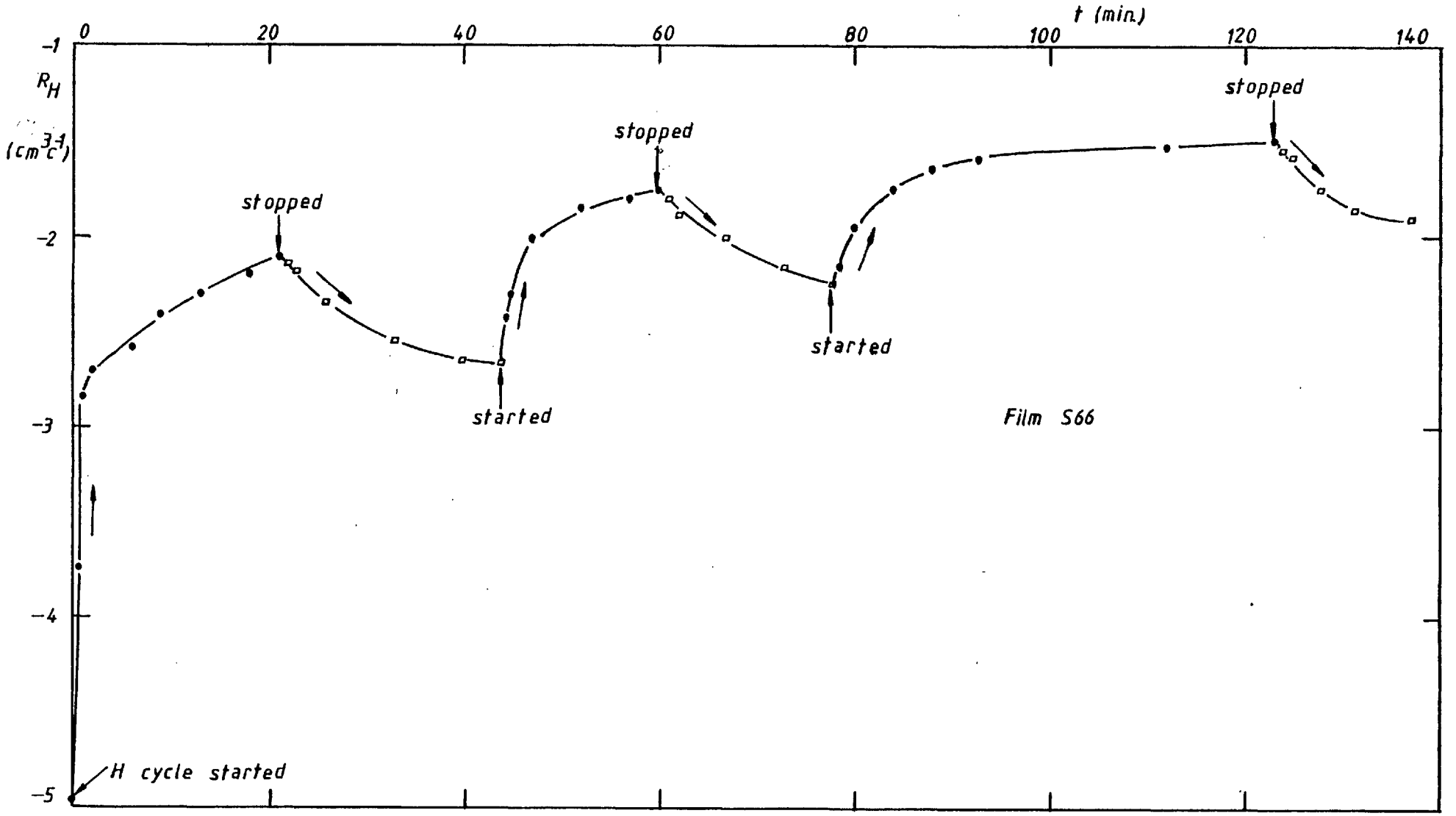

Fig. 5.4 Interrupted H cycles on a 'virgin' n-type film

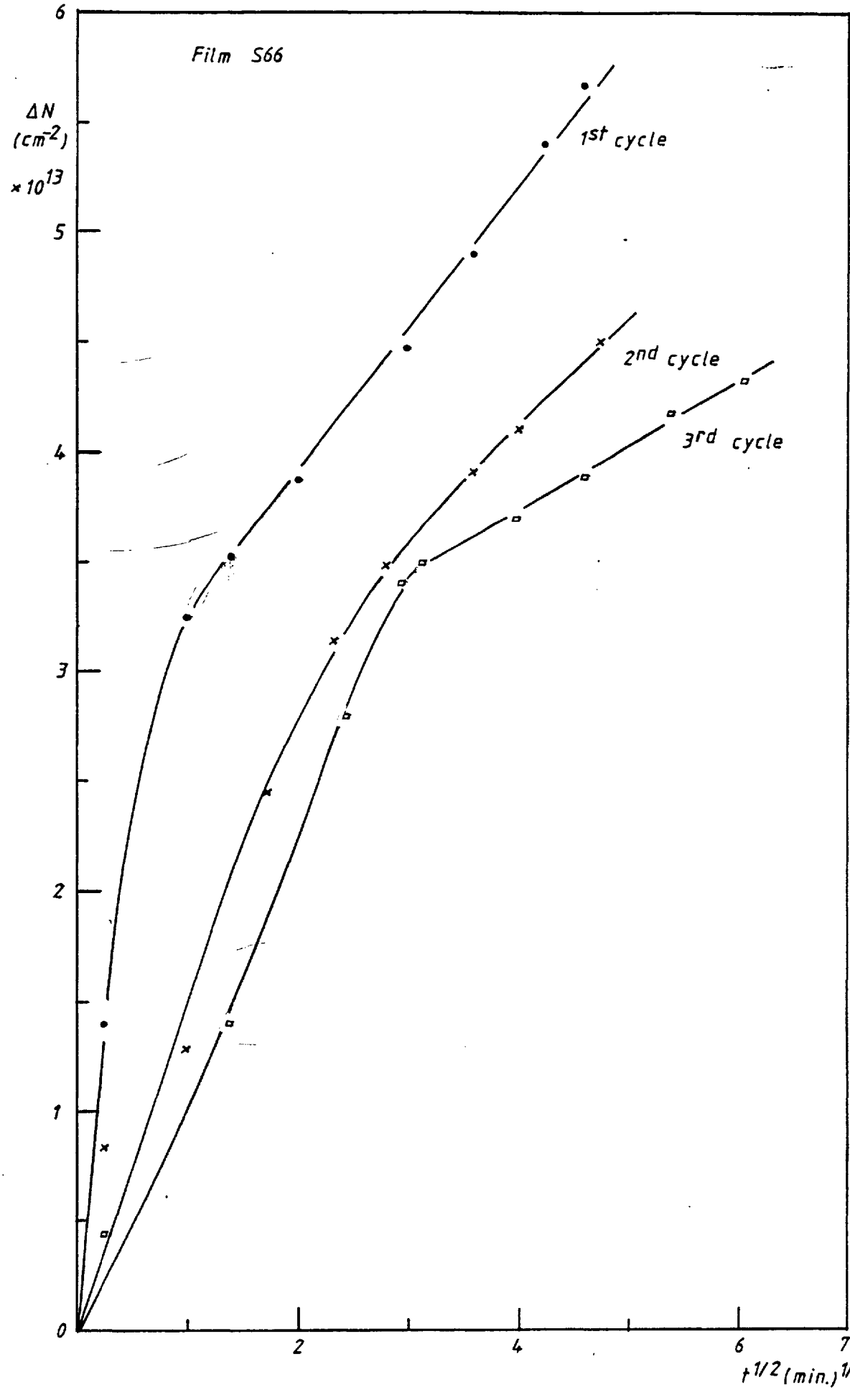

Fig. 5.5 Interrupted H-kinetics of a 'virgin' n-type film

$|R_H|$ during the period the filament was on. A graph of ΔN vs $t^{\frac{1}{2}}$ for these interruptions is shown in Fig. 5.5. The slopes of first, second and third cycle were 8.3×10^{11} $cm^{-2}s^{-\frac{1}{2}}$, 6.8×10^{11} cm^{-2} $s^{-\frac{1}{2}}$ and 3.8×10^{11} $cm^{-2}s^{-\frac{1}{2}}$ respectively which meant that the rate of gas-uptake became progressively slower with each cycle.

Shown in Fig. 5.6 are the kinetics of H-uptake for O_2-driven p-type films. Compared with 'virgin' n-type films, both the rate and amount of gas uptake was smaller. A summary of these results is shown in Table 5.2.

5.2.2 O_2 Kinetics

The kinetics described first are concerned with H saturated n-type films.

In Fig. 5.7, a graph of $-\Delta N$ vs ℓnt is shown for two films, S6 and S7. These were air-exposed prior to H cycle and the films remained n-type even after long air exposures at atmospheric pressure. Both of these films followed ℓnt dependence.

Fig. 5.8(a) and Fig. 5.8(b) show the kinetics of O_2-uptake for films S25 and S33. In both cases, the rate of gas-uptake was higher for the first cycle. As the films were cycled through H-O_2 cycles, the amount of gas-uptake decreased and it followed ℓnt dependence more faithfully. The pressure dependence of O_2 kinetics for H saturated n-type film S50 is shown in Fig. 5.9.

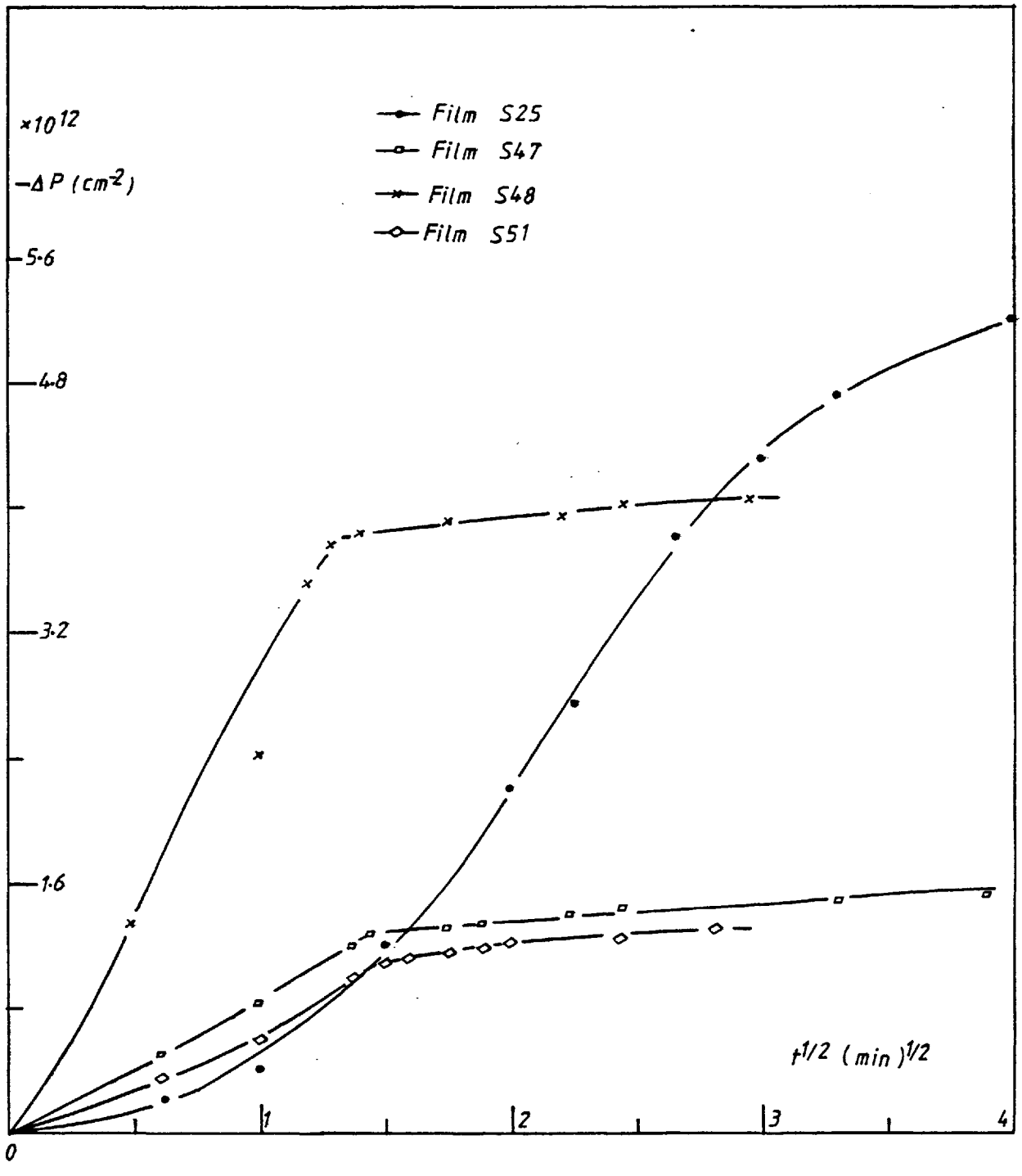

Fig. 5.6 H-kinetics of O_2-driven p-type films.

Film	Conductivity type (virgin)	Deposition temperature ^{o}C	Film Thickness $\overset{o}{A}$	Slope = $\frac{d\Delta N}{dt^{\frac{1}{2}}}$ $cm^{-2}sec^{-\frac{1}{2}}$	Diffusion Coefficient, D cm^2/sec	$pH_2 x10^{-4}$ torr
S27	n-type	250	2940	5.78×10^{11}	3.63×10^{-14}	2
S34	n-type	200	4100	5.39×10^{11}	7.1×10^{-14}	2
S37	n-type	175	2946	2.74×10^{11}	0.66×10^{-14}	0.5
S49	n-type	175	3400	0.88×10^{11}	0.39×10^{-14}	0.6
S50	n-type	175	2900	1.17×10^{11}	0.33×10^{-14}	0.6

Table 5.1

(H-effect on 'virgin' n-type films at room temperature)

Film	Conductivity type prior to gas cycle	Deposition temperature ^{o}C	Film thickness $\overset{o}{A}$	Slope = $\frac{d\lvert\Delta P\rvert}{dt^{\frac{1}{2}}}$ $cm^{-2}sec^{-\frac{1}{2}}$	$pH_2 \times 10^{-4}$ torr
S47	p-type	175	2900	1.3×10^{10}	0.4
S48	p-type	175	2000	1.94×10^{10}	0.6
S51	p-type	175	2049	1.89×10^{10}	0.6

Table 5.2

(H-effect on O_2-driven p-type films at room temperature)

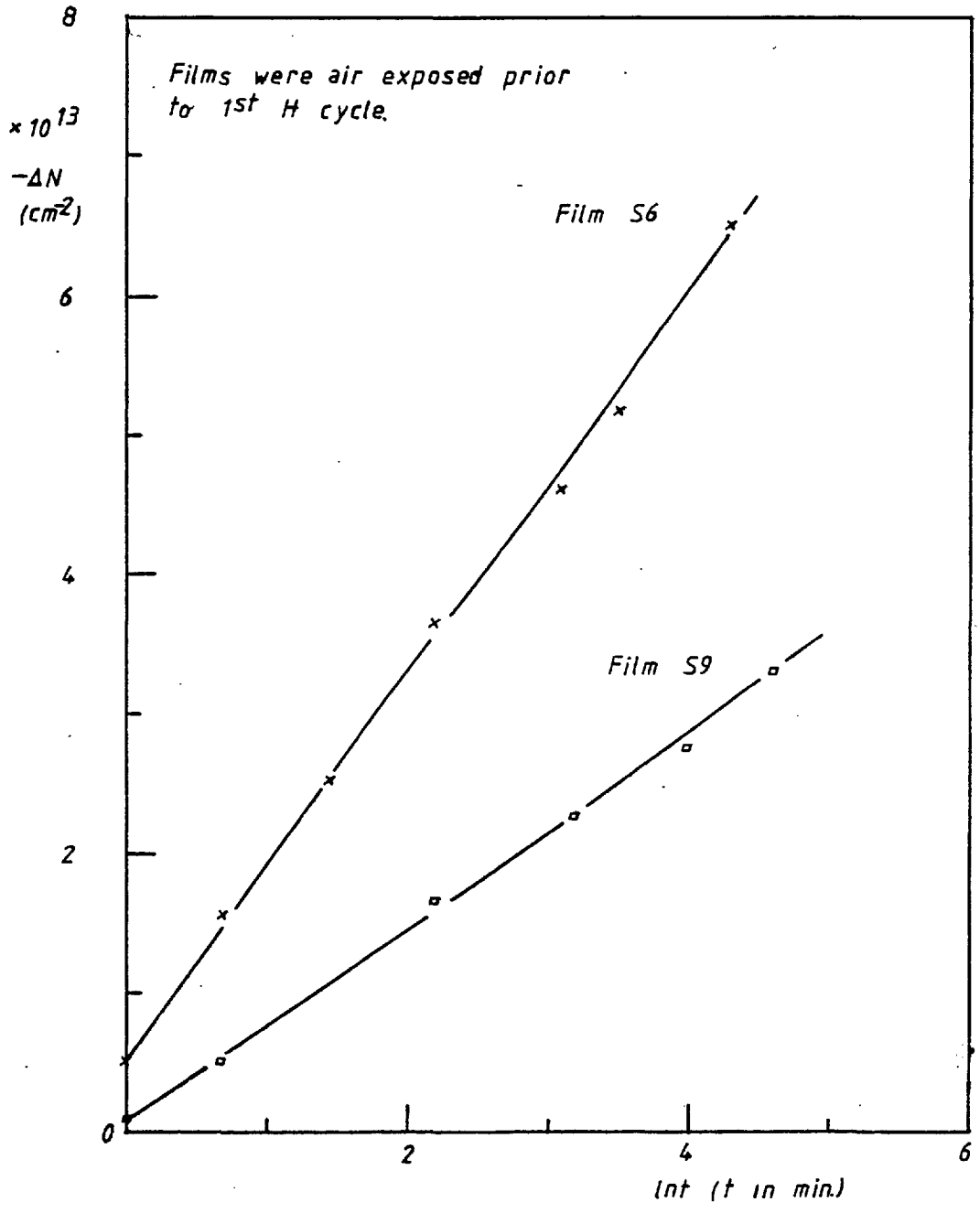

Fig.5.7 O_2^- kinetics of hydrogenated films

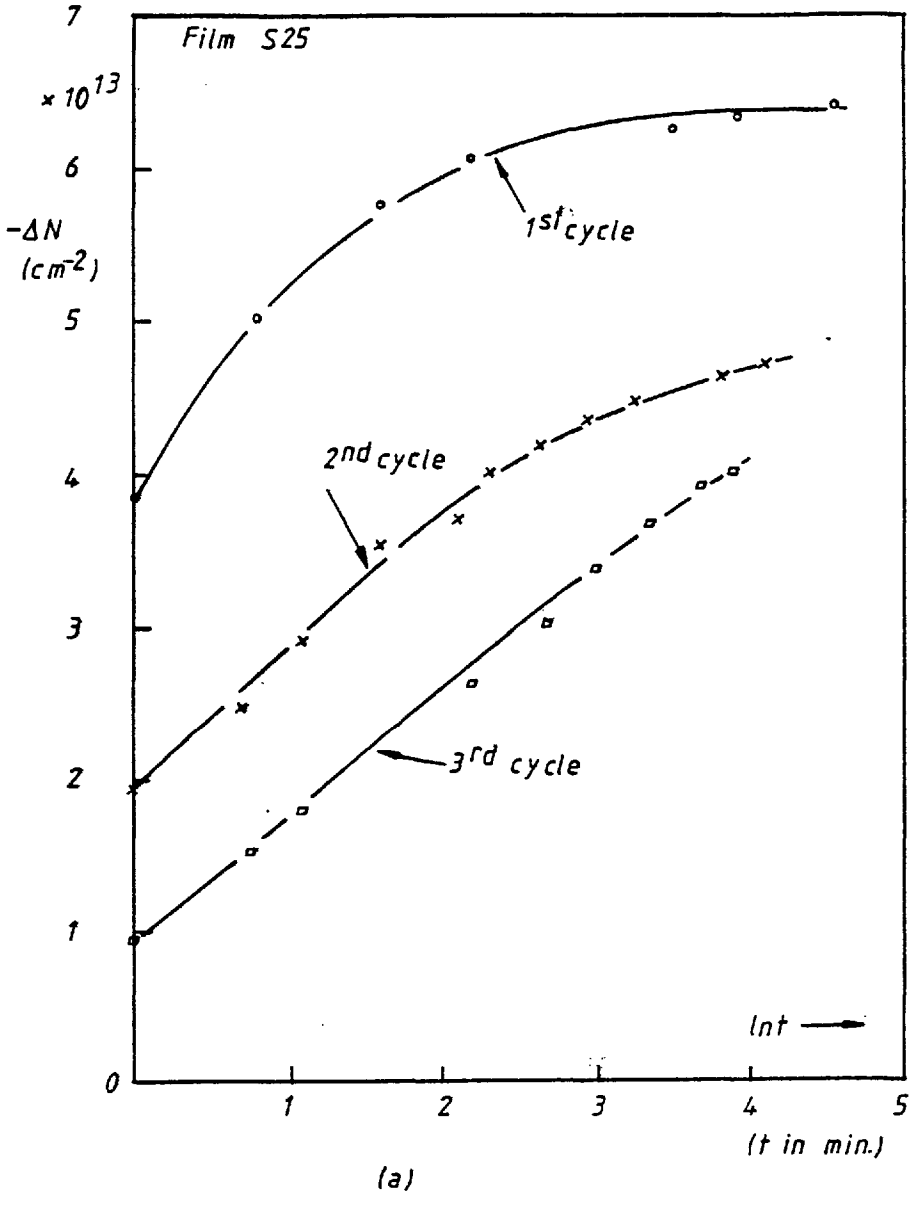

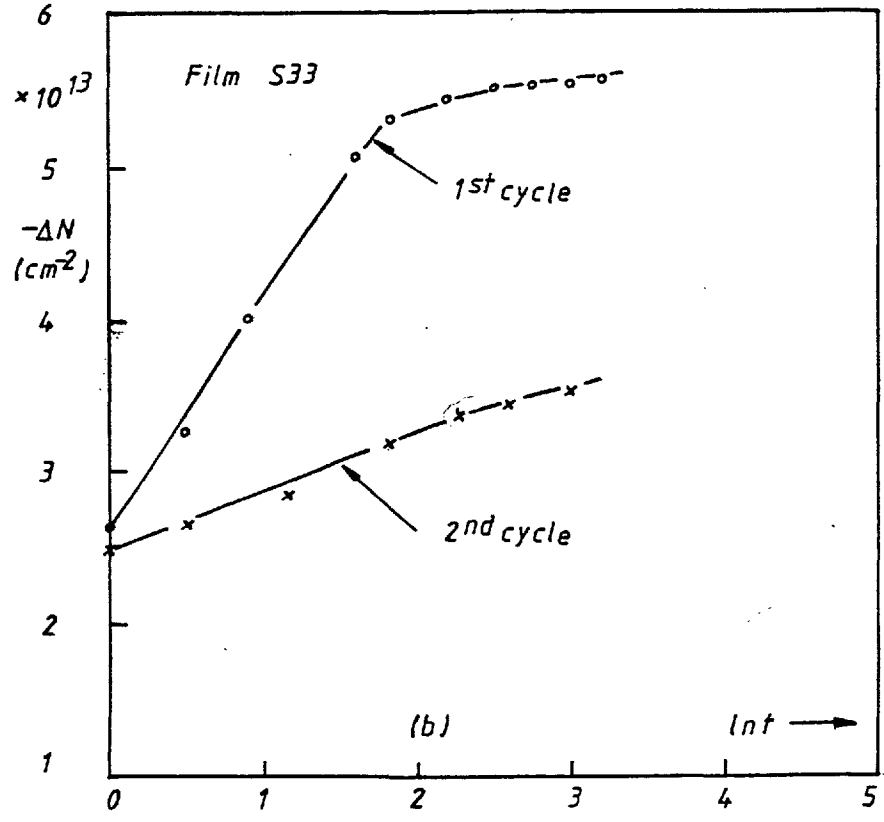

Fig. 5.8 O_2-kinetics of H-saturated films.

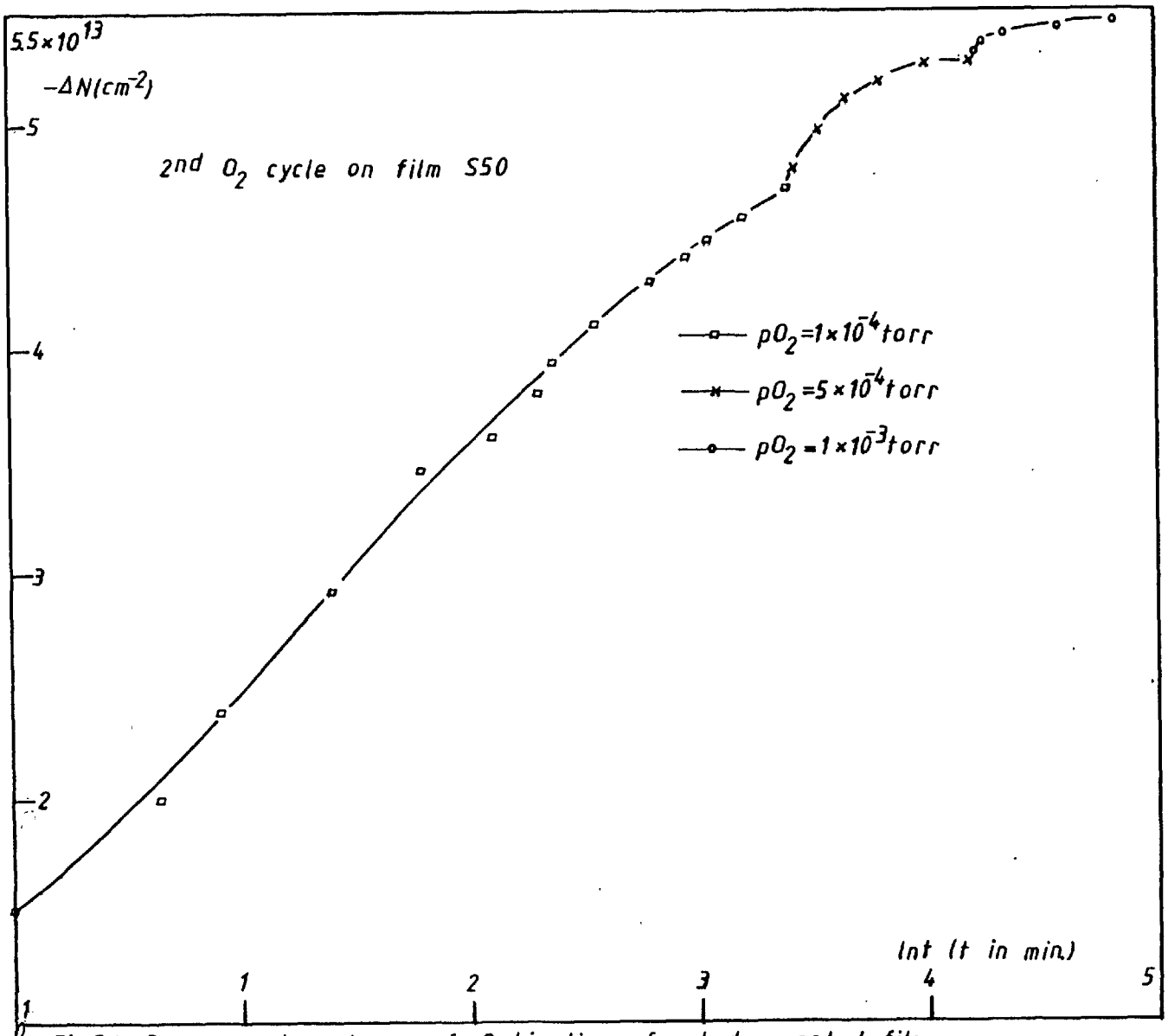

Fig.5.9 Pressure dependence of O_2 kinetics of a hydrogenated film

The changes in R_H as a function of time, t are shown in Fig. 5.10 for a 'virgin' n-type film when exposed to O_2 at 1 x 10^{-4} torr. The film turned p-type after 22 mins and when R_H reached a value of 24 cm^3/C, the O_2 supply was stopped and film S53 was kept in a vacuum of $\sim$1 x 10^{-6} torr for 38 mins. During this period, changes in R_H were small as seen from Fig. 5.10. When the O_2 supply was restored at 1 x 10^{-4} torr, R_H started to increase again. The film was left at this pressure overnight and as a result R_H rose to 53 cm^3/C and when the film was exposed to air at atmospheric pressure, R_H decreased to 8.5 cm^3/C within 3 mins. Film S53 was driven n-type and 'saturated' with H and exposed to O_2 at 1 x 10^{-4} torr again. The kinetics of O_2-uptake are shown in Fig. 5.11(a). The oxygen supply was terminated for 25 mins. During the first 18 mins of this interruption, R_H changed from -23.5 cm^3/C to -25.4 cm^3/C but during the next 7 mins, it rose to -43.3 cm^3/C. When the O_2 supply was restarted, the kinetics followed by the O_2-uptake are shown in Fig. 5.11(b). As the two graphs show, the amount of gas-uptake for the first O_2 cycle was higher than that for the second cycle (after 25 mins pause).

Fig. 5.12 shows the effect of exposing 'virgin' p-type film to O_2. Plots of ΔP vs ℓnt and ΔP vs $t^{\frac{1}{2}}$ are shown in this figure.

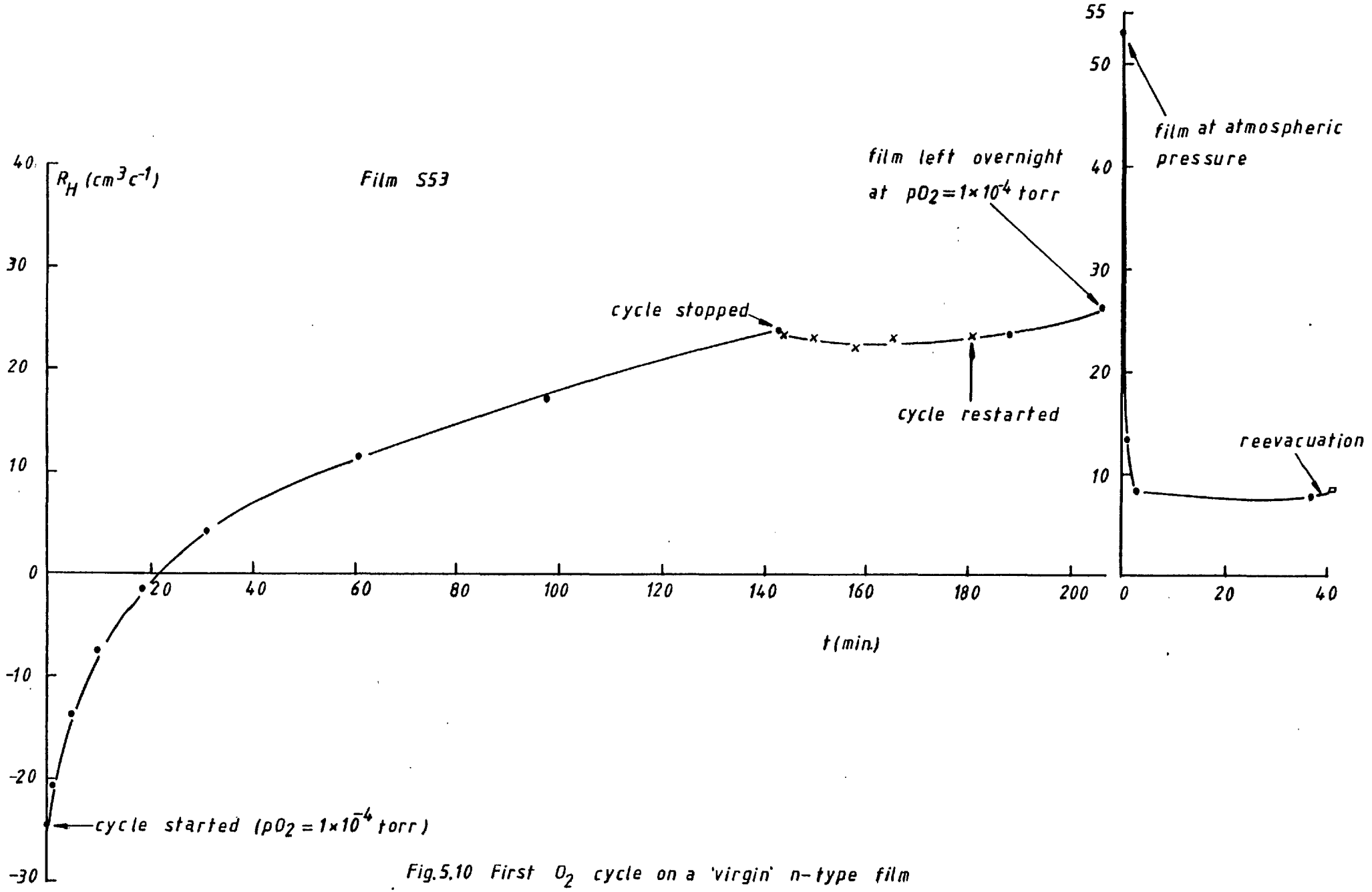

Fig.5.10 First O_2 cycle on a 'virgin' n-type film

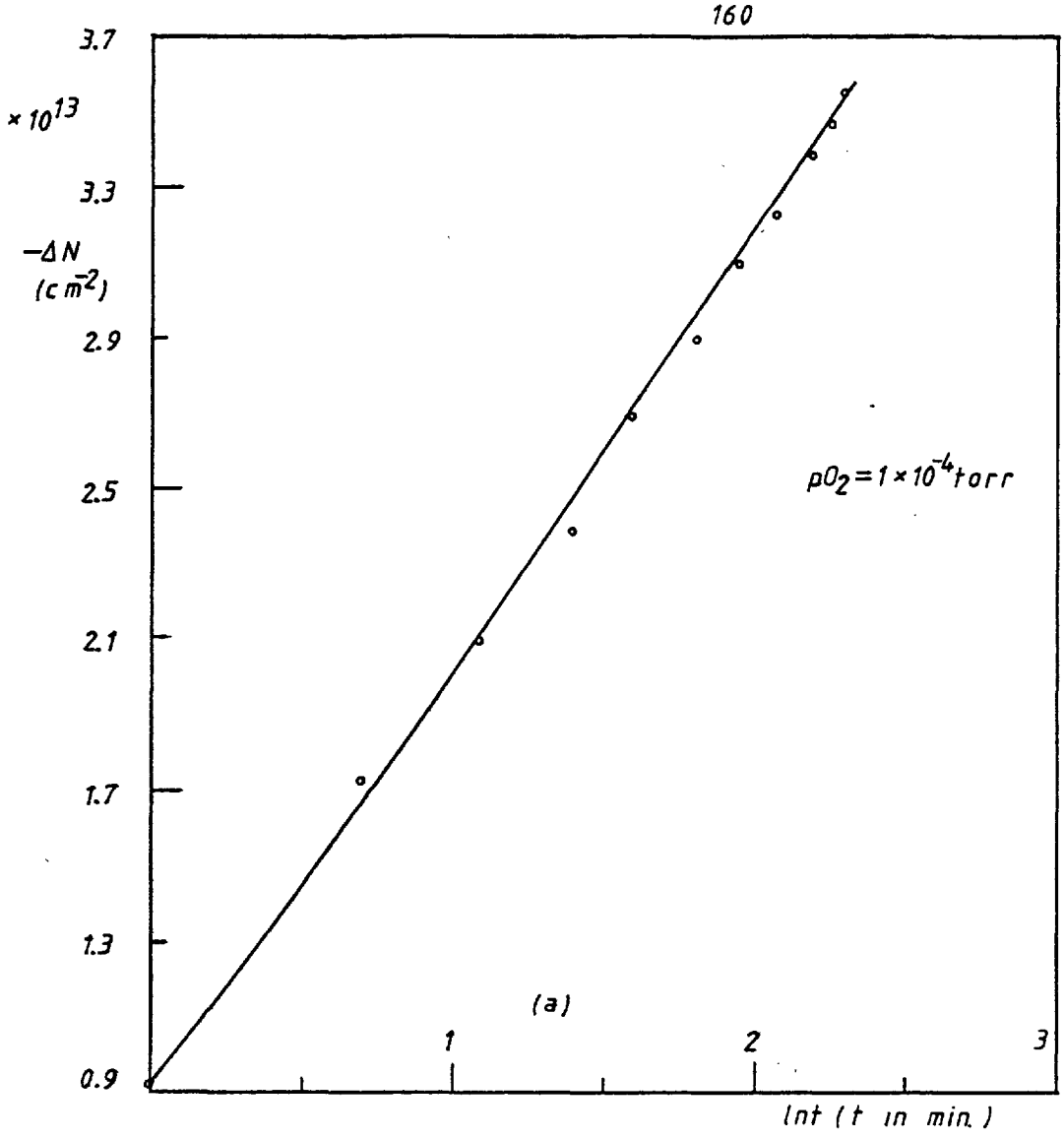

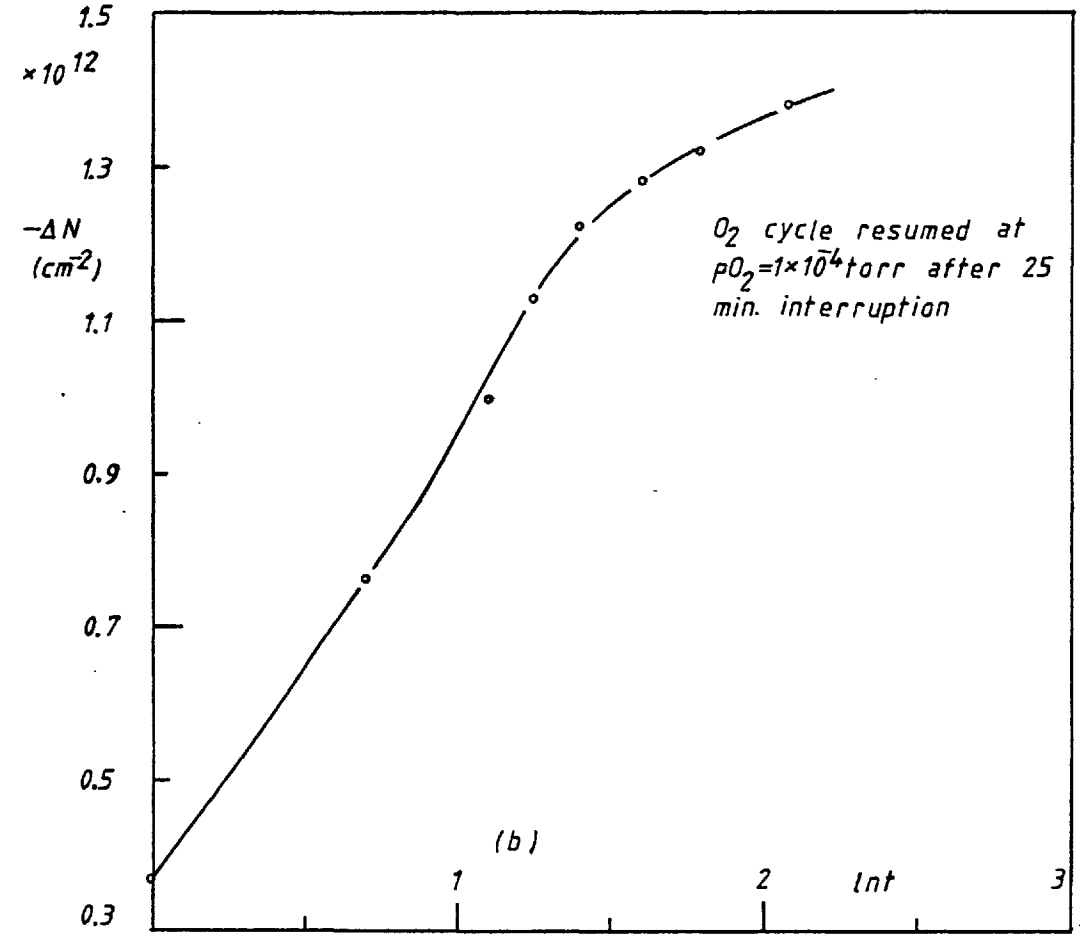

Fig.5.11 O_2^- kinetics of hydrogenated film S53 (2nd cycle)

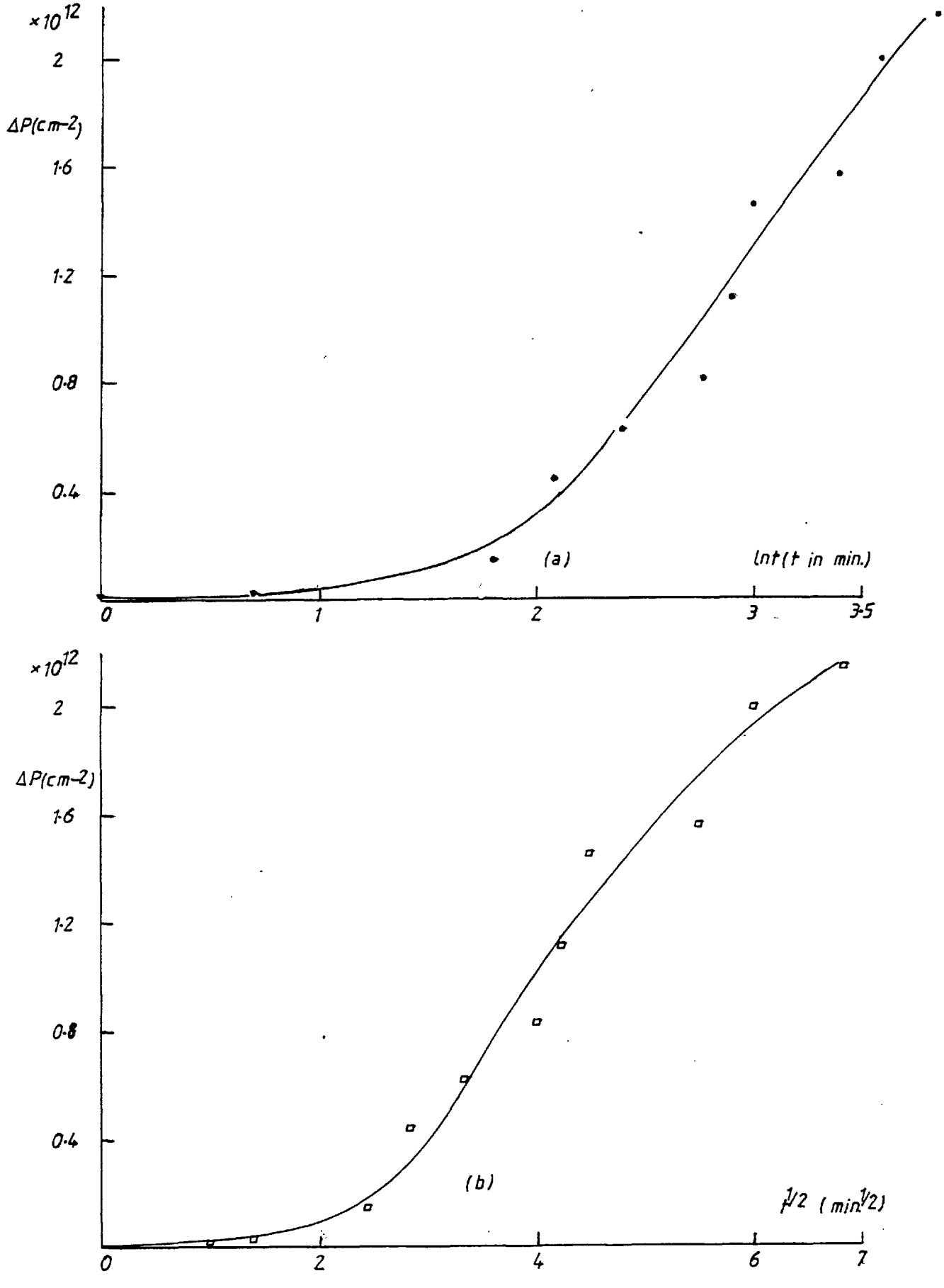

Fig. 5.12 O_2 Kinetics of film S51

5.3 DISCUSSION OF RESULTS

5.3.1 H Effect

The following points can be made at the outset.

(i) H_2 had no observable effect on PbTe films

(ii) H had a donor-like effect on PbTe films

An attempt will now be made to resolve the question of mechanism(s) of gas-uptake by considering the results of kinetic studies as well as the theoretical models described in chapter 4.

5.3.1 (a) 'Virgin' n-type Films

If H effect can be described as a surface effect, then H occupies lead vacancies at the surface and donates an electron to the conduction band. This will result in an accumulation layer being formed at the surface. As time progresses, the accumulation layer will grow and so will the band bending. Bearing in mind the values of ΔN involved ($>10^{13}$ cm^{-2} - see Fig. 5.2), two questions may be raised regarding the surface model.

(i) What is the band bending for such values of ΔN?

(ii) What is the influence of surface quantisation?

Many et al. (M4) give a relationship between the excess surface carrier density ΔN and the bulk value,

n_b.

$$\Delta N = n_b L G^+ (u_b, v_s) \qquad (5.14)$$

where L is the Debye length and graphical representation of the surface function $G^+(u_b, v_s)$ as a function of u_b and v_s is given by Many et al. (M4). In order to evaluate v_s from equation (5.14), the flat-band (v_s=0) condition must be known. If one assumes that the bands are flat prior to the gas cycle, estimates of v_s can be made for experimentally observed values of ΔN. Although there was no experimental justification for this assumption, it was assumed that the bands were flat prior to H cycle in order to estimate the order of magnitude of v_s. This is shown in Table 5.3. As can be seen from Table 5.3, a charge accumulation in excess of 10^{13} cm^{-2} was produced. This raises the possibility of quantisation effects.

In case of strong accumulation carriers become confined in a deep potential well at the surface and momentum of the carriers in the direction normal to the surface becomes quantised (M6). In the case of quantisation, band bending is larger for a given surface space charge compared with the classical case. Under such conditions, expressions for surface charge given by Many et al. (M4) for a classical case or Seiwatz and Green (S11) for a degenerate case cannot be used since both of these treatments neglect quantum effects. This implies that the surface function requires

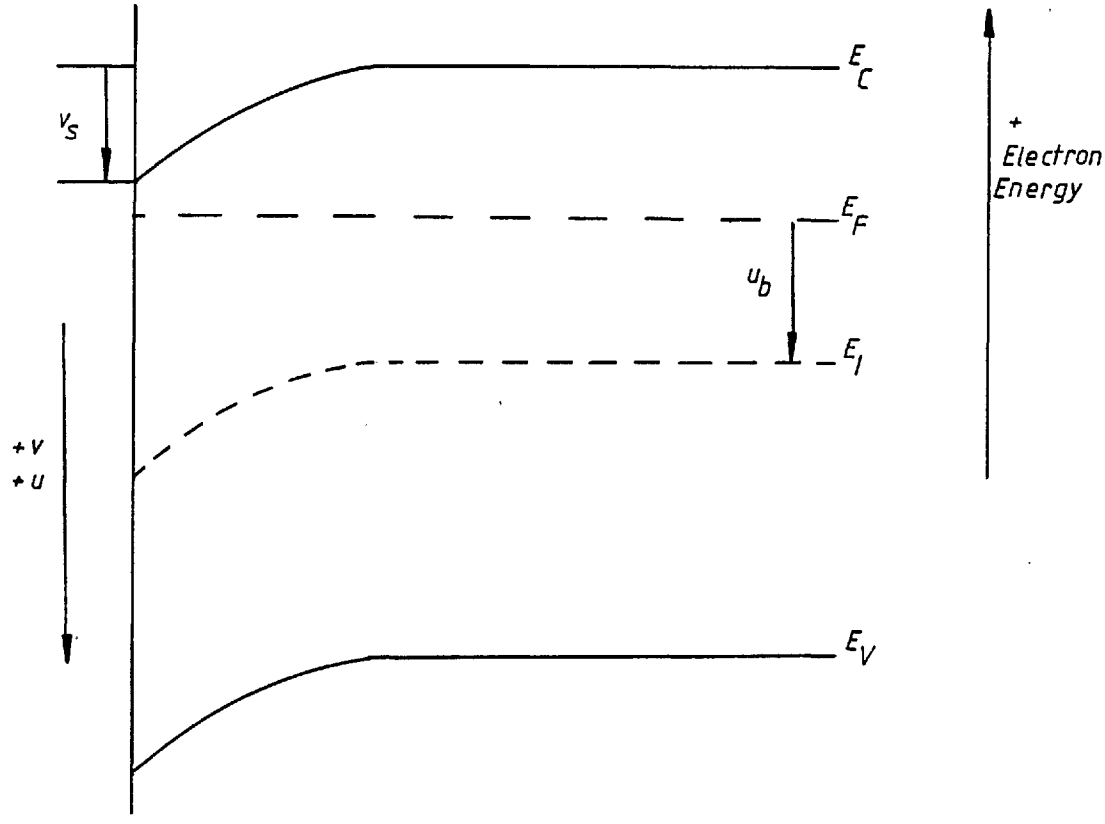

(Definition of energy parameters)

Fig. T.1: n-type semiconductor under accumulation

n_b (cm^{-3})	Film	Deposition temp. °C	Film thickness Å	u_b (in kT)	L (in Å)	ΔN $cm^{-2} x10^{13}$	v_s (kT)
$4x10^{16}$	S49	175	3400	1.68	1198	1	5.5
$4.5x10^{16}$	S27	250	2940	1.8	1138	5	8.5
$3.26x10^{17}$	S34	200	4100	3.8	433	4	6
$1.26x10^{18}$	S66	150	3400	5	220	5	5.3

H effect on 'virgin' n-type films

Table 5.3

modification to take quantisation into account. According to Greene (G8), correction for surface function becomes significant in the case of strong accumulation when the electric field, E_s due to the space charge region,

$$E_s \geq 6 \times 10^4 \left(\frac{m_d^*}{m_o}\right) \text{ volt cm}^{-1} \qquad (5.15)$$

at room temperature where m_d^* is the density of states effective mass and m_o is the free electron mass. For PbTe at room temperature $E_s \sim 1.5 \times 10^4$ V cm^{-1} which give gives a space charge, $Q_{sc} \sim 3.5 \times 10^{12}$ cm^{-2}. As mentioned earlier, a space charge in excess of 10^{13} cm^{-2} was encountered suggesting that the quantisation might have occurred. But as Fig. 5.13 shows, quantisation did not have an adverse effect on the Hall mobility of electrons. Using equation (5.16),

$$\% \text{ change in } \mu_H = \left(\frac{\mu_{HO}-\mu_{Ht}}{\mu_{HO}}\right) 100 \qquad (5.16)$$

where μ_{HO} is the Hall mobility prior to H cycle and μ_{Ht} is the Hall mobility after time, t during the gas cycle. Maximum change observed in μ_H was 8.2% for S66, 6.9% for S49, 12% for S34 and 13.6% for S27. Zemel and Kaplit (Z6) also found that μ_H for p-type PbSe films grown on NaCℓ was substantially independent of the surface charge ($\sim 5 \times 10^{13}$ cm^{-2}).

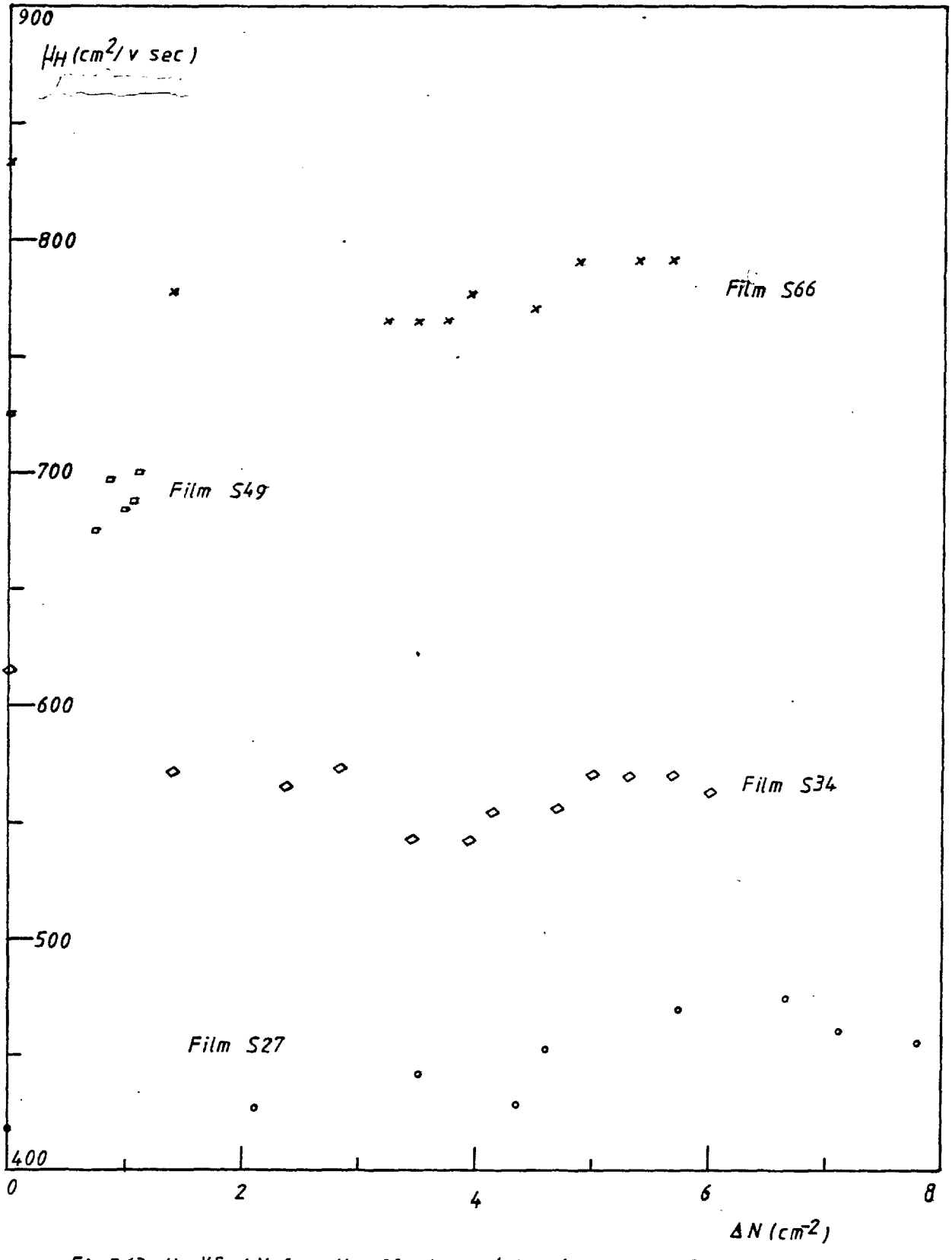

Fig.5.13 μ_H vs. ΔN for H effect on 'virgin' n-type films

The effect of interrupted H cycles on 'virgin' n-type films is shown in Fig. 5.4 and Fig. 5.5. This was typical behaviour of the three films for which this effect was investigated at room temperature. Two points are worth noting.

(i) After each interruption, the rate of gas-uptake is slower (Fig. 5.5).

(ii) Changes in $|R_H|$ during the period the filament is 'on' are greater compared with changes in $|R_H|$ during the period the filament is 'off' even though the two periods are approximately of the same duration (Fig. 5.4).

From the above it may be inferred that the mechanism of H uptake is not a unique one. If the mechanism of gas-uptake was just a surface model, then changes in $|R_H|$ during the 'on' and 'off' periods should be the same. If,on the other hand, the mechanism is a diffusion type process, then there should be no *appreciable* changes in $|R_H|$ during the 'off' period. Progressively slower rates of gas-uptake after each interruption seems to suggest that some H has permanently been incorporated into the film (even when the 'off' period was extended to 23 hours in vacuum of $\sim 10^{-6}$ torr, R_H of film S66 was -2.42 cm^3/C whereas R_H was -4.95 cm^3/C before the gas cycle commenced). Consequently, the concentration

gradient between the gaseous ambient and the film becomes progressively shallower. Relatively fast initial uptake after each interruption also suggests that some out-diffusion of H during the 'off' period may have occurred.

Kinetics of H uptake shown in Fig. 5.2 suggest that after the initial fast rise, the gas-uptake is a diffusion limited mechanism. It was possible to fit ℓnt dependence for kinetics of the initial H uptake. This is shown in Fig. 5.14. This is in common with Egerton and Crocker (E4) who observed similar kinetics for H uptake on PbTe films. A similar $t^{\frac{1}{2}}$ dependence of H uptake for thin film epitaxial films of PbSe (M7) and $Pb_{1-x}Sn_xTe$ (H1) has also been observed. However, it must be noted that the films used by McLane (M7) were air exposed prior to H cycle. If the mechanism of H uptake is a diffusion process, one may pose the following questions.

(i) Is H diffusing into the film? and

(ii) can the diffusion coefficient of H be associated with the self-diffusion coefficient of lead in PbTe?

The value of the self-diffusion coefficient of lead D_{Pb} in PbTe at room temperature can be extrapolated from previously published data. This, unfortunately, can give rise to large discrepancies in D_{Pb}. For example, $D_{Pb} \sim 2.5 \times 10^{-15}$ cm^2s^{-1} in p-type PbTe single crystal with $p = 10^{17}$ cm^{-3} (R1) whereas $D_{Pb} \sim 10^{-18}$ cm^2s^{-1} for

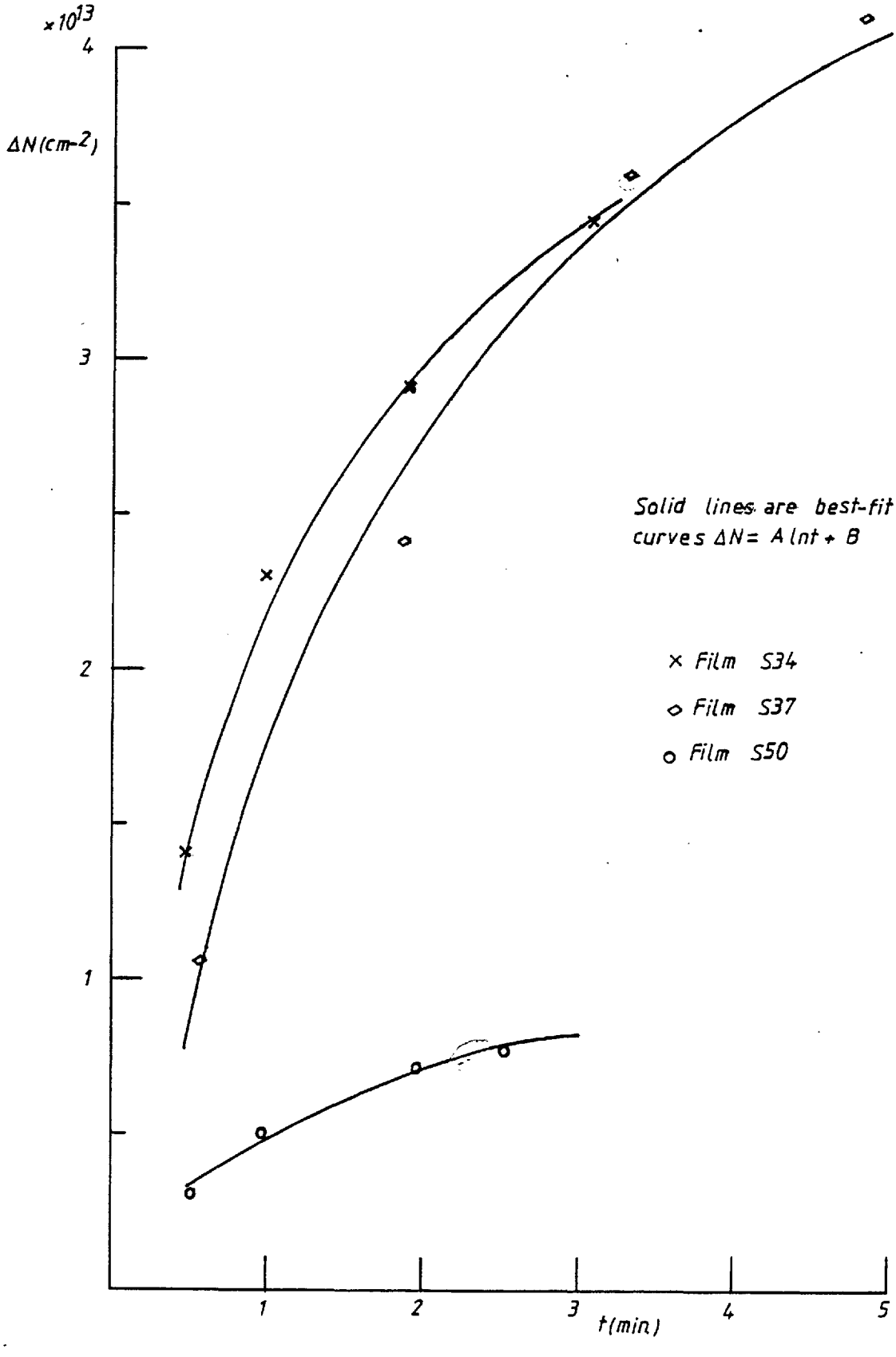

Fig. 5.14 ---- ΔN vs. t For Initial Uptake Of H

p-type single crystal PbTe, with p = 3 x 10^{18} cm^{-3} (G9). Calawa et al (C7) give a value of D_{Pb} ~1.9 x 10^{-21} cm^2s^{-1} for single p-type PbSe. The values of diffusion coefficient in the present study are in the range 10^{-14}-10^{-15} cm^2s^{-1}. Similar values of diffusion coefficient were obtained by Young (Y3) for H effect on epitaxial PbSe films grown on NaCℓ but his films were air exposed and p-type. Therefore, it is difficult to compare the values of diffusion coefficient obtained during the present study with the values obtained by other workers.

5.3.1(b) H Effect on O_2-driven p-type Films

Typical examples of H effect on O_2-driven p-type films are shown in Fig. 4.3 to Fig. 4.6 (chapter 4) where H turns the films less p-type by neutralising the excess hole concentration. In terms of the surface model, H creates a depletion layer on the surface of a p-type bulk. Once again the determination of the resultant band bending is difficult since it is not known whether the bands are flat prior to H exposure. However, a tentative estimation of v_s may be made as follows.

The range of values of v_s for the theoretical R_H vs ρ curve predicted by the computer program was from -10 kT to 20 kT, i.e. it embraced regions of accumulation and depletion (see Fig. 4.11). By

superimposing the experimental values of R_H and ρ prior to H cycle with the theoretical values, the corresponding band bending could be estimated. In cases of films S25 and S51, there was an accumulation layer giving rise to a band bending of $\sim$-1 kT whereas for films S47 and S48 the bands were flat prior to the H cycle. In Table 5.4, the estimated values of v_s and other pertinent parameters are shown. Surface functions given by Many et al. (M4) were used to estimate v_s. As can be seen from Table 5.4, $v_s > 2\ u_b$ in all cases, i.e. inversion has occurred and the majority carriers in the surface region are electrons. This implies that a large electric field would be set up due to the space charge at the surface.

As mentioned in chapter 4, the fit between the theoretical and experimental R_H vs ρ curve during the initial stages of H cycle is very good. Fig. 4.11 is a typical example of this. Therefore, it is tempting to infer that the surface adsorption model describes H uptake during the initial stages. Since $t^{\frac{1}{2}}$ dependence (Fig. 5.6) is followed by H uptake after the initial fast uptake, this further suggests that surface adsorption precedes diffusion.

The mechanism of H uptake in the case of air exposed film is complicated further when one considers the possibility of an oxide growth due to the interaction of the film with air. A recent study by Bettini and

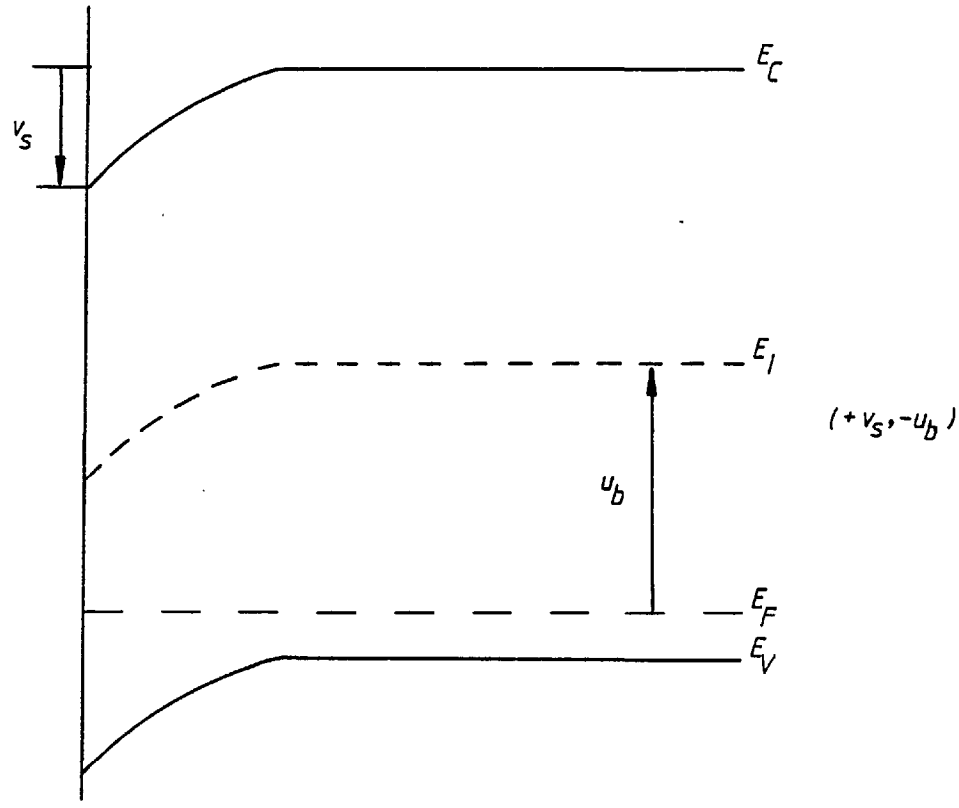

Fig. T.2: p-type semiconductor under depletion

Film	Deposition temp. ^oC	Film thickness Å	P_b cm^{-3} x 10^{17}	L (in Å)	$-u_b$ (kT)	No. of holes neutralised $-(\Delta P)$ cm^{-2}	v_s (kT)
S47	175	2900	2.68	477	3.3	1.4×10^{12}	8
S48	175	2000	2.65	480	3.3	4	9.3
S51	175	2049	3.93	394	3.7	1.2	9.4
S25	170	2038	3.69	407	3.6	4	10.7

H effect on O_2-driven p-type films

Table 5.4

Richter (B10) has provided evidence for oxide growth on epitaxial films of PbTe when the films were exposed to air. They investigaged the oxidation of PbTe films, 5-10 μm in thickness, grown on BaF_2 with carrier concentration $\sim 10^{17}$-10^{18} cm^{-3} using the techniques of x-ray photo-electron spectroscopy (XPS) and LEED in ultra-high vacuum system. They concluded that the surface became oxidised after a prolonged exposure to air (several days) where PbO and TeO_2 were the oxidation products.

5.3.1(c) H Effect on 'Virgin' p-type Films

Fig. 4.6 and Fig. 4.7 (chapter 4) illustrate the effect of first H cycle on 'virgin' p-type films. This behaviour was typical of all 'virgin' p- type films (four in all). Interpretation of results in this case is difficult because of the following reasons.

(i) All the 'virgin' p-type films had low carrier concentration (i.e. x 10^{16} cm^{-3}, see Table 4.2) and it was found difficult during the present study to grow p-type films.

(ii) Almost instantaneous change-over (see Table 4.2) from p-type to n-type is difficult to reconcile with either surface or diffusion model.

(iii) Since the films not only change over from p- to n-type but also from two carrier type to substantially single

carrier type, the kinetic study of gas-uptake becomes obscure.

However, once the films become n-type (single carrier) H uptake may be plotted as a function of time. This has been done for films S25 and S33 and is shown in Fig. 5.15. Film S33 was grown at 175°C and its thickness was 2600Å.

In order to resolve the question of an instantaneous turnover from p- to n-type, a typical R_H vs time curve of H effect on an O_2-driven p-type film (S48) has been plotted in Fig. 5.16. As can be seen from Fig. 5.16, once R_H starts to decrease after reaching a peak the changeover from p- to n-type is rather fast. For example, R_H changed from 105.3 cm^3/C to -173 cm^3/C in 4 mins. Even though this changeover is slower than that for 'virgin' p-type films (see Table 4.2), it indicates that the value of R_H of 'virgin' p-type films prior to first H cycle lies in the range FC in Fig. 5.1.

Before concluding the discussion of H effect on PbTe films, possibilities of H incorporation into PbTe film other than through lead vacancy occupation will now be discussed.

As mentioned previously, there exists a large discrepancy in the extrapolated value of self-diffusion coefficient of lead D_{Pb}(reported in the literature)in PbTe and other lead salts. Furthermore, the value of D_{Pb} for thin films will be different compared with the

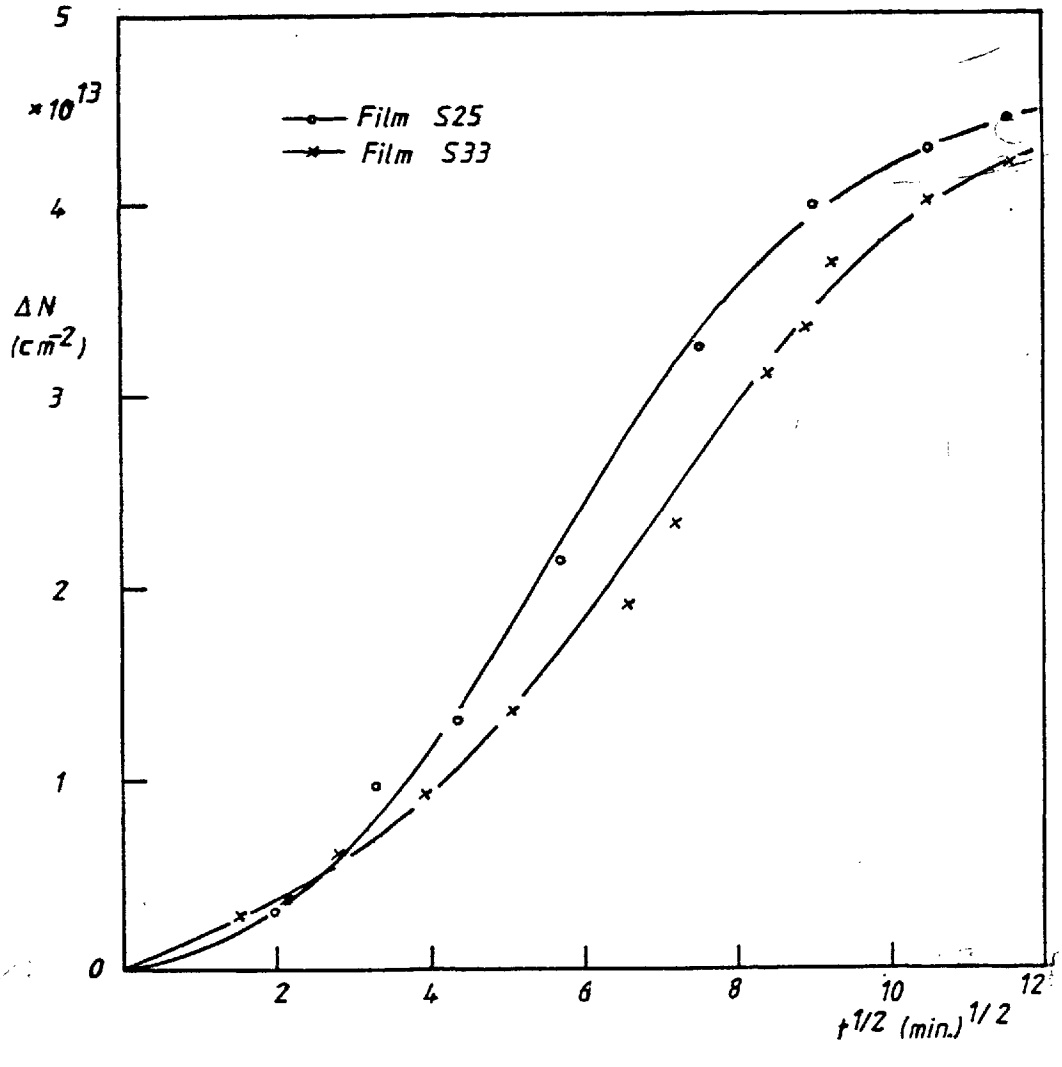

Fig. 5.15 1st H cycle on 'virgin' p-type films

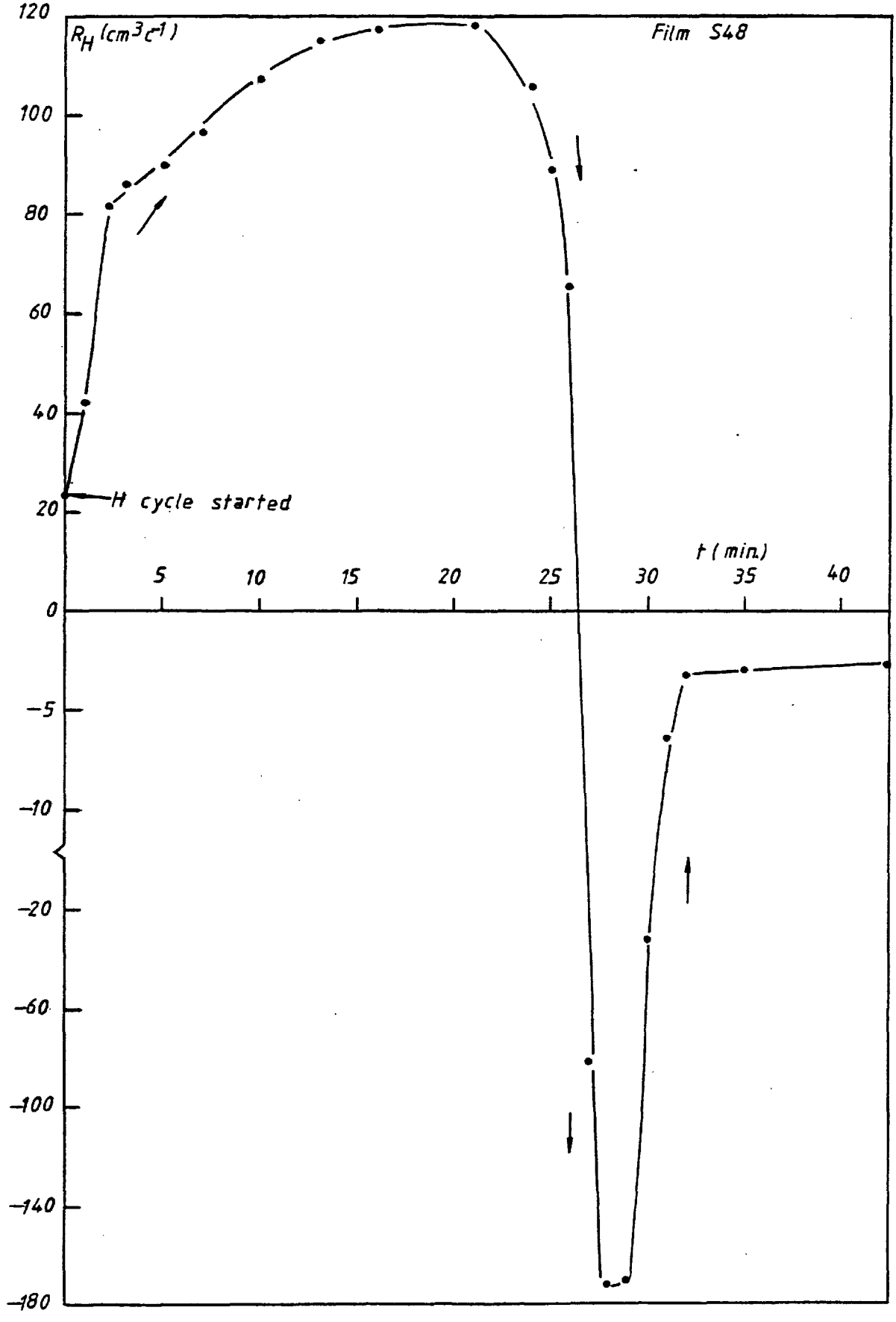

Fig. 5.16 H effect on an O_2 driven p-type film

single crystal value. For example, Zemel (Z8) estimated D_{Pb} in PbSe epitaxial films to be 10^4 times higher than that for PbSe single crystal. It is, therefore, difficult to correlate D_{Pb} values for thin film and single crystal and identify the value of diffusion coefficient estimated during the present study with self-diffusion coefficient of lead in PbTe. In any case, for efficient self-diffusion of lead to take place, there must be a high concentration of V_{Pb}. There is evidence in the literature suggesting that in undoped PbTe ionised lead and tellurium vacancies are the sources of free holes and electrons (B7,H6,B8,K5) and it is normally heavily compensated (Y4). On the other hand, H in-diffusion is also possible via short circuit paths such as dislocations and grain boundaries during the initial stages of the gas cycle followed by diffusion into the crystallites (G10). In general, short circuit diffusion is faster than the lattice diffusion (B13). However, since no data are available (to the best of the author's knowledge) on H diffusion in single crystal PbTe, it is not possible to compare the diffusion coefficients of H for thin film and single crystal PbTe. Therefore, it is difficult to discuss H diffusion along the short circuit paths.

H entering an interstitial site and ionising to act as a donor is an another possibility but Zemel (Z4, Z7) has expressed doubts on the compatibility of this model with the experimental data. Ionisation of H once it occupies a lead vacancy seems to be the most

acceptable model (Z4,Z7,Y4). Therefore, a p-type PbTe film is driven n-type because H neutralises the effect of lead vacancies. To establish this model experimentally, PbTe films must be grown with controlled concentration of V_{Pb} which in the present case was not possible.

5.3.2 O_2 Effect

The following points are noteworthy.

(i) Compared with a 'virgin' n-type film O_2 exposures at higher pressures and for longer periods are required to turn a hydrogenated film p-type. (See section 4.3.2.1, chapter 4.) For instance, film S53 ('virgin' n-type) turned p-type after 22 mins when exposed to O_2 at $p_{O_2} = 1 \times 10^{-4}$ torr (Fig. 5.10) whereas some H saturated films took days at atmospheric pressure to turn p-type.

(ii) Reversal of H effect was quicker when O_2 was leaked in at higher pressure (Fig. 5.9).

(iii) Films like S6 and S9 did not turn p-type at all (S6,S9 were air-exposed prior to H cycle).

Initially it was thought that there might be an oxide growth on the surface of such films as S6 and S9 which prevented O_2 penetration. Cooling films S6 and S9 to liquid N_2 temperature in an attempt to crack the oxide layer,if any, failed to turn the films p-type, although Band (B2) and Hing (H1) had some success using this method with their stable H saturated n-type films. This suggested that the films S6 and S9 were permanently doped n-type.

From the previous argument it may also be inferred that O_2 reverses H effect by removing it probably in the form of H_2O (E4,Y3) which is desorbed at the surface. But since most H saturated films are eventually turned p-type, a second mechanism in addition to H removal is necessary to explain total O_2 uptake.

Various models of O_2 uptake on lead salts (PbS, PbSe and PbTe) have been proposed in the past where the surfaces of these salts were obtained by epitaxial growth, by crushing or cleaving single crystals. This is partly due to the fact that different workers have used different experimental conditions and techniques (such as change in ambient pressure due to gas-uptake (H2), changes in transport properties in conventional vacuum and ultra-high vacuum (B3,M2,E2,P8), ultra-violet photo-electron spectroscopy (S8)) to study O_2 effect. Based on the evidence presented in the literature, O_2 uptake on lead salts occurs in at least two stages and it is both pressure and temperature dependent.

Initial O_2 uptake for low p_{O_2} is a surface phenomenon. Green and Lee (G4) proposed that surface adsorption of O_2 was consistent with the formation of a peroxide surface complex whereas Lee (L5) explained O_2 uptake on n-type epitaxial PbS films in terms of surface stoichiometry effect where he suggested that formation of oxide molecules at the surface changed the surface stoichiometry thereby removing more electrons than valence band states. Considering O_2 effect on PbSe films, Hagström and Fahlman (H4) postulated that an oxide growth of monolayer range was formed. Hillenbrand (H3) who studied O_2 uptake on polycrystalline PbS films proposed that total gas-uptake was the sum of three processes operating together which were, (a) the ionisation of oxygen at PbS surface by capturing carrier electrons present in n-type polycrystalline films; (b) adsorption of oxygen atoms by PbS surfaces in amounts that approach one atom of oxygen per lead atom in the surface layer and (c) the incorporation into the PbS lattice by replacement of the sulphur atoms followed by a partial evolution of S as SO_2.

Other workers such as Egerton and Juhasz (E2) and Parker and Williams (P8) put forward a diffusion model as an alternative mechanism for O_2 uptake on epitaxial PbTe films. By basing their model on the model proposed by Bloem and Kröger (B9) for interstitial diffusion of Cu in PbS single crystal, Egerton and Juhasz (E2) suggested that atomic oxygen diffused interstitially to occupy tellurium vacancies, whereas Parker and Williams postulated that interstitial Pb was diffusing out to

the surface to interact with O_2 during the initial stages of the gas exposure.

A second slower mechanism of oxygen uptake on epitaxial PbTe films at pressure of 10^{-1} torr sec was characteristic of oxidation process according to Sun et al (S8). Galat et al (G5) concluded that oxygen chemisorption was followed by the formation of a heterophase layer of lead tellurate, $PbTeO_4$. Bode and Levistein (B1) who measured the effect of O_2 adsorption on conductivity and thermoelectric power of n-type PbTe films suggested that surface adsorption of O_2 was followed by its diffusion along the grain boundaries. Therefore, in the past, total O_2 uptake on lead salts have been discussed in terms of surface adsorption, oxide formation and diffusion.

It is suggested that as far as hydrogenated films were concerned, the first stage of O_2 uptake involves effective removal of H. As far as 'virgin' n-type films are concerned, O_2 chemisorbs on the film surface giving rise to band bending. Direct evidence of this band-bending due to chemisorption of O_2 on PbTe epitaxial films has been provided by Sun et al (S8). The second stage of O_2 uptake for both types of films involves diffusion of the gas into the bulk probably to occupy tellurium vacancies. Low sticking coefficient of O_2 for the latter stage of gas exposure seems to explain why prolonged exposures at higher pressures are necessary to turn films p-type and also why O_2 effect is partially

reversible by evacuating the films to a vacuum of $\sim 10^{-6}$ torr. A unique interpretation of kinetics of O_2 uptake is difficult since not only Elovich type kinetics (ℓn (t) dependence) and $t^{\frac{1}{2}}$ dependence are indicative of chemisorption and diffusion mechanism respectively but these kinetics also describe oxidation processes (H7,F2,R2).

CHAPTER 6

SUMMARY AND CONCLUSIONS

A summary of experimental results obtained during the present study will be given in this chapter. Conclusions drawn from the study together with some suggestions for future work will also be presented.

6.1 TRANSMISSION ELECTRON MICROSCOPY AND THE HALL MEASUREMENTS

Lead telluride grew epitaxially on air-cleaved muscovite mica in the temperature range 150-225^{o}C. The deposited material had (111) plane parallel to the surface of the substrate as previously reported (E3, G1, S6). The salient feature of the microstructure was the existence of double positioning boundaries enclosing domains of single crystal orientation. The size of the triangular based nuclei and the domain increased as the substrate temperature was increased.

The Hall measurements were carried out in air on 18 films grown on mica substrate. Four films considered to be representative of this work are discussed in chapter 3. These four films (n-type) were grown in the temperature range 150-200^{o}C and thickness of the films was in the range 2900-4100$\mathring{A}$. The Hall effect measurements were performed using a standard d.c. technique in the temperature range 77-300^{o}K. Carrier concentration

at room temperature was in the 10^{17}-10^{18} cm^{-3} range and the Hall mobility at room temperature ranged from 590-883 cm^2/V sec compared with the best value of μ_H = 1200 cm^2/V sec obtained by Egerton (E1) at room temperature for his n-type PbTe film grown on mica at 260°C.

In all cases, μ_H decreased as the temperature was increased and the temperature dependence of μ_H was described by the power law $\mu_H \alpha T^{-s}$. Furthermore, the temperature dependence of μ_H became weaker in the temperature range 77-150°K. In the temperature range 200-300°K, the value of s was 1.45 for film S10 and 1.75 for film S17 (see Table 3.1, chapter 3). This compares poorly with s = 2.5 for thin films of lead telluride grown on alkali halides (Z1, L1, L2). Matthiessen's rule was used to isolate the contribution of defect scattering such as dislocation and grain boundary scattering often considered to be dominant scattering sources in thin polycrystalline films (A6). The temperature dependence deduced for defect scattering in the case of the present films was incompatible with the known temperature dependence of dislocation and grain boundary scattering. It was proposed that intergrain potential barriers might be responsible for departure from $\mu_H \alpha T^{-2.5}$ dependence. In the past, $\mu_H \alpha T^{-2.5}$ temperature dependence has been interpreted in terms of the combined effect of acoustic phonon scattering and temperature dependent effective mass (A3).

The Hall coefficient was weakly temperature dependent. For instance in the case of film S66, R_H changed from -4.06 cm^3/C to -3.91 cm^3/C in the temperature range 77-300°K. A change of about 18% in R_H may be explained in terms of changing carrier statistics from degenerate to classical.

6.2 GASEOUS EXPERIMENTS

Most of the films studied during the present study of gaseous effects were n-type (out of about 40 films grown for these experiments, only 5 were 'virgin' p-type). In spite of this, an attempt was made to perform gas cycles in different sequences and the cycles were repeated to establish reproducibility of the gas interaction with thin films of lead telluride. Changes in R_H and ρ were continuously monitored during the gas cycle. The following points can be made at the outset.

(i) Molecular hydrogen had no observable effect on PbTe thin films.

(ii) Paths traversed by successive $H-O_2$ cycles were never the same.

(iii) Some reversibility of the gas effect was evident when a particular gas cycle was interrupted, for example, re-evacuating an air exposed film. But initial values of R_H and ρ were not obtained.

6.2.1(a) H. Effect

When a 'virgin' n-type film was exposed to atomic hydrogen, the film turned more n-type. For example, in the case of film S37, R_H changed from $-22.3\ cm^3/C$ to $-2.1\ cm^3/C$, whereas in the case of films S27 R_H changed from $\sim -139\ cm^3/C$ to $-2.3\ cm^3/C$. The corresponding change in ρ for the latter case was from $0.33\ \Omega$ cm to $0.0051\ \Omega$ cm. In either case, $R_H\sigma$ product was almost constant during the gas cycle.

There was a marked difference between the H effect on 'virgin' p-type film and oxygen driven p-type film. As far as the oxygen driven p-type film was concerned, there was an initial increase in the values of R_H and ρ such that $R_H\sigma$ was almost constant, whereas in the case of 'virgin' p-type film there was no initial increase in the value of R_H and ρ. Furthermore, 'virgin' p-type film turned n-type much more quickly ($\sim$90 secs for film S29) compared with oxygen driven p-type film ($\sim$47 mins for film S25).

6.2.1(b) Oxygen Effect

Oxygen turned 'virgin' p-type film more p-type. Film S51 was an example of this behaviour. In this case, R_H decreased from $71.3\ cm^3/C$ to $12.7\ cm^3/C$ during the gas cycle. When films treated with atomic hydrogen were exposed to oxygen, the films became progressively less n-type and the reversal of the H effect was quicker for higher pressures of oxygen. It was also noted that 'virgin' n-type films were driven p-type by oxygen more

quickly compared with hydrogenated films. For example, film S47 ('virgin' n-type) turned p-type in 4 mins. However, once film S47 was treated with atomic hydrogen and then exposed to oxygen, it took ∿20 hours to turn p-type.

6.2.2 Theoretical Models

Two theoretical models were used to interpret the results of gaseous experiments, namely surface adsorption model and diffusion model.

6.2.2(a) Surface Adsorption Model

In this model, it was assumed that the gaseous species was adsorbed onto the surface of the film and the changes produced in R_H and ρ of the film were due to the existence of surface space charge region.

Planar form of Poisson's equation was used to formulate the problem mathematically. A computer program using a two-band non-parabolic model and degenerate statistics was used to generate a series of values of R_H and ρ for assumed values of surface band bending, v_s. Accuracy of the fit between the theoretical and the experimental R_H vs ρ curve was taken as evidence for the validity of the model. A very good fit was achieved between the two curves in the initial linear region of R_H vs ρ curve. In the past (E1, B2), major objection to this model has been the requirement of an excessive amount of band bending (∿20 kT) for a p-type film to turn n-type.

Levine (L6) has calculated the three-dimensional electrostatic potential surrounding a square array of fixed charges on an insulator. Using Levine's results, calculation suggests that for a static dielectric constant of 400 planar model and three-dimensional model can be used indiscriminatly for a space charge of $\sim 10^{13}$ cm^{-2}. In the present study, inferred value of the space charge density was in 10^{12} - 10^{13} cm^{-2} range. Therefore, use of the three-dimensional model of Poisson's equation can remove some of the limitations imposed by the planar form. Greene et al (G6) have given a three-dimensional formulation of Poisson's equation for a non-degenerate electron gas with an array of localised charges on the semiconductor surface. Based on their results, the effective band bending would be lower compared with the one-dimensional model for the same space charge density. Therefore, the objection of excessive band bending required to turn a p-type film n-type in the case of the planar model can be removed to some extent by using the three-dimensional formulation of Poisson's equation. However, the three-dimensional form of Poisson's equation was not used to obtain a theoretical R_H vs ρ curve during the present study.

As mentioned earlier, there was a marked difference in H effect on 'virgin' p-type films and oxygen driven p-type films. In addition, the carrier concentration deduced from R_H in the case of 'virgin' p-type films was comparable to the intrinsic carrier

concentration (see Table 4.2, chapter 4). Therefore, assuming the bulk of the film to be intrinsic and using classical statistics and planar form of Poisson's equation, expressions for R_H and ρ were developed in order to compare the theoretical and the experimental R_H vs ρ curve for H effect on 'virgin' p-type films. This model correctly predicted the shape of R_H vs ρ curve but exact fit with the experimental curve was not possible.

6.2.2(b) Diffusion Model

In this model, it was assumed that gaseous species had diffused into the bulk as a result of concentration gradient between the ambient and the film bulk. This model was considered to account for irreversible changes in R_H and ρ of the film.

Fick's laws were used to formulate the problem. The following simplifying assumptions were made.

(i) Exponential profile of the diffusant was assumed.

(ii) Surface concentration of the diffusant was constant.

(iii) Unidirectional diffusion coefficient was independent of concentration.

(iv) Charge neutrality was assumed.

(v) All impurities were considered ionised.

Expressions for R_H and ρ were developed but the fit between the theoretidal and experimental curve was not exact. Expressions for R_H and ρ were also developed where condition of charge neutrality was not assumed (i.e. planar form of Poisson's equation was solved for a diffusant with exponential profile).

6.2.3 Kinetic Studies

In order to distinguish between surface adsorption and diffusion as being possible mechanisms of gas uptake, kinetic studies were also undertaken. Most of the kinetic studies were carried out at room temperature.

After the initial fast uptake, H effect kinetics followed a $t^{\frac{1}{2}}$ dependence suggesting that H uptake was a diffusion process. Similar kinetics have been noted for H effect on thin films of PbTe, PbSe and $Pb_{1-x}Sn_xTe$ (E4, M7, H1). Interrupted kinetics of H effect on 'virgin' n-type film indicated that after each interruption, rate of gas uptake was becoming progressively slower. For example, in the case of film S66, the ^{slope} of H uptake during first cycle was 8.32×10^{11} cm^{-2} $sec^{-\frac{1}{2}}$, 6.79×10^{11} cm^{-2} $sec^{-\frac{1}{2}}$ for second cycle and 3.79×10^{11} cm^{-2} $sec^{-\frac{1}{2}}$ for third cycle.

The value of diffusion coefficient for H effect on 'virgin' n-type films was in 10^{-14}-10^{-15} cm^2s^{-1} range at room temperature and in agreement with the value for H effect on PbSe film (Y3). But it was not possible to associate this value of diffusion coefficient with

self diffusion coefficient of lead D_{Pb} in PbTe since there were large discrepancies in the values of D_{Pb} given in the literature. For example, the value of D_{Pb} given by Goldstein (G9) and Ravich et al (R1) is 10^{-15} cm^2 s^{-1} and 10^{-18} cm^2 s^{-1} respectively at room temperature. Kinetic study of H effect on oxygen driven p-type films showed that under similar experimental conditions, the rate of gas uptake was slower compared with 'virgin' n-type films. This could be attributable to oxide growth on PbTe film surface due to its exposure to oxygen. Evidence of oxide growth as a result of oxygen interaction with lead chalcogenides has been provided by some recent studies (B10, H4, S8). For instance, Bettini and Richter (B10) studied the oxidation and thermal desorption of PbTe epitaxial layers grown on BaF_2 (5-10 μm in thickness, $n = 10^{17}$-10^{18} cm^{-3}). using XPS and LEED in ultra high vacuum and concluded that prolonged exposure of PbTe at room temperature to air at atmospheric pressure led to the formation of PbO and TeO_2.

Kinetics of oxygen uptake on hydrogenated films followed ℓnt dependence more faithfully after the first $H\text{-}O_2$ cycle indicating that atomic hydrogen recombined with oxygen at the surface. Since the reversal of H effect was faster for higher oxygen pressure this further supports the above proposal. Young (Y3) also concluded that atomic hydrogen incorporated into a PbSe film

recombined with oxygen on the surface of the film to form water. The rate of oxygen uptake on a 'virgin' p-type film was plotted using $t^{\frac{1}{2}}$ and ℓnt time dependence and it was noted that both time dependences were operative over parts of the curve. In any case, since oxygen effect was examined on only one 'virgin' p-type film, no firm conclusions could be drawn.

6.3 CONCLUSIONS AND SUGGESTIONS FOR FUTURE WORK

Under appropriate conditions both theoretical models (surface adsorption and diffusion model) predicted the correct shape of R_H vs ρ curve but exact fit between the theoretical and the experimental curve in either case was lacking.

As far as H effect is concerned combined evidence of theoretical models and kinetic studies suggest that mechanism of gas uptake is a two stage process, namely in-diffusion of H preceded by its surface adsorption. It is possible for H to be incorporated into PbTe thin film and influence its electrical properties if H diffuses along grain boundaries or occupies interstitial sites or occupies lead vacancies. Although value of the diffusion coefficient for H effect deduced during present study was comparable to those previously reported values of H effect on lead chalcogenides, it could not be identified with the self diffusion coefficient of Pb in PbTe. Since no data are available (to the best of the author's knowledge) for H effect on single crystal

PbTe, it is not possible to compare the two diffusion coefficients and postulate whether H is diffusing along grain boundaries. Occupation of an interstitial site by H was not substantiated experimentally, since if H were to occupy every available interstitial site and ionise, the resultant change in carrier concentration, for example, would be incompatible with present experimental data. Therefore, the proposed mechanism of H incorporation into PbTe thin film is through its occupation of lead vacancies.

Oxygen effect is also a two stage process. In the case of hydrogenated films, oxygen reverses the H effect by removing H and reversal of H effect is faster the higher the oxygen pressure. Since unhydrogenated films turned p-type more quickly compared with hydrogenated films under similar experimental conditions, this further supports the above proposal. As far as 'virgin' films are concerned, it is suggested that chemisorption of oxygen is followed by its in-diffusion to occupy tellurium vacancies. This suggestion is based on the evidence given in current literature (H4, S8, Z4). The influence of an oxide growth on PbTe films (due to its interaction with oxygen) on H effect still remains poorly understood.

During present study, it was found difficult to grow p-type films and little control over carrier concentration of 'virgin' films was possible. The latter is expected in view of the experimental technique used

(single and open source evaporation technique, pressure $\sim 10^{-6}$ torr) to grow thin films. Furthermore, almost entire kinetic studies were limited to room temperature. Removal of these experimental limitations in addition to having a clean surface is essential in furthering the understanding of mechanisms of H uptake on PbTe thin films. Although there have been recent studies of O_2 interaction with PbTe thin films using ultra high vacuum (S8, P6, B10), there has not been an investigation of H effect under similar conditions. For future work, it is proposed that H effect on PbTe thin films should be carried out in UHV sytem. It is important to have a clearer insight into the mechanisms of gas uptake (H and O_2) if devices based on PbTe thin films are to have practical applications other than in the field of infra-red detection.

APPENDIX A

R_H, σ EXPRESSIONS FOR AN INTRINSIC BULK IN THE PRESENCE OF A SURFACE SPACE CHARGE REGION

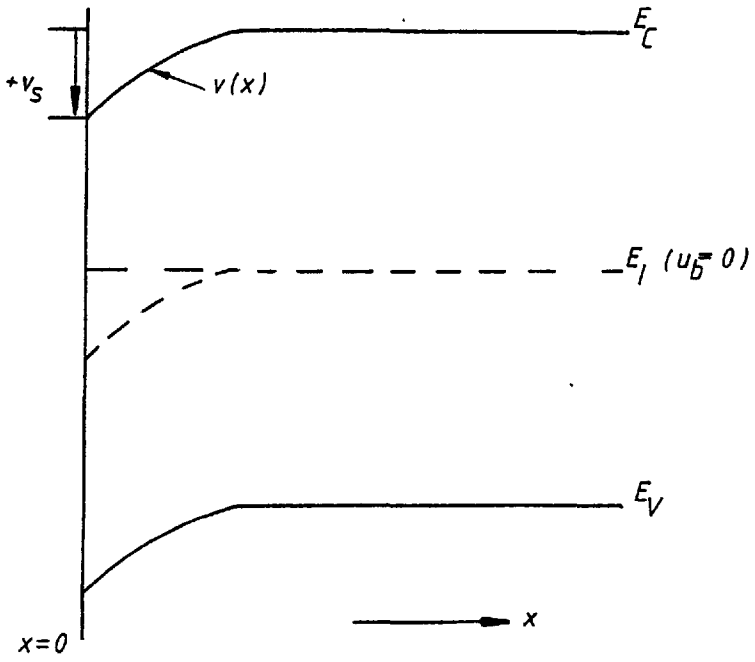

Fig.A.1: Intrinsic semiconductor with surface space charge

Using Poisson's equation in the planar form and reduced potential notation,

$$\frac{d^2v}{dx^2} = - \frac{q\rho}{\varepsilon_o \varepsilon_r kT} \qquad (A.1)$$

For the case of complete ionisation, uniform impurity concentration and non-degenerate statistics (M4),

$$\frac{d^2v}{dx^2} = - \frac{q^2}{\varepsilon_o \varepsilon_r kT} \left(n_b - p_b + p_b \exp -v - n_b \exp v\right) \qquad (A.2)$$

Defining $$L = \left[\frac{\varepsilon_o \varepsilon_r kT}{q^2(n_b+p_b)} \right]^{\frac{1}{2}} \qquad (A.3)$$

where q is the electronic charge, k is the Boltzmann's constant, T is the temperature, ε_o is the permittivity of free space, n_b and p_b are the electron and hole concentrations in the bulk.

Equation (A.2) becomes,

$$\frac{d^2v}{dx^2} = \frac{1}{L^2} \left[\frac{\sinh(u_b+v)}{\cosh u_b} \right] - \tanh u_b \qquad (A.4)$$

From Many et al (M4),

$$\frac{x}{L} = \int_{v_s}^{v} \frac{dv}{\pm F(u_b,v)} \qquad (A.5)$$

where

$$F(u_b,v) = \sqrt{2} \left[\frac{\cosh(u_b+v)}{\cosh u_b} - v \tanh u_b - 1 \right]^{\frac{1}{2}} \qquad (A.6)$$

In the case of intrinsic semiconductor $u_b = 0$

$$\therefore \quad F(0,v) = \pm 2 \sinh (v/2) \qquad (A.7)$$

From equations (A.5) and (A.7),

$$\frac{x}{L} = \ln \left[\frac{\tanh(v_s/4)}{\tanh v/4} \right] \qquad (A.8)$$

or $$v(x) = 4 \tanh^{-1} \{ \tanh(v_s/4) \exp - \frac{x}{L} \} \qquad (A.9)$$

Expressions for p and n in space charge region can now be written in terms of their respective bulk concentrations as follows:

$$n = n_b \exp\left[4 \tanh^{-1} \{\tanh(^{v}s/4) \exp - \frac{x}{L}\}\right] \quad (A.10)$$

and

$$p = p_b \exp-\left[4 \tanh^{-1}\{\tanh(^{v}s/4) \exp- \frac{x}{L}\}\right] \quad (A.11)$$

Assuming that the carrier mobility is independent of x, conductivity can be written as follows:

$$\sigma d = e\mu_n \int_o^d n(x)\, dx + e\mu_p \int_o^d p(x)\, dx = I_1 + I_2 \quad (A.12)$$

where d is the thickness of the film.

$$I_1 = e\mu_n \int_o^d n(x)dx \quad (A.13)$$

and

$$I_2 = e\mu_p \int_o^d p(x)dx \quad (A.14)$$

Evaluating I_1 first, from equations (A.9) and (A.13)

$$I_1 = \alpha \int_o^d \exp\left[4 \tanh^{-1}\{\tanh(^{v}s/4) \exp - \frac{x}{L}\}\right] dx \quad (A.15)$$

where $\alpha = e\mu_n n_b$ (A.16)

$$\text{Put } \tanh(^{V}s/4) = A \tag{A.17}$$

$$\text{and } Y = \tanh(^{V}s/4) \exp - \frac{x}{L} = A \exp - \frac{x}{L} \tag{A.18}$$

$$\therefore \quad dx = - L \frac{dY}{Y} \tag{A.19}$$

From equations (A.15), (A.17), (A.18) and (A.19),

$$I_1 = - \alpha L \int \frac{\exp(4 \tanh^{-1} Y)}{Y} \tag{A.20}$$

where the limits of integration have been omitted for the time being.

$$\text{Put } P = 4 \tanh^{-1} Y \tag{A.21}$$

$$\therefore \quad dY = \left[\frac{1}{4} \operatorname{sech}^2(^{P}/4) \right] dP \tag{A.22}$$

From equations (A.20), (A.21) and (A.22),

$$I_1 = - \frac{\alpha L}{2} \int \frac{\exp P}{\sinh(^{P}/2)} dP \tag{A.23}$$

or

$$I_1 = - \alpha L \int \frac{\exp(^{P}/2)}{1 - \exp(-P)} dP \tag{A.24}$$

$$\text{Put } D = \exp {}^{P}/2 \tag{A.25}$$

$$dP = 2 \frac{dD}{D} \tag{A.26}$$

Substitute equations (A.25) and (A.26) in equation (A.24)

$$I_1 = - 2\alpha L \int \frac{D^2}{(D^2-1)} dD \tag{A.27}$$

Equation (A.27) can now be integrated to give,

$$I_1 = -\alpha L\left[\, 2D + \ell n\, \left(\frac{D-1}{D+1}\right) \right] \quad \text{iff } D^2 > 1 \tag{A.28}$$

In order to evaluate equation (A.28), limits of integration must be included in the expression. Substitute equation (A.25) in equation (A.28)

$$I_1 = -\alpha L\left[\, 2 \exp {}^{P}/2 + \ell n \left[\frac{\exp {}^{P}/2 - 1}{\exp {}^{P}/2 + 1}\right]\right] \tag{A.29}$$

From equations (A.21) and (A.29)

$$I_1 = -\alpha L\left[\, 2 \exp(2 \tanh^{-1}Y) + \ell n\left[\frac{\exp(2 \tanh^{-1}Y)}{\exp(2 \tanh^{-1}Y) + 1}\right]\right] \tag{A.30}$$

Substitute equation (A.18) in equation (A.30)

$$I_1=\alpha L\left[\ell n\left(\frac{\exp 2\left[\tanh^{-1}\{\tanh {}^{V}s/4 \exp - \frac{x}{L}\}\right]+ 1}{\exp\left[2 \tanh^{-1}\{\tanh {}^{V}s/4 \exp - \frac{x}{L}\}\right]- 1}\right) -2 \exp \left[2 \tanh^{-1}\{\tanh {}^{V}s/4 \exp - \frac{x}{L}\}\right]\right]_{o}^{d}$$

$$I_1=\alpha L\left[\ell n\left[\left(\frac{\exp 2\left[\tanh^{-1}(\tanh {}^{V}s/4 \exp - \frac{d}{L})\right]+ 1}{\exp 2 \tanh^{-1}(\tanh {}^{V}s/4 \exp - \frac{d}{L}) -1}\right)\left(\frac{\exp {}^{V}s/2 - 1}{\exp {}^{V}s/2 + 1}\right)\right] + 2 \exp {}^{V}s/2 -2 \exp \; 2\left[\tanh^{-1} (\tanh {}^{V}s/4 \exp - \frac{d}{L})\right]\right] \tag{A.31}$$

Recalling $I_2 = e\mu_p^d \int_o p(x)\, dx$

From equation (A.12),

$$I_2 = \beta \int_o^d \exp - \left[4 \tanh^{-1}(\tanh {}^{v}s/4 \exp - \frac{x}{L})\right] dx \qquad (A.32)$$

Integral I_2 can be integrated using the substitutions used in the case of I_1. This finally gives,

$$I_2=\beta L\left[\ell n\left[\left(\frac{1+\exp-2\left[\tanh^{-1}(\tanh {}^{v}s/4 \exp - \frac{d}{L})\right]}{1-\exp-2\left[\tanh^{-1}(\tanh {}^{v}s/4 \exp - \frac{d}{L})\right]}\right)\left(\frac{1-\exp-{}^{v}s/2}{1+\exp - \frac{{}^{v}s}{2}}\right)\right] + 2\exp-{}^{v}s/2 - 2\exp-2\left[\tanh^{-1}(\tanh {}^{v}s/4 \exp - \frac{d}{L})\right]\right] \qquad (A.33)$$

where $\beta = e\mu_p p_b \qquad (A.34)$

Recalling $\sigma = \frac{1}{d}\left[I_1 + I_2\right]$

$$\therefore \quad \sigma^2 d = \frac{1}{d}\left[I_1 + I_2\right]^2 \qquad (A.35)$$

The Hall coefficient can be evaluated as follows,

$$R_H \sigma^2 d = e\mu_p^2 \int_o^d p(x)dx - e\mu_n^2 \int_o^d n(x)dx \qquad (A.36)$$

From equations (A.13), (A.14) and (A.36)

$$R_H \sigma^2 d = \mu_p I_2 - \mu_n I_1 \qquad (A.37)$$

From equations (A.35) and (A.37) one gets,

$$R_H = d\left[\frac{\mu_p I_2 - \mu_n I_1}{(I_1 + I_2)^2}\right] \qquad (A.38)$$

$$\rho^{-1} = \sigma = \frac{1}{d}\left[I_1 + I_2 \right] \tag{A.39}$$

Since the bulk is intrinsic $p_b = n_b = n_i$.

Integrals I_1 and I_2 can be evaluated as functions of surface band bending v_s since α, β, d and L are known. One major limitation of the model is that it breaks down for $v_s = 0$, i.e. it does not predict the flat band values of R_H and ρ. However, the model works for $v_s > 0$ and $v_s < 0$.

For the sake of completeness, expressions for ΔN and ΔP are also given for the case of intrinsic bulk. By definition,

$$\Delta N = \int_o^\infty (n-n_b)dx \tag{A.40}$$

and

$$\Delta P = \int_o^\infty (p-p_b)dx \tag{A.41}$$

Changing the variable to v (M4),

$$\Delta N = n_b L \int_{v_s}^{o} \frac{\exp(v)-1}{\pm F(u_b,v)}\, dv \tag{A.42}$$

and

$$\Delta P = \pm p_b L \int_{v_s}^{o} \frac{\exp(-v) - 1}{F(u_b,v)} \tag{A.43}$$

In the case of intrinsic bulk,

$$\Delta N = \pm \int_{v_s}^{o} \frac{\exp(v) - 1}{2 \sinh^{v}/2} \, dv = \pm 2 n_b L \left[\exp \frac{v}{2} \right]_{v_s}^{o}$$

or

$$\Delta N = 2 n_b L(\exp \frac{v_s}{2} - 1) \tag{A.44}$$

Similarly,

$$\Delta P = 2 p_b L \left[\exp(- \frac{v_s}{2}) - 1 \right] \tag{A.45}$$

APPENDIX B

R_H AND σ EXPRESSIONS FOR A SINGLE CARRIER FILM IN THE PRESENCE OF A SURFACE SPACE CHARGE DUE TO DONOR DIFFUSION

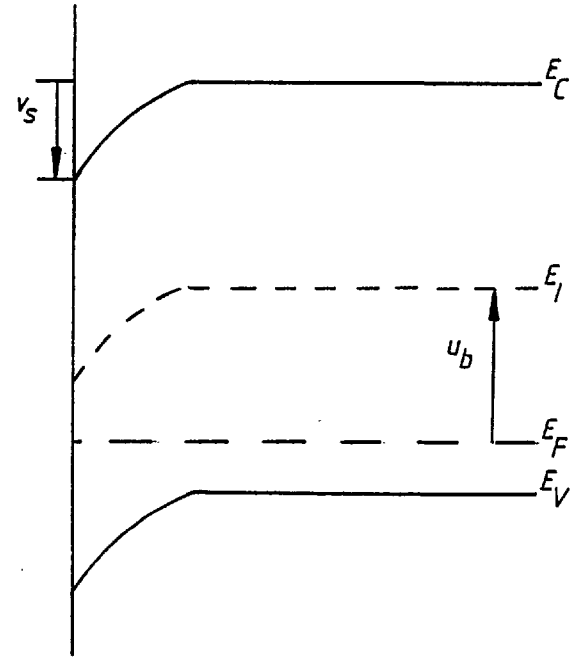

Fig. B.1: P-type Semiconductor under depletion

For assumptions see chapter 4.

Donors are diffusing into a p-type semiconductor with an exponential profile, i.e.

$$N_d = N_o \exp - \frac{x}{\ell} \qquad (B.1)$$

where $\ell = 2\sqrt{Dt}$, D = unidirectional diffusion coefficient and t is the time.

$$\text{Charge density } \rho = e\,(N_d - N_a) = e\,N_o\left(\exp\left(-\frac{x}{\ell}\right) - \frac{N_a}{N_o}\right) \qquad (B.2)$$

Using the planar form of Poisson's equation in reduced potential notation,

$$\frac{d^2v}{dx^2} = - \frac{e^2 N_o}{\varepsilon_o \varepsilon_r kT} \left[\exp(- \frac{x}{\ell}) - \frac{N_a}{N_o} \right] \qquad (B.3)$$

Define $$L_D = \left(\frac{\varepsilon_o \varepsilon_r kT}{e^2 N_o} \right)^{\frac{1}{2}} \qquad (B.4)$$

$$\therefore \quad \frac{d^2v}{dx^2} = - \frac{1}{L_D^2} \left[\exp(- \frac{x}{\ell}) - \frac{N_a}{N_o} \right] \qquad (B.5)$$

Integrating equation (B.5) with respect to x,

$$\int_{x=0}^{x=x_j} \frac{d^2v}{dx^2} dx = - \frac{1}{L_D^2} \int_{x=0}^{x=x_j} (\exp(- \frac{x}{\ell}) - \frac{N_a}{N_o}) \, dx \qquad (B.6)$$

$$\left. \frac{dv}{dx} \right|_{x=x_j} - \left. \frac{dv}{dx} \right|_{x=0} = - \frac{1}{L_D^2} \left[- \ell \exp(- \frac{x}{\ell}) - \frac{N_a}{N_o} x \right]_{x=0}^{x_j} \qquad (B.7)$$

where x_j is the value of x when $\rho = 0$.

i.e. $$x_j = \ell \, \ell n \, (\frac{N_o}{N_a}) \qquad (B.8)$$

Equation (B.7) becomes,

$$\left. \frac{dv}{dx} \right|_{x=x_j} - \left. \frac{dv}{dx} \right|_{x=0} = \frac{1}{L_D^2} \left[\ell \exp[- \frac{x_j}{\ell}] + \frac{N_a}{N_o} x_j - \ell \right] \qquad (B.9)$$

Integrating equation (B.9) w.r.t. x again,

$$v(x_j) - v(0) = \frac{1}{L_D^2}\left[\ell^2 x_j \exp[-\frac{x_j}{\ell}] + \frac{N_a}{N_o} x_j^2 - \ell x_j\right] \quad (B.10)$$

From equations (B.8) and (B.10)

$$v(x_j) = v(0) + (\frac{\ell}{L_D})^2\left[\frac{N_a}{N_o}\ell n \frac{N_o}{N_a} + \frac{N_a}{N_o}\{\ell n (\frac{N_o}{N_a})\}^2 - \ell n(\frac{N_o}{N_a})\right] \quad (B.11)$$

Put $A = \left[\frac{N_a}{N_o}\ell n \frac{N_o}{N_a} + \frac{N_a}{N_o}\{\ell n(\frac{N_o}{N_a})\}^2 - \ell n(\frac{N_o}{N_a})\right]$ (B.12)

$$\therefore \quad v(x_j) = v(0) + A(\frac{\ell}{L_D})^2 \quad (B.13)$$

At $x = 0$, $v(0) = v_s$ = surface band bending.

$$\therefore \quad v(x_j) = v_s + A(\frac{\ell}{L_D})^2 \quad (B.14)$$

Since A is constant, $v(x_j)$ can be evaluated in terms of v_s for a given value of $\ell = 2\sqrt{Dt}$. Once $v(x_j)$ is known, R_H and ρ can be evaluated as follows.

$$R_H = \frac{1}{ep} \quad (B.15)$$

and

$$\rho = \sigma^{-1} = \frac{1}{e\mu_p p} \quad (B.16)$$

where $$p = N_a \exp[-v(x_j)] \quad (B.17)$$

Value of N_a in equation (B.17) is deduced from the Hall coefficient before starting the gas cycle.

APPENDIX C

R_H AND σ EXPRESSIONS USING THE DIFFUSED LAYER MODEL

For assumptions, see chapter 4.

Consider donor diffusion into a p-type semiconductor with bulk hole concentration of N_a. Assuming the donors have exponential profile, i.e.,

$$N_d = N_o \exp - \frac{x}{\ell} \tag{C.1}$$

where $\ell = 2\sqrt{Dt}$ as defined in Appendix B and where N_o is donor concentration for $t \to \infty$. The distribution of carriers in the diffused layer is given by,

$$n(x) = \left[N_o \exp(- \frac{x}{\ell}) - N_a \right] \tag{C.2}$$

Using Petritz's model (P9),

$$\sigma d = \int_{x=0}^{x'} e\mu_n n(x)\, dx + \int_{x'}^{d} e\mu_p N_a dx \tag{C.3}$$

where d is the film thickness and x' is given by the following equations,

$$n(x) = 0$$

or

$$x' = \ell \ell n(\frac{N_o}{N_a}) \tag{C.4}$$

Integrating equation (C.3),

$$\sigma d = \left[e\mu_n \{-\ell N_o \exp - \frac{x}{\ell} - N_a x\}_o^{x'} + e\mu_p N_a (d-x') \right] \tag{C.5}$$

$$\sigma = \frac{1}{d}\left[e\mu_n \ell N_o \left(1-\exp\left[-\frac{x}{\ell}\right]-\frac{N_a}{N_o}\frac{x'}{\ell}\right) + e\mu_p N_a (d-x')\right] \qquad (C.6)$$

From equations (C.4) and (C.6),

$$\sigma(\ell) = \frac{e\mu_n \ell N_o}{d}\left(1 - \frac{N_a}{N_o} + \frac{N_a}{N_o}\ell n \frac{N_a}{N_o}\right) + \frac{e\mu_p N_a}{d}\left(d + \ell\ell n \frac{N_a}{N_o}\right) \qquad (C.7)$$

$$R_H \sigma^2 d = e\mu_p^2 \int_{x'}^{d} N_a dx - e\mu_n^2 \int_{x=0}^{x'} n(x)dx \qquad (C.8)$$

From equations (C.2) and (C.8),

$$R_H \sigma^2 d = e\mu_p^2 N_a(d-x') - e\mu_n^2 N_o \ell \left(1- \exp\left[-\frac{x'}{\ell}\right]-\frac{N_a}{N_o}\frac{x'}{\ell}\right) \qquad (C.9)$$

Substitute equation (C.4) in equation (C.9)

$$R_H \sigma^2 d = e\mu_p^2 N_a\left(d+ \ell\ell n \frac{N_a}{N_o}\right) - e\mu_n^2 N_o \ell\left(1- \frac{N_a}{N_o} + \frac{N_a}{N_o}\ell n \frac{N_a}{N_o}\right) \qquad (C.10)$$

From equations (C.7) and (C.10) one gets,

$$R_H = \frac{\frac{e\mu_p^2 N_a}{d}\left(d+ \ell\ell n \frac{N_a}{N_o}\right) - \frac{e\mu_n^2 N_o \ell}{d}\left(1 - \frac{N_a}{N_o} + \frac{N_a}{N_o}\ell n \frac{N_a}{N_o}\right)}{\left[\frac{e\mu_p N_a}{d}\left(d + \ell\ell n \frac{N_a}{N_o}\right) + \frac{e\mu_n N_o \ell}{d}\left(1 - \frac{N_a}{N_o} + \frac{N_a}{N_o}\ell n \frac{N_a}{N_o}\right)\right]^2} \qquad (C.11)$$

Using equations (C.7) and (C.11), $\sigma = \rho^{-1}$ and R_H can be evaluated as functions of $\ell = 2\sqrt{Dt}$ since N_a, N_o, μ_p, μ_n and d are all known.

When $t = 0$; $\ell = 0$, $\therefore \sigma = \rho^{-1} = e\mu_p N_a$ from equation (C.7)

and $R_H = 1/e N_a$ from equation (C.11).

References

A

A1 Allgaier, R.S., J. Appl. Phys (Suppl), 32 (1961) 2185

A2 Allgaier, R.S. and Scanlon, W.W., Phys. Rev., 111 (1958) 1029

A3 Allgaier, R.S. and Houston, B.B., Proc. Int. Conf. Semicond. Phys., Exeter (1962) (London, Institute of Physics and Physical Society) 172

A4 Azaroff, L.V. and Buerger, M.J., "The Powder Method in X-ray Crystallography", McGraw Hill (1958)

A5 Allison, J., "Electronic Engineering Materials and Devices", McGraw Hill, London (1971)

A6 Anderson, J.C., Advan. Phys., 19 (1970) 311

A7 Allgaier, R.S., Phys. Rev., 152 (1967) 808

B

B1 Bode, D.E. and Levinstein, H., Phys. Rev., 96 (1954) 259

B2 Band, K.S., Ph.D. Thesis, University of London (1972)

B3 Brodsky, M.H. and Zemel, J.N., Phys. Rev., 155 (1967) 780

B4 Brennan, D. and Fletcher, P.C., Proc. Royal Soc. (Lond.) Series A, 250 (1959) 389

B

B5 Blakemore, J.S., "Semiconductor Statistics", Pergamon Press (1962)

B6 Boltaks, B.I., "Diffusion in Semiconductors", Infosearch, London (1963)

B7 Brebrick, R.F. and Gubner, E., J. Chem. Phys., 36 (1962) 1283

B8 Bauer, G. et al., J. Appl. Phys., 47 (1976) 1721

B9 Bloem, J. and Kröger, F.A., Philips Res. Rept., 12 (1957) 281

B10 Bettini, M. and Richter, H.J., Surface Sci., 80 (1979) 334

B11 Beer, A.C., Solid State Phys. Suppl. 4 (1963)

B12 Berry, R.W. et al., "Thin Film Technology", D. Van Nostrand Ltd. (1968)

B13 Balluffi, R.W. and Blakely, J.M., Thin Solid Films, 25 (1975) 363

C

C1 Cuff, K.F. et al., Proc. 7th Int. Conf. Phys. Semicond., Paris (1964) 677

C2 Cuff, K.F. et al., J. Appl. Phys., 32 (1961) 2179

C3 Chernik, I.A. et al., Sovt. Phys. - Semicond., 2 (1968) 645

C

C4 Cullity, B.D., "Elements of X-ray Diffraction", Addision-Wesley Publ. (1956)

C5 Crank, J., "The Mathematics of Diffusion", Oxford (1956)

C6 Crocker, A.J., J. Phys. Chem. Solids, 28 (1967) 1903

C7 Calawa, A.R. et al., Trans. Met. Soc., AIME, 242 (1968) 374

C8 Cohen, M.H., Phys. Rev., 121 (1961) 387

C9 Crocker, A.J. and Rogers, L.M., Brit. J. Appl. Phys., 18 (1967) 563

D

D1 Dalven, R., Infrared Phys., 9 (1969) 141

D2 Dubrovskaya, I.N. and Ravich, Y.I., Sovt.Phys.-Solid State, 8 (1966) 1160

D3 Dhere, R.G., Private Communication

D4 Dawar, A.L. et al., Solid State Elec., 22 (1979) 117

D5 Dexter, D.L. and Seitz, F., Phys. Rev., 86 (1952) 964

D6 Dixon, J.R. and Riedl, H.R., Phys. Rev., 138 (1965) A873

E

E1 Egerton, R.F., Ph.D. Thesis, University of London, (1968)

E2 Egerton, R.F. and Juhasz, C., Thin Solid Films, 4 (1969) 239

E3 Egerton, R.F., Phil. Mag., 20 (1969) 547

E4 Egerton, R.F. and Crocker, A.J., Surface Sci., 27 (1971) 117

F

F1 Frankl, D.R., "Electrical Properties of Semiconductor Surfaces", Pergamon Press Ltd. (1967)

F2 Fehlner, F.P. and Mott, N.F., Oxid. Met., 2 (1970) 59

G

G1 Green, M., Surface Sci., 26 (1971) 549

G2 Gudkin, T.S. et al., Sovt. Phys.-Semicond., 8 (1975) 1453

G3 Green, M. and Miles, R.E., J. Phys. D: Appl. Phys., 6 (1973) L45

G4 Green, M. and Lee, M.J., J. Phys. Chem. Solids, 27 (1966) 797

G

G5 Galat, J. et al., Oxid. Met., 9 (1975) 497

G6 Greene, R.F. et al., J. Vac. Sci. Techn., 8 (1971) 75

G7 Grove, A.S., "Physics and Technology of Semiconductor Devices", John Wiley and Sons (1967)

G8 Greene, R.F., Surface Sci., 2 (1964) 101

G9 Goldstein, M.L., C.R. Acad. Sci., Paris, 268 (1969) 686

G10 Green, M., Private Communication

H

H1 Hing, L.A., Ph.D. Thesis, University of London (1975)

H2 Hillenbrand, L.J., J. Chem. Phys., 41 (1964) 3971

H3 Hillenbrand, L.J., J. Chem. Phys., 73 (1969) 2902

H4 Hagström, A.L. and Fahlman, A., Physica Scripta, 16 (1977) 432

H5 Hickmott, T.W., J. Chem. Phys., 32 (1960) 810

H6 Hemstreet, L.A., Phys. Rev. (B), 12 (1975) 1212

H7 Hapse, M.G. et al., Surface Sci., 12 (1968) 85

H8 Harman, T.C. et al., J. Phys.Chem.Solids, 24 (1963) 835

J

J1 Jones, R.H., Proc. Phys. Soc. (B), 70 (1957) 704

J2 Jones, R.H., Proc. Phys. Soc. (B), 70 (1957) 1025

J3 Juhasz, C., Ph.D. Thesis, University of London (1967)

J4 Juhasz, C., Private Communications

J5 Jayadevaiah, T.S. and Kirby, R.E., Thin Solid Films, 6 (1970) 343

K

K1 Kolomoets, N.V. et al., Sovt.Phys.-Semicond., 1 (1968) 1020

K2 Kanai, Y. and Shohno, K., Jap. J. Appl. Phys., 2 (1963) 6

K3 Kondratov, A.V. et al., Sovt. Phys.-Semicond., 7 (1973) 124

K4 Kittel, C., "Introduction to Solid State Physics", John Wiley (1971)

K5 Kuchar, F. et al., J. Phys. C: Solid State Phys., 10 (1977) 5101

K6 Kane, E.O., J. Phys. Chem. Solids, 1 (1957) 249

L

L1 Lopez-otero, A., Thin Solid Films, 49 (1978) 3

L2 Lopez-otero, A., J. Appl. Phys., 48 (1977) 446

L3 Lundström, I. et al., Appl. Phys. Lett., 26 (1975) 55

L4 Lundström, I. et al., J. Appl. Phys., 46 (1975) 3876

L5 Lee, R.N., Jap. J. Appl. Phys. Suppl. 2, pt. 2, (1974) 311

L6 Levine, J.D., Surface Sci., 10 (1968) 313

L7 Lehovec, K. and Slobodskoy, A., Solid State Elec., 3 (1961) 45

L8 Logothetis, E.M. and Holloway, H., Solid State Comm., 8 (1970) 1937

M

M1 Makino, Y., J. Phys. Soc., Japan, 19 (1964) 580

M2 McLane, G.F. and Zemel, J.N., Thin Solid Films, 7 (1971) 229

M3 Myers, J.H. et al., J. Appl. Phys., 42 (1971) 5578

M4 Many, A. et al. "Semiconductor Surfaces", North-Holland Publ. Co. (1971)

M

M5 Makino, Y. and Hoshina, T., J. Phys. Soc., Japan, 19 (1964) 1242

M6 Many, A., CRC Crit. Rev. in Solid State Sci., 4 (1974) 515

M7 McLane, G.F., Ph.D. Thesis, University of Pennsylvania (1971)

O

O1 Ota, T., Proc. 7th Int. Vac. Congr. and 3rd Int. Conf. Solid Surfaces, Vienna (1977) 1713

O2 Okuyama, K., Thin Solid Films, 33 (1976) 165

P

P1 Putley, E.H., "Materials used in Semiconductor Devices", Ed. Hogarth, C.A. (1965) 71

P2 Piccioli,N. et al., J. Phys. Chem. Solids., 35 (1974) 971

P3 Poh, K.J. and Anderson, J.C., Thin Solid Films, 3 (1969) 139

P4 Palatnik, L.S. et al., Sovt. Phys.-Solid State, 11 (1970) 2086

P5 Putley, E.H., "The Hall Effect and Related Phenomena", Butterworths, London (1960)

P

P6 Parker, E.H.C. and Williams, D., Solid State Elec., 20 (1977) 567

P7 Palatnik, L.S. et al., Sovt. Phys.-Solid State, 15 (1973) 963

P8 Parker, E.H.C. and Williams, D., Thin Solid Films, 35 (1976) 373

P9 Petritz, R.L., Phys. Rev., 110 (1958) 1254

P10 Parada, N.J. and Pratt, G.W., Phys. Rev. Lett., 22 (1969) 180

R

R1 Ravich, Y.I. et al., "Semiconducting Lead Chalcogenides", Plenum Press, New York (1970)

R2 Ritchie, I.M. and Hunt, G.L., Surface Sci., 15 (1969) 524

R3 Rogers, L.M., Brit. J. Appl. Phys., 18 (1967) 1227

R4 Ravich, Y.I. et al., Phys. Stat. Sol. (B), 43 (1971) 11, 453

R5 Rogalski, A., ACTA Physica Polonica, A55 (1979) 45

S

S1 Scanlon, W.W., Solid State Phys., 9 (1959) 83

S2 Stavitskaya, T.S. et al., Sovt. Phys.-Semicond., 1 (1968) 952

S3 Silverman, S.J. and Levinstein, H., Phys. Rev., 94 (1954) 871

S4 Shivaraman, M.S., J. Appl. Phys., 47 (1976) 3592

S5 Steele, M.C. and MacIver, B.A., Appl. Phys. Lett., 28 (1976) 687

S6 Sealy, B.J. and Crocker, A.J., Thin Solid Films, 26 (1975) 135

S7 Smith, R.A., "Semiconductors", Cambridge University Press (1968)

S8 Sun, T.S. et al., J. Vac. Sci. Tech., 15 (1978) 585

S9 Schilz, W., J. Phys. Chem. Solids, 30 (1969) 893

S10 Stephenson, G., "Mathematical Methods for Science Students", Longman (1971)

S11 Seiwatz, R. and Green, M., J. Appl. Phys. 29 (1958) 1304

T

T1 Tuck, B., "Introduction to Diffusion in Semiconductors", Peter Peregrinus Ltd. (1974)

T2 Tauber, R.N. et al., J. Appl. Phys., 37 (1966) 4855

W

W1 Wallace, C.A. and Ward, R.C.C., J. Appl. Cryst., 8 (1975) 255

Y

Y1 Yasuoka, Y. et al., Jap. J. Appl. Phys., 7 (1968) 1186

Y2 Young, J.J. and Zemel, J.N., Thin Solid Films, 31 (1976) 25

Y3 Young, J.J., Ph.D. Thesis, University of Pennsylvania (1974)

Y4 Yang, C.Y. and Rabii, S., Int. J. Quantum Chemistry Symp. No. 10, (1976) 313

Z

Z1 Zemel, J.N. et al., Phys. Rev., 140 (1965) A330

Z2 Zhitinskaya, M.K. et al., Sovt. Phys.-Solid State, 8 (1966) 246

Z

Z3 Zemel, J.N., "Solid State Surface Science", Ed. Green, M., vol. 1 (1969) 292

Z4 Zemel, J.N., "Surface Physics of Phosphors and Semiconductors", Ed. Scott, C.G. and Read, C.E., Academic Press, London (1975) 523

Z5 Zemel, J.N., Research/Development, 28 (1977) 38

Z6 Zemel, J.N. and Kaplit, M., Surface Sci., 13 (1969) 17

Z7 Zemel, J.N. et al., CRC Crit. Rev. in Solid State Sci., 5 (1975) 369

Z8 Zemel, J.N., "The Use of Thin Films in Physical Investigations", Ed. Anderson, J.C., Academic Press, London (1966) 319